Photocatalytic degradation of toluene in an annular LED-based photoreactor

Effect of controlled periodic illumination, radiation profile, and process control

Francisco O. Galnares

TU Delft

Photocatalytic degradation of toluene in an annular LED-based photoreactor

Effect of controlled periodic illumination, radiation profile, and process control

by

Francisco O. Galnares

to obtain the degree of Master of Science

at the Delft University of Technology,

to be defended publicly on 20 July, 2017 at 13:00

Faculty of Electrical Engineering, Mathematics and Computer Science

Sustainable Energy Technology

Department of Process & Energy, Faculty 3mE

Section of Intensified Reactors & Separation Systems

Student number:	4516796	
Report number:	P&E-2681	
Project duration:	August 22, 2016 – May 24, 2017	
Thesis committee:	Prof. dr. ir. A. Stankiewicz,	TU Delft, supervisor
	Prof. D. Roekaerts,	TU Delft
	Prof. A. Smets,	TU Delft
	Ir. F. M. Khodadadian,	TU Delft

An electronic version of this thesis is available at http://repository.tudelft.nl/.

TU Delft

Abstract

Despite the fact that photocatalysis has been proposed as an attractive and sustainable technology to completely mineralize organic pollutants, its large-scale economic development has been hindered, among other factors, by a low efficiency in illumination. In this work, gas phase toluene was degraded as model contaminant in an annular LED-based photocatalytic reactor under various light irradiance and illumination modes as a means to enhance the efficiency in illumination.

The effect of controlled periodic illumination was first studied by exploring the effect of the duty cycle and the period and compared to continuous illumination at equivalent light irradiance. Controlled periodic illumination is based on the hypothesis that introducing photons in an alternate fashion rather than continuously avoids the buildup of charges and consequently, diminishes electron-hole recombination. The results show that under a kinetic-limited regime, there is no difference between the conversion of toluene under controlled periodic illumination and continuous illumination at equivalent average irradiance. Consequently, the photonic efficiency for controlled periodic illumination and continuous illumination at equivalent irradiance is also the same. Nonetheless, the photonic efficiency diminished with increasing average light irradiance. This behaviour is ascribed to increasing electron-hole recombination with increasing duty cycle for controlled periodic illumination and with increasing light irradiance for continuous illumination.

The second illumination technique investigated was the following of different radiation profiles along the reactor length. The LED array of the annular photoreactor was controlled with five different power supplies, each controlling one-fifth of the reactor length; thus, allowing to test experimentally different light irradiance per section of reactor. It was hypothesized that since at the inlet of the reactor the mass transfer driving force is larger than at the outlet of the reactor, a lower irradiance at the inlet would still yield good toluene conversion while at the same time decreasing the energy input. Experimentally, both an increasing and decreasing light irradiance profiles were tested and compared to a uniform profile at equivalent light irradiance. The results show that an increasing irradiance profile yielded a slightly higher conversion than uniform illumination; however, the difference was not statistically significant. In addition, a mathematical model of five photocatalytic reactors in series was developed to further explore the effect of following different irradiation profiles. By solving an optimization problem to minimize both the irradiance and outlet concentration of toluene, it was noted that the highest toluene conversion is always achieved under a uniform illumination of the reactor.

Finally, this thesis presents the experiments to design the irradiation process control. The effect of relative humidity and toluene inlet concentration perturbations on the degradation of toluene, production of carbon dioxide, and mineralization are also analyzed. The results show that increasing the relative humidity to a certain value will stop catalyst deactivation and will augment the mineralization of toluene. In contrast, an increase in toluene inlet concentration will diminish the mineralization of toluene. Furthermore, a PI feedback controller was designed and validated manually. The feedback controller was able to maintain the conversion of toluene at the set-point at experimental conditions with no perturbations and at experimental conditions with perturbations such as catalyst deactivation, and changes in relative humidity and toluene inlet concentration.

Keywords: *photocatalysis, electron-hole recombination, UV-LEDs, controlled periodic illumination, continuous illumination, average irradiance, kinetic-controlled regime, radiation profile, process control.*

Graphical Abstract

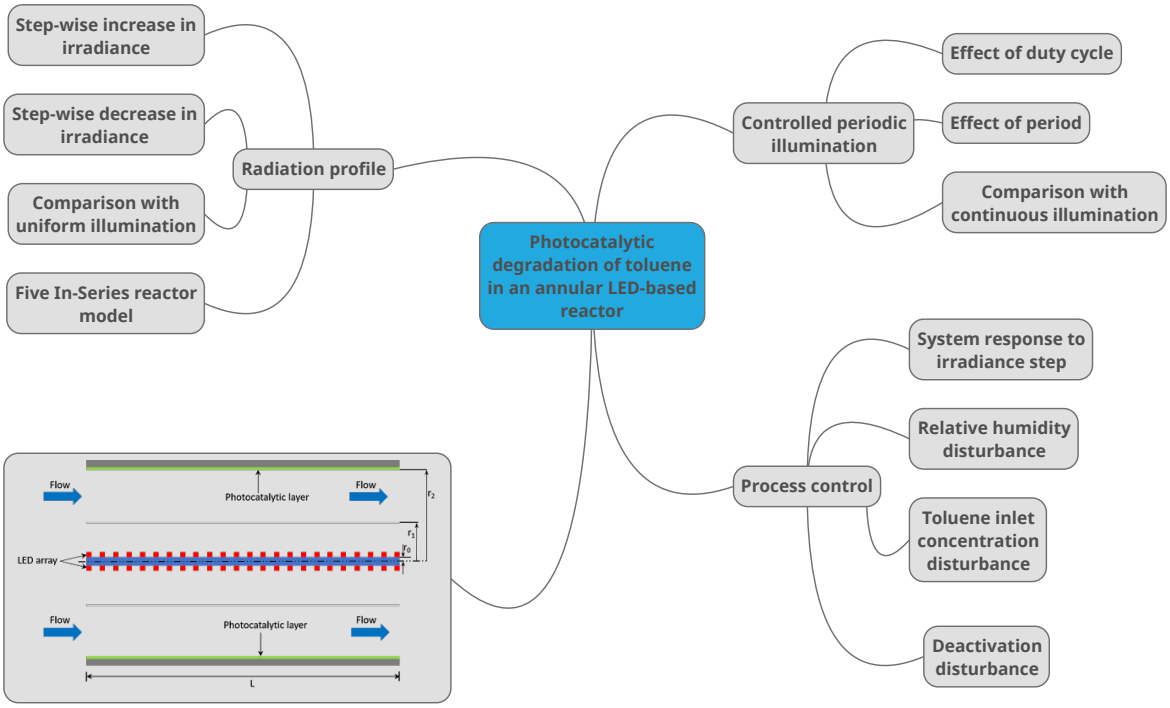

Acknowledgments

I am especially thankful for the hard work and commitment of my daily supervisor, Maryam Khodadadian, who helped me without hesitation throughout my thesis. Maryam, you are a person who works very hard towards your goals. I have no doubt you will succeed in your future endeavors. I must also recognize the generous support of Michel van den Brink, who did not hesitate to help when needed in the lab.

I would like to express my gratitude to Professor Andrzej Stankiewicz and Prof. Ruud van Ommen, for their insights regarding the photocatalytic part of this project and to Dr. Richard Lakerfield, for his insights and help through the process control part.

I must also express my gratitude to Prof. Dirk Roekaerts and Prof. Arno Smets for their comments on this thesis and for being party of my thesis committee.

Additionally, I must express my appreciation to CONACyT, for which without their financial support for the past two years I would not have been able to study my Master's Degree at TU Delft.

To my family and friends, I owe unconditional gratitude for their encouragement and support for the past two years.

Contents

1 Introduction

In the past decades, urban areas around the world have not just grown in number, but also in population and complexity [1]. This growth in population, added to the constant increase in human wealth, consequently has increased the consumption of non-renewable resources to satisfy the needs of the society. To date, non-renewable resources have been widely used to produce electricity, heat, transportation fuels, as well as the vast majority of chemical and biochemical products used by society. However, with the current level of consumption of non-renewable resources, the environmental degradation has become more apparent and concern has extended not just to significant pollutants such as carbon dioxide, but also to micro and emerging contaminants.

As non-renewable resources continue to deplete, chemical engineering research in the 21st century needs to focus on the development of technically- and economically-feasible and energy efficient technologies based on renewable feedstocks [2]. Photocatalysis, in which the energy of the sun can be utilized to carry out a chemical reaction is a major advancement in the direction of sustainable chemical processes. The use of light to drive chemical or biochemical reactions may yield a more sustainable process for two reasons [2]:

1. the process selectivity to specific products may increase due to the following of a different chemical pathway or due to the operation at a low or ambient temperature
2. the energy consumption may drastically decrease due to the operation at low temperature, the use of solar energy, or electricity generated via renewable energy resources

1.1. Photocatalysis

Photocatalysis is an attractive technology due to its various potential applications in areas such as selective chemical synthesis [3], environmental technology [4], and medicine [5]. In selective processes, photocatalysis has been utilized for the synthesis of fine chemicals such as the reduction of carbon dioxide into methanol [6–8], water splitting for hydrogen production [3, 4, 9], and selective oxidation of organic compounds such as alcohols to carbonyls [3]. Cancer treatment is one of the most important applications associated with photocatalysis [5]. For instance, a 30-minute illumination in the presence of TiO_2 leads to complete killing of *human U*937 monocytic leukemia cells [10]. Finally, non-selective applications are mainly employed in environmental remediation of non-biodegradable molecules from water and air [4] where the organic contaminants are mineralized into stable inorganic molecules such as carbon dioxide, water, and salts.

However, two of the main reasons large-scale photocatalytic industrial applications have remained limited are [8]:

1. low efficiency of illumination (photon transfer limitations)
2. limited contact between the activated catalyst and the reactants (mass transfer limitations)

With respect to photon transfer limitations, light may be absorbed on the way to the catalyst since it has to travel through the fluid. Thus, making it very difficult to achieve optimal irradiance throughout the catalyst surface. The light irradiance also decreases inversely with the square of the distance from the source of light. Hence, a small distance between the light source and the catalyst is usually preferred. With respect to mass transfer limitations, both the contact between the catalyst and the reactants and the removal of the formed products should be maximized [8].

1.1.1. Heterogeneous photocatalytic mechanism

The overall heterogeneous photocatalytic process follows the same steps as conventional heterogeneous catalysis [6]. The main difference with conventional heterogeneous catalysis is that photoinduced reactions are activated by the absorption of a photon rather than by thermal energy [6]. As Figure 1.1 illustrates, the reactants first have to diffuse from the fluid phase to the surface of the catalyst, where they are adsorbed. Once adsorbed, they react on the surface of the catalyst. Afterward, the products are desorbed from the catalyst surface and diffuse into the fluid phase.

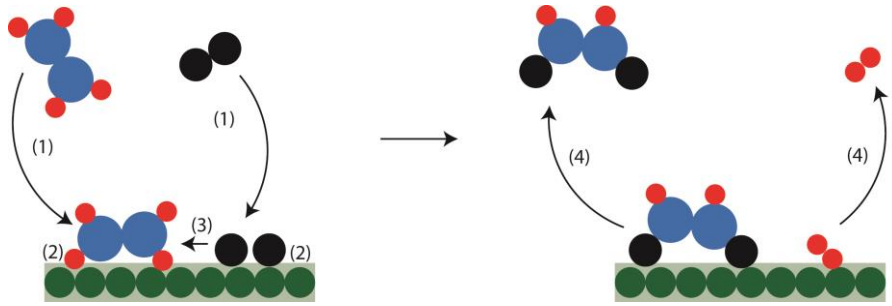

Figure 1.1: Schematic representation of the main steps in heterogeneous catalysis: (1) transfer of reactants from the fluid phase to the surface of the catalyst; (2) adsorption of the reactants on the surface of the catalyst; (3) reaction in the adsorbed phase; (4) desorption of the products onto the bulk phase (based on [11])

When a semiconductor catalyst is illuminated with photons with equal or greater energy than the band gap of the catalyst, these photons are absorbed and an electron-hole (e^--h^+) pair is generated. Although thermal energy is inadequate to activate the photocatalyst, the temperature of operation is still an important parameter [12]. Operating at low temperatures favors adsorption; hence, the desorption of the products will limit the overall reaction rate. On the opposite, operating at high temperature limits the adsorption of the reactants on the catalytic surface and promotes the recombination of charge carriers. As a consequence, the optimum operating temperature has been found between 20°C and 80°C [6].

Figure 1.2 presents a schematic of the photocatalytic process when a photocatalyst is excited with adequate photon energy ($h\nu$), together with some of the oxidation-reduction (redox) reactions that take place [4, 8, 12].

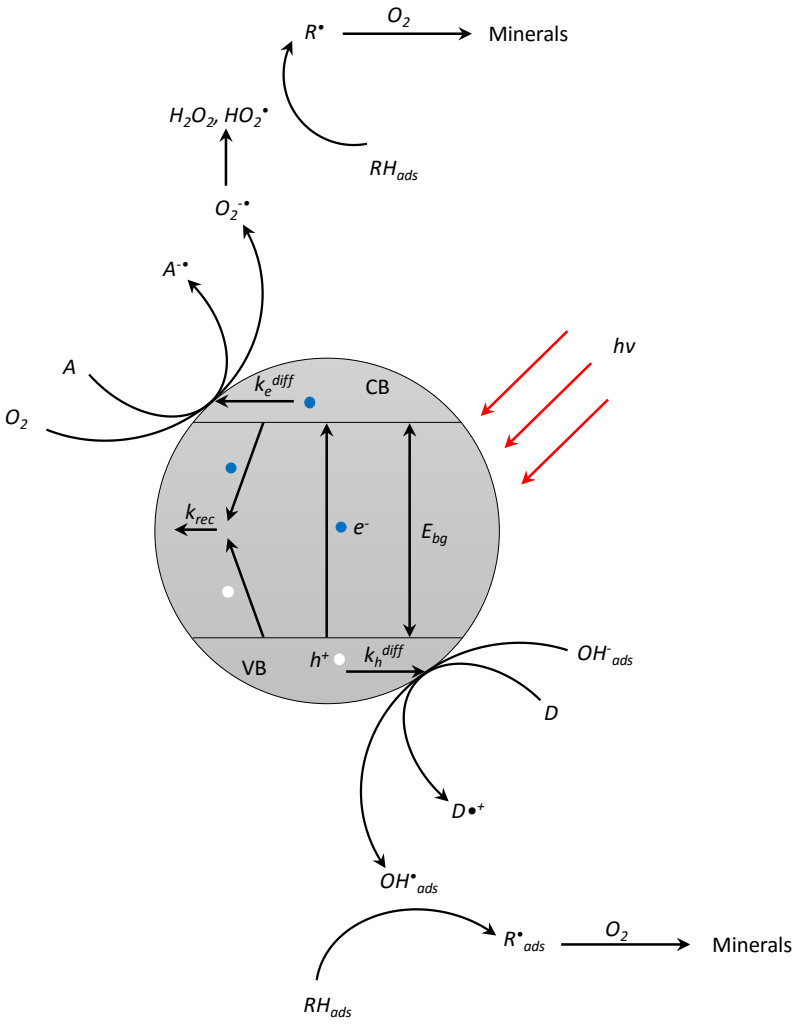

Figure 1.2: Schematic mechanism of electron-hole formation of a spherical TiO_2 particle together with some of the redox reactions that take place (based on [4]).

As the photon is absorbed, the electron (e^-) is promoted from the valence band to the conduction band (e^-_{CB}), generating a hole in the valence band (h^+_{VB}):

$$TiO_2 + h\nu \rightarrow h^+_{VB} + e^-_{CB} \tag{1.1}$$

Generally, during the transport of the photogenerated electrons and holes to the catalyst surface two things can happen: they either recombine and dissipate energy as heat (Equations 1.2 and 1.3)

$$e^-_{CB} + \{>Ti^{IV}OH^{\bullet}\}^+ \rightarrow Ti^{IV}OH \tag{1.2}$$

$$h^+_{VB} + \{>Ti^{III}OH\} \rightarrow Ti^{IV}OH \tag{1.3}$$

or if a suitable scavenger or surface defect is available to trap the electron or hole (Equations 1.4 to 1.6), recombination is prevented and the subsequent reduction and oxidation processes are initiated (Equations 1.7 and 1.8) [6–8].

$$h^{+}_{VB} + \{>Ti^{IV}OH\} \rightarrow \{>Ti^{IV}OH^{\bullet}\}^{+} \tag{1.4}$$

$$e^{-}_{CB} + \{>Ti^{IV}OH\} \leftrightarrow \{>Ti^{III}OH\} \tag{1.5}$$

$$e^{-}_{CB} + \{>Ti^{IV}\} \leftrightarrow \{Ti^{III}\} \tag{1.6}$$

The photogenerated electron that reaches the surface of the catalyst ($>Ti^{III}OH$) must react to avoid recombination, hence, electron acceptors or scavengers must be present. Oxygen is the most commonly used electron acceptor [4].

$$\{>Ti^{III}OH\} + Ox \rightarrow Ti^{IV}OH + Ox^{\bullet+} \tag{1.7}$$

After the photogenerated hole diffuses towards the surface of the catalyst ($>Ti^{IV}OH^{\bullet+}$), it either reacts with the adsorbed solvent molecules, or with an adsorbed reactant by interfacial electron transfer, oxidizing the adsorbed species [4, 13, 14].

$$\{>Ti^{IV}OH^{\bullet}\}^{+} + Red \rightarrow >Ti^{IV}OH + Red^{\bullet+} \tag{1.8}$$

Overall, the photoinduced process may be summarized with Equation 1.9:

$$(Ox_1)_{ads} + (Red_2)_{ads} \xrightarrow[\text{semiconductor}]{h\nu \geqslant E_{bg}} Red_1 + Ox_2 \tag{1.9}$$

The characteristic times for each of the primary photocatalytic processes were estimated by Hoffmann et al. [15] on the basis of laser flash photolysis experiments [16, 17] and are presented in Table 1.1. As Table 1.1 illustrates, charge-carrier recombination is primarily mediated by $\{>Ti^{III}OH\}$ in the first 10 nanoseconds. It also appears that the rate determining step is the interfacial charge transfer by trapped electrons since it happens in the millisecond scale. However, the overall chemical kinetics may vary depending on the pollutant [18].

Table 1.1: Characteristic times of primary processes in TiO_2 semiconductor photocatalysis. Notation: h^{+}_{VB} = valence band hole, e^{-}_{CB} = conduction band electron, $\{>Ti^{IV}OH^{\bullet}\}^{+}$ = trapped hole, and $\{>Ti^{III}OH\}$ = trapped electron.

Primary process		Characteristic time
Charge-carrier generation		
$TiO_2 + h\nu \rightarrow h^{+}_{VB} + e^{-}_{CB}$	1.1	Very fast (fs)
Charge-carrier recombination		
$e^{-}_{CB} + \{>Ti^{IV}OH^{\bullet}\}^{+} \rightarrow Ti^{IV}OH$	1.2	Slow (100 ns)
$h^{+}_{VB} + \{>Ti^{III}OH\} \rightarrow Ti^{IV}OH$	1.3	Fast (10 ns)
Charge-carrier trapping		
$h^{+}_{VB} + >Ti^{IV}OH \rightarrow \{Ti^{IV}OH^{\bullet}\}^{+}$	1.4	Fast (10 ns)
$e^{-}_{CB} + >Ti^{IV}OH \leftrightarrow \{Ti^{III}OH\}$	1.5	Shallow trap (100 ps)
$e^{-}_{CB} + >Ti^{IV} \rightarrow Ti^{III}$	1.6	Deep trap (10 ns)
Interfacial charge transfer		
$\{>Ti^{III}OH\} + Ox \rightarrow Ti^{IV}OH + Ox^{\bullet+}$	1.7	Very slow (ms)
$\{>Ti^{IV}OH^{\bullet}\}^{+} + Red \rightarrow >Ti^{IV}OH + Red^{\bullet+}$	1.8	Slow (100 ns)

1.1.2. Semiconductor photocatalysts

Several oxide and sulfide semiconductors have bandgap energies capable of catalyzing a wide range of chemical reactions of environmental interest. Among these semiconductor catalysts, zinc oxide (ZnO), zirconium dioxide (ZrO_2), titanium dioxide (TiO_2), cerium(IV) oxide (CeO_2), cadmium sulphite (CdS), and iron(III) oxide (Fe_2O_3) have been investigated for photocatalytic processes [6]. Nonetheless, the best photocatalytic performances have always been obtained with TiO_2 [19–24]. Figure 1.3 illustrates some of the aforementioned catalysts together with the redox potential of some organic compounds.

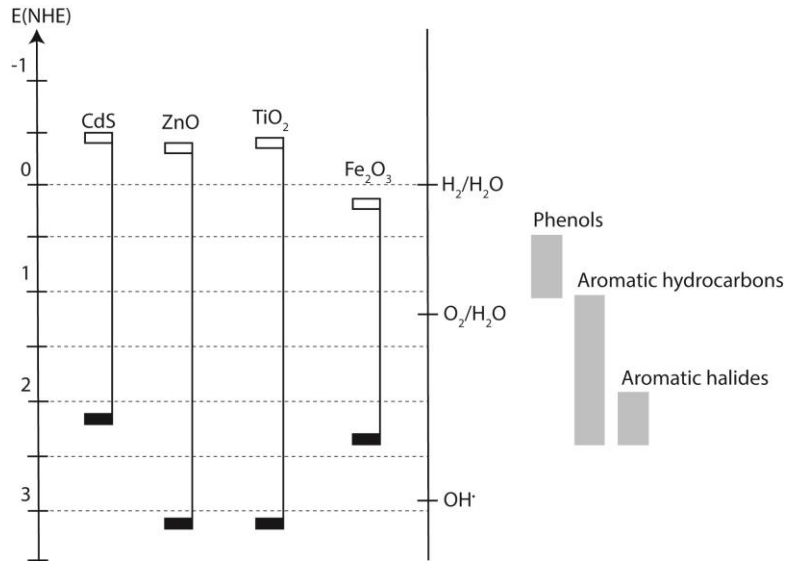

Figure 1.3: Band positions (top = valence band, bottom = conduction band) of several semiconductors together with the redox potential of some organic compounds (based on [3]).

The two main criteria for a good semiconductor catalyst to degrade organic compounds are that the redox potential of the $H_2O/HO^{\bullet}$ couple lies within the bandgap of the semiconductor and that the semiconductor must be stable over large periods of time [15]. Both the sulfide semiconductors and the iron oxide semiconductors are unsuitable based on the stability requirements. The former ones undergo photoanodic corrosion, whereas the latter ones undergo photocathodic corrosion [25]. Additionally, although ZnO appears to be a good alternative to TiO_2 as illustrated in Figure 1.3, it undergoes inactivation over time [16]. With the exception of CdS, which has been reported as a suitable visible light photocatalyst [26, 27], the bandgap of these catalysts falls within the UV activation wavelength.

Titanium dioxide, with a bandgap of 3.0 eV for rutile and 3.2 eV for anatase, is the most active photocatalyst under the photon energy corresponding to the wavelength between 300 and 390 nm [12] and has the advantages of being chemically and biologically inert, photocatalytically stable, cheap, easy and safe to manufacture and use, and catalyzes efficiently reactions [6, 19].

1.1.3. Radiation sources for heterogeneous photocatalysis

The reaction rate of a photocatalytic process does not only depend on the concentration of the chemical species, but also on the number of photons absorbed by the catalyst. Generally, at low irradiance, the reaction rate has a linear dependence with the absorbed photons, whereas at higher irradiance, the dependence has been reported to be square root [7, 28]. The reason behind this is that at high irradiance, the rate of charge carrier recombination becomes higher than the reaction rate at the surface of the catalyst [28]. The transition between the linear and square root dependency has been estimated to happen above one sun equivalent [29]. Although one sun is not quantitatively defined, the sun emits about 1 and 2 mW/cm^2 for wavelengths below 350 and 400 nm, respectively [30]. Nonetheless, this transition also depends on the catalyst material, the reactor configuration, and on whether or not there are mass transfer limitations [31]. Additionally, at very high light irradiance, Ollis et al. [32] reported a dependency which approximated zero. They concluded that at very high light irradiance, the transport of the reactants towards the catalyst surface limits the overall reaction. The optimal power utilization corresponds to the regime where the reaction rate and the irradiance have a linear dependence [33].

Since the reaction rate depends on the number of absorbed photons by the catalyst, the radiation source is of critical importance in heterogeneous photocatalysis. As mentioned in Chapter 1.1.2, TiO_2 is the most active photocatalyst under ultraviolet radiation. Ultraviolet radiation (UV) refers to electromagnetic radiation in the 200-400 nm wavelength range and is further divided into UVA, UVB, and UVC, depending on the wavelength. UVA covers from 315 to 400 nm, UVB from 280 to 315 nm, and UVC from 200 to 280 nm [34]. Solar radiation reaching the Earth's surface is mainly composed of visible radiation, which accounts for about 50% of the spectrum, and infrared radiation, which accounts for about 40% of the spectrum. Since UV radiation represents less than 10%, one of the most active areas of research is shifting the photocatalyst bandgap to be able to use the visible part of the spectrum [35].

The efficient utilization of solar radiation in heterogeneous photocatalysis is advantageous as it will decrease energy costs considerably [8]. For instance, a life cycle assessment performed by Muñoz et al. [36] to determine the environmental impact of heterogeneous photocatalysis comparing the use of UV lamps and solar radiation among different advanced oxidation processes (AOPs), determined that heterogeneous photocatalysis using UV lamps has the highest environmental impact because of the high electrical consumption required. Even though the utilization of sunlight as a natural source of UV irradiation is cost-effective, it is not readily available in all geographic locations and current highly efficient solar photoreactors are cost-intensive and require complex designs and components [37].

For heterogeneous photocatalysis to be energy efficient, both the photon generation process and photon utilization processes must be efficient and cost-effective. An efficient artificial radiation source for heterogeneous photocatalysis is one that provides optimal illumination of the catalytic surface, minimizes heat loss during operation, and can be easily incorporated into the reactor design [37]. Artificial light devices used in heterogeneous photocatalysis include UV lamps, lasers, and light-emitting diodes (LEDs).

UV lamps are by far the most utilized artificial radiation sources in photocatalytic reactions. The most common commercially available UV lamps are low, medium, and high pressure mercury arc lamps. Mercury arc lamps consist of a sealed quartz tube with electrodes at both ends. The tube is filled with a small amount of mercury and an inert gas such as argon. UV light is generated when mercury vapor, excited by the discharge produced by applying a high voltage across the electrodes, returns to a lower energy state. The inert gas prevents any atmospheric electrochemical influence on the lamp; thus, extending the life of the electrode and reducing thermal losses [38]. Despite having a narrower emission spectrum than solar radiation, UV lamps emission spectrum is broader when compared to UV lasers and LEDs.

Several studies have compared the photocatalytic degradation of pollutants under solar and artificial UV radiation. For example, Bhaktende et al. [39] compared the degradation of nitrobenzene under concentrated solar radiation and UV lamps. The results showed a much faster degradation using artificial UV lamps as the useful UV component present in the artificial light source was greater than in sunlight.

UV lasers possess unique characteristics compared to other artificial light devices, such as high monochromaticity and low beam divergence. However, they have had a very limited used in photocatalysis mainly because of their high costs, their safety concerns, the incompatibility for reactor design, and the high specialized training required for their operation [40]. Nevertheless, the interest in using UV lasers is increasing since Gondal et al. [40] and Yahaya et al. [41] reported that the UV light produced by the laser beam may enhance both the photonic efficiency and the conversion of desired products.

After Chen et al. [42] demonstrated the possibility of using LEDs as an alternative UV radiation source for heterogeneous photocatalysis in 2005, the studies employing LEDs in the literature have continuously grown. LEDs are solid-state light (SSL) sources which use inorganic semiconductors that have a junction with hole-carrying p-layer and an electron-carrying n-layer to generate photons [43]. The recombination of the electron-hole pairs within the device after the application of a forward voltage releases photons [37]. UV LEDs provide a higher overall efficiency in photon generation and utilization compared to UV lamps because the electrical power is converted directly into optical power [44, 45]. Moreover, unlike incandescent lamps which efficiency is limited by the heat loss in the filament, the efficiency of SSL devices increases exponentially with advances in semiconductor technology, material science and optics [46].

Despite their low power output, UV LEDs possess multiple advantages when compared to conventional UV lamps. Their rated lifetime is about 100,000 hours, which lies between 10 and 100 times greater than conventional UV lamps. Their size is small, which means they can be easily incorporated into the reactor design, and they achieve full brightness instantly rather than in seconds [37, 47–49]. A summary of the comparison between UV lamps and UV LEDs is presented in Table 1.2.

Table 1.2: General comparison between conventional UV lamps and UV LEDs. (Adapted from [50])

	Conventional UV lamps	UV LEDs
Rated life time [h]	1,000 - 17,000	100,000
Emission spectra	Polychromatic	Quasi-monochromatic
Toxicity	May contain toxic substances like mercury	Non-toxic
Power output [W]	Up to 1,000	Up to 1
Failure mode	Abrupt failure	Gradual failure
Response time	Full brightness in several seconds	Full brightness almost instantly
Wall-plug efficiency	Up to 23%	Up to 35%
External quantum efficiency	7 - 15%	Up to 40%
Size	Large	Small
Durability	Fragile	Durable
Operating technology	Plasma physics and optics	Semiconductor technology and optics
Thermal radiation	High	Negligible
Integration with reactor	Difficult	Easy
Purchase cost	Low	High but reducing rapidly

In general, using LEDs as radiation source offer several new degrees of freedom in the design of photocatalytic reactors [51]. Due to its small size, each LED can be positioned flexibly in the reactor design to control the reaction rate locally. Nevertheless, studies on LED-based photocatalytic reactor modelling and optimization of the LEDs position have remained limited. For instance, Wang et al. [52] studied the photocatalytic degradation

of dimethyl sulfide. Their work showed that the position of the LED array relative to the catalyst surface strongly affects both the radiation intensity and uniformity. The closer the lamp to the catalyst surface, the less uniform the illumination profile. In contrast, although a more uniform profile was observed by increasing the distance between the LED array and the catalyst, the photon flux reaching the catalyst surface was lower due to dispersion. The authors found an optimal dimethyl sulfide removal performance when the LED array was positioned at a distance between 1.5 and 3 cm relative to the catalyst surface. At these conditions, the radiation field became more uniform and the dispersion of the photon flux was not high enough.

In a second study, Khodadadian et al. [51] modelled and optimized a continuous annular LED-based photocatalytic reactor for the degradation of gas phase toluene. The authors found that the optimized reactor design involves a trade-off between residence time, mass transfer limitations, and average irradiance and that a uniform irradiance profile does not necessarily translates into an optimal design when the costs of the LEDs are considered. In addition, the authors also illustrated how for a desired concentration profile along the reactor length, the LEDs are not uniformly distributed, hence, demonstrating the flexibility of LEDs to be located in a manner that allows manipulating reaction rates locally.

1.1.4. Efficiency of photocatalytic processes

To indicate the efficiency of a heterogeneous photocatalytic process, multiple terms such as quantum yield, apparent quantum yield, and photonic efficiency have been used in the literature. The term quantum yield, often called quantum efficiency, predates heterogeneous photocatalysis as it is a common term to express the efficiency in homogeneous photochemistry. In homogeneous photochemistry, quantum yield indicates the efficiency of an absorbed photon to produce a certain event. However, in heterogeneous photocatalysis, quantum yield has sometimes been used incorrectly referring to the number of photons incident on the catalyst surface [53].

Serpone et al. [53] argued that in any photoinduced process, the term quantum yield is only useful when referring to the absorbed photons. For a species C, the quantum yield Φ is defined as the number of molecules changed divided by the number of absorbed photons [15]:

$$\Phi = \frac{\pm \mathrm{d}\,[\mathrm{C}]/\mathrm{dt}}{\mathrm{d}[h\nu]_{\mathrm{abs}}/\mathrm{dt}} \tag{1.10}$$

When determining the quantum yield in semiconductor photocatalysis, a combination of the total pathway probabilities for the holes and electrons must be considered [15]. Hence, the quantum yield is directly proportional to the charge carriers transfer rate (k_{CT}) and inversely proportional to the sum of the charge transfer rate and the charge carrier recombination rate (k_{rec}) illustrated in Figure 1.2.

$$\Phi \propto \frac{k_{CT}}{k_{CT} + k_{rec}} \tag{1.11}$$

Thus, the overall quantum yield is determined by two critical processes [15, 16]:

1. the competition between charge carrier recombination (Equations 1.2 and 1.3) and trapping (Equations 1.4 to 1.6), at a time scale of picoseconds to nanoseconds
2. the competition between trapped carrier recombination (Equations 1.2 and 1.3) and interfacial charge transfer (Equations 1.7 and 1.8), at a time scale of microseconds to

milliseconds

Trapping is a process that suppresses the recombination of charge carriers. Surface and bulk irregularities occur naturally in the preparation of semiconductor photocatalysts and help prevent electron-hole recombination by trapping the charge carriers. These irregularities are associated with surface electron states which have a different energy than the bands present in the bulk semiconductor [54]. Figure 1.4 illustrates a schematic representation of the surface and bulk electron trapping together with bulk and surface recombination of charge carriers.

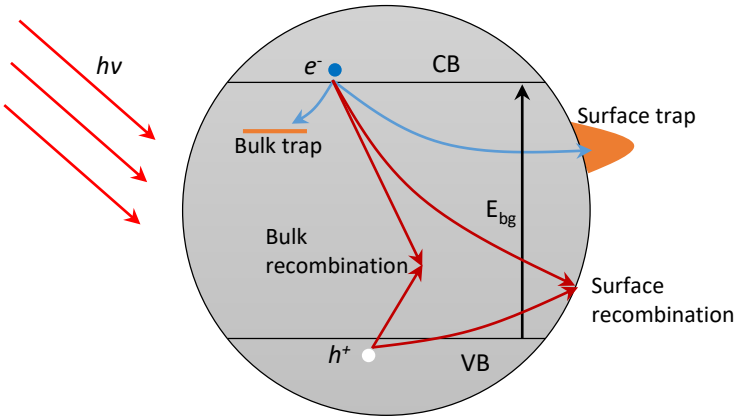

Figure 1.4: Schematic representation of surface and bulk electron carrier trapping along with bulk and surface recombination. (Based on [54] and [6]).

Overall, an increase in either the recombination lifetime of the charge carriers or the interfacial electron transfer rate constant may result in higher quantum yields [15]. When there is no electron-hole recombination, the quantum yield will have an ideal value of one [54]. Nevertheless, charge carrier recombination is always present in real systems [32], and hence the need to promote the trapping of electrons and holes for a more efficient charge transfer process.

The determination of quantum yields is experimentally difficult due to the effects of scattering, reflection, absorption, and transmission of photons. Thus, most studies calculate the photonic efficiency rather than the quantum yield. Photonic efficiency, also called *apparent* quantum yield, was a term proposed by Serpone et al. [53] to avoid further confusion with the term quantum yield used in homogeneous photochemistry. The photonic efficiency of a given reaction describes the initial rate of formation of a product or disappearance of a reactant divided by the number of photons incident on the catalyst surface. Therefore, the photonic efficiency is a lower limit of the quantum yield since the extent of light scattered or reflected is not accounted [53].

$$\zeta = \frac{\pm \mathrm{d}\,[\mathrm{C}]/\mathrm{dt}}{\mathrm{d}[h\nu]_{\mathrm{inc}}/\mathrm{dt}} \tag{1.12}$$

In a later work by Serpone et al. [55, 56], they suggested that the term photonic efficiency had little or no meaning describing process efficiencies due to the need of stipulating reactor geometry, light source, and photocatalyst properties. They proposed the term *relative* photonic efficiency, which was reactor independent and could be used to compare experiments from different studies. The relative photonic efficiency compares the photonic efficiency of a determined species to the photonic efficiency of phenol at constant incident

photon flux. Phenol was chosen as base molecule as its molecular structure is present in many organic pollutants and is degraded by an oxidative pathway rather than a reductive one.

$$\zeta_r = \frac{d[C]_{reactant}/dt}{d[C]_{phenol}/dt} \Big/ \frac{d[h\nu]_{inc}/dt}{d[h\nu]_{inc}/dt} \tag{1.13}$$

Since both initial rates are obtained under identical photon fluxes, there is no strict need to measure the photon flux and Equation 1.13 can be further simplified to:

$$\zeta_r = \frac{d[C]_{reactant}/dt}{d[C]_{phenol}/dt} \tag{1.14}$$

The work by Serpone et al. [56] also proposed a method to ultimately calculate the quantum yield. Once the relative photonic efficiency is known, it is just necessary to determine the quantum yield of phenol. Afterward, the quantum yield of the studied system can be calculated as:

$$\Phi = \zeta_r \Phi_{phenol} \tag{1.15}$$

To determine the efficiency and economic feasibility of a photocatalytic process, Bolton et al. [57] suggested the use of two figures of merit: Electric Energy per Order of Magnitude (E_{EO}) for low contaminant concentrations and Electric Energy per Unit Mass (E_{EM}) for high contaminant concentrations. These figures of merit relate the electrical energy consumption to the efficiency factors of photon absorption irrespective of the system; hence, they also allow a direct comparison among different AOPs. For example, Natarajan et al. [58] compared the E_{EO} of the photocatalytic degradation of Congo Red dye using just UV LEDs and using different synthesized TiO_2 nanotube arrays (TNA) together with UV LEDs. Their study showed over a ten-fold decrease in energy consumption in the presence of the TNA due to the generation of hydroxyl radicals.

For diluted systems (e.i. overall first-order reactions with respect to the contaminant), the required electrical energy to diminish one order of magnitude the contaminant concentration is independent of the concentration. Thus, the E_{EO} is defined as the electrical energy in kWh required to degrade a contaminant by one order of magnitude in one cubic meter of water or air and can be calculated as:

$$E_{EO} = \frac{P}{F \times \ln(c_o/c_f)} \tag{1.16}$$

where P is the rated power in kW, F is the flow rate in $m^3\ h^{-1}$, c_o and c_f are the initial and final concentrations of the contaminant in mol L^{-1}, respectively,

In contrast, for systems where the concentration of the contaminant is high (e.i. phenomenologically zero-order reactions with respect to the contaminant), the rate of contaminant removal is directly proportional to the electrical energy use. Hence, E_{EM} is defined as the electrical energy in kWh required to degrade one kilogram of contaminant:

$$E_{EM} = \frac{P \times t \times 1000}{V \times M \times 60 \times (c_o - c_f)} \tag{1.17}$$

where V is the volume in L treated in the time t in min, and M is the molecular weight of the contaminant in g mol^{-1}.

1.1.5. Enhancement of photocatalytic efficiency

To enhance the efficiency of photocatalytic processes, various methods have been investigated. One of the most reported methods in the literature is the surface modification of the catalyst. To date, the inhibition of charge-carrier recombination, the improvement of light absorption, and the enhancement of selectivity of a target product are three benefits of modifying the catalyst surface that have been widely studied [54, 59, 60]:

Metal semiconductor modification [59], composites semiconductors [61], surface sensitization [62], and transition metal doping [63] are among the methods employed to modify the surface of the catalyst. Figure 1.5 illustrates some of these examples.

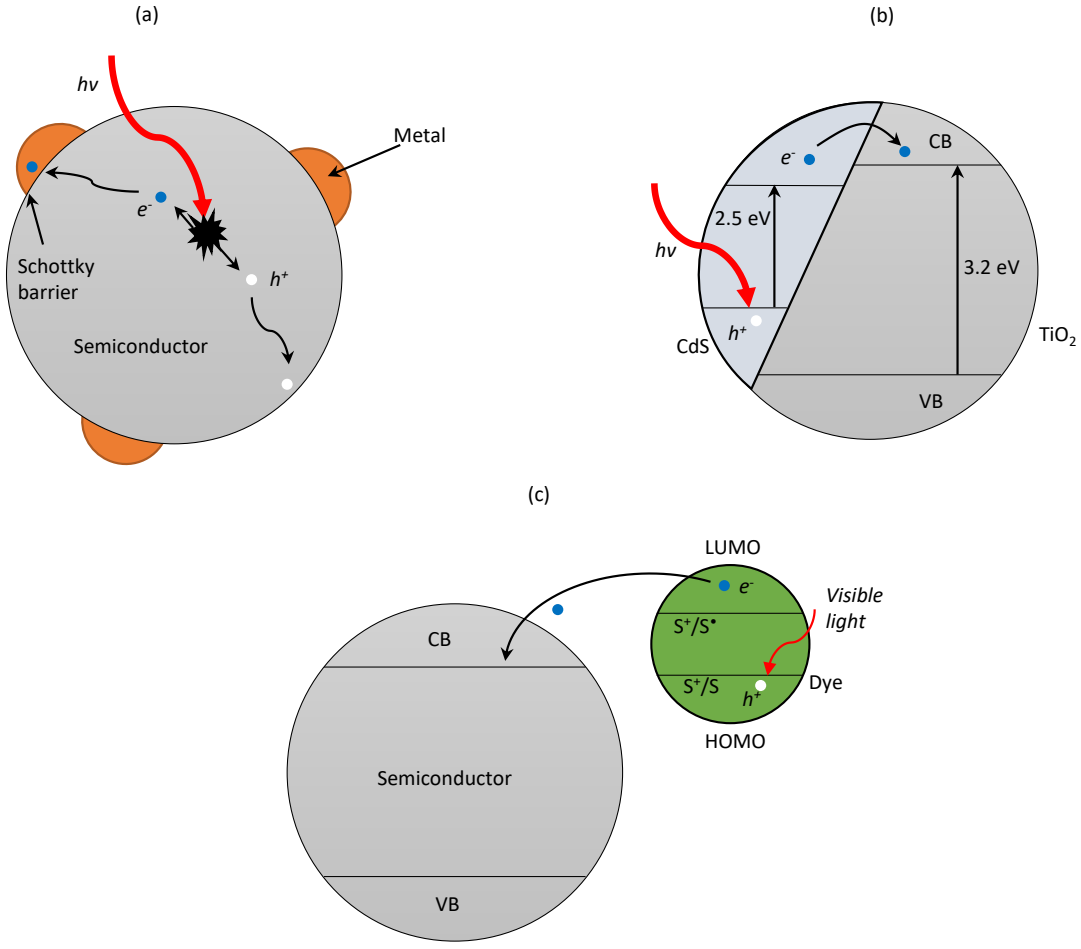

Figure 1.5: Particle surface modification to enhance the efficiency of photocatalytic processes: (a) Metal surface modified semiconductor photocatalyst (based on [54]); (b) Composite semiconductor-semiconductor (based on [54]); and (c) Dye sensitized semiconductor photocatalyst (based on [64]). CB stands for conduction band, VB for valence band, LUMO for lowest unoccupied molecular orbital, HOMO for highest occupied molecular orbital, and S for sensitizer. The Schottky barrier represents the space-charge barrier formed at the metal-semiconductor interface.

A second method to enhance photonic efficiency is the introduction of an extra electric field across the catalyst [65–68]. Electro-assisted photocatalysis is based on the fact that electrons and holes are particles with different electrical properties. When an electric field is introduced, the electrons and holes are promoted into different directions preventing their recombination and the energy bandgap of the semiconductor catalyst bends upwards or downwards depending on the electric field [68].

A third method to enhance photonic efficiency was proposed in 1993 by Sczechovski et al. [69]. The authors reported a five-fold increase in the photonic efficiency through a technique called controlled periodic illumination (CPI). CPI is based on the hypothesis that upon illumination of the photocatalyst, there is a critical time during which oxidizing species are generated. These oxidizing species react with the reactants either on the catalyst surface or in the bulk fluid. Since no photons are required for this latter step, it can take place in the dark.

Continuous illumination of the photocatalyst promotes a build-up of electron-hole pairs which consequently result in their recombination. In contrast, controlled periodic illumination may reduce the build-up of intermediates as the particles are illuminated for short intervals [69]. Nonetheless, for over two decades CPI has been a controversial subject of research as it has been both validated by initial experiments and disproved by subsequent experiments [70].

1.2. Controlled periodic illumination (CPI)

Controlled periodic illumination (CPI) is based on a series of alternate light (t_{ON}) and dark periods (t_{OFF}) as illustrated in Figure 1.6, which prevent the continuous introduction of photons.

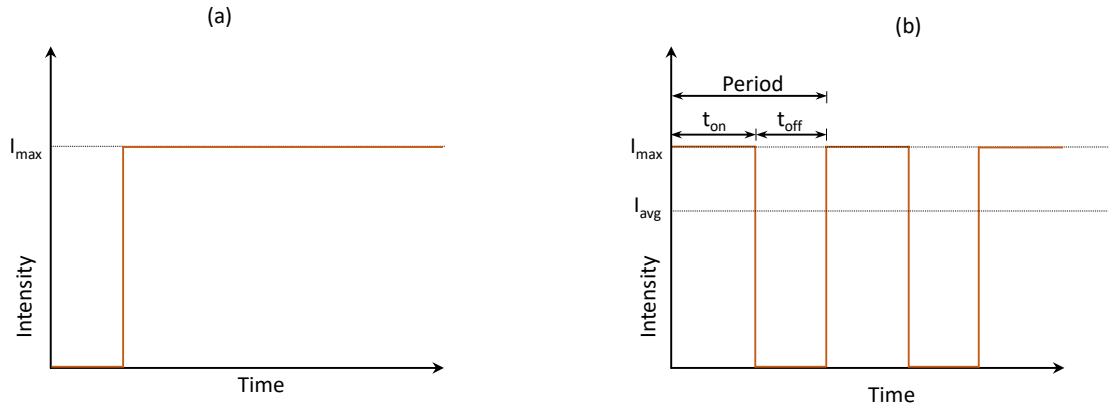

Figure 1.6: Time profile of (a) Continuous illumination; and (b) Controlled periodic illumination pulses

Generally, for CPI experiments, the main controllable parameters are the period (τ) and the duty cycle (γ). The period is the time taken for a complete light and dark time cycle:

$$\tau = t_{ON} + t_{OFF} \tag{1.18}$$

and the duty cycle refers to the fraction of the period equivalent to a light time:

$$\gamma = \frac{t_{ON}}{t_{ON} + t_{OFF}} \tag{1.19}$$

At light times, the illumination intensity is maximum (I_{max}); hence, for an experiment under CPI, the average intensity of illumination (I_{avg}) is calculated as:

$$I_{avg} = \gamma I_{max} \tag{1.20}$$

1.2.1. CPI studies in heterogeneous photocatalysis

In the early study by Sczechowski et al. [69], the authors investigated the influence of the duty cycle on the photonic efficiency of formate ions oxidation in a slurry reactor under CPI conditions. To regulate the light and dark cycles, certain sections of the photoreactor were covered by alumina foil. Their results showed a 5-fold increase in the photonic efficiency when the duty cycle decreased from a value of 1 (continuous illumination) to a value of 0.05 (with a light time of 72 milliseconds and a dark time of 1.45 seconds). They suggested that this increase in the photonic efficiency was due to a lower buildup of intermediates, which subsequently resulted in lower recombination rates; thus, favoring the oxidation of formate ions.

A later work by Sczechowski et al. [71] in 1995 used a Taylor vortex photoreactor that incorporated light and dark times via fluid mixing. This novel reactor generated the periodic illumination conditions allowing the fluorescent light bulbs to remain on continuously. This work demonstrated coinciding results with their former investigation as the photonic efficiency in the degradation of formate ion increased nearly three times under CPI compared to continuous illumination.

Stewart et al. [72] investigated both the oxidation of 1-octanol to 1-octanal and the reduction of *p*-nitroacetophenone to *p*-aminoacetophenone. The photonic efficiency of the oxidation augmented 1.8 times at longer dark times, whereas the reduction reaction showed no significant improvement. They suggested that a dark recovery time improved the photonic efficiency for oxidation processes.

In 1996, Foster et al. [73] investigated the mechanism of CPI using a rotating ring disk photoelectrochemistry. Their results demonstrated that photocatalytic reaction rates are highly dependent on both the illumination intensity and the light and dark times between periods. They also suggested that photocatalytic reactors will only show high photonic efficiencies at low light intensities, whereas high photonic efficiencies at high light intensities could only be achieved if the catalyst was illuminated periodically.

Following the experimental work by Sczechowski et al. [69], Upadyha et al. [74] performed a transient kinetic mathematical modeling of the oxidation of formate under CPI conditions. In their work, they assumed that the entire photocatalytic process took place on a single TiO_2 particle. Their model suggested that the rapid consumption of the adsorbed reactants by holes accounted for the high efficiency under CPI conditions, and that the low adsorption of oxygen, and/or electron transfer to oxygen was responsible for the low efficiency under continuous illumination.

The hypothesis by Sczechowski et al. [69] was later challenged in 1999 by Buechler et al. [75], who investigated the effect of CPI on the photodegradation of formate in a rotating disk photoreactor. To control the dark and light times of the black lamps they used a mechanical shutter. Their results showed an increase in the photonic efficiency from 5% under continuous illumination to 20% under CPI. Nonetheless, they found that at low light

intensities, CPI did not enhance photonic efficiency. They suggested that at low intensities, the observed reaction rate is controlled by the surface reaction; thus, the addition of photons increases the reaction rate. In contrast, at high light intensities, the mass transfer of oxygen to the photocatalyst surface limits the reaction. In this regime, if the dark time is long enough, the concentration of oxygen at the surface of the catalyst will equal the bulk concentration, which will result in a higher observed rate of reaction when photons are reintroduced.

Based on their previous work, Buechler et al. [76] further investigated the gaseous oxidation of trichloroethylene under CPI at kinetic- and diffusion-limited flow regimes. Their results showed that in the kinetic-limited regime the photonic efficiency was constant regardless of the illumination method used. In contrast, in the diffusion-limited regime, the photonic efficiency almost doubled when using CPI. Overall, their conclusion was that either intraparticle diffusion or mass transport of oxygen to the catalyst surface or a combination of both processes were responsible for the photonic efficiency increase under CPI conditions.

In 2001, both Buechler et al. [77] and Cornu et al. [78] investigated the photocatalytic oxidation of formate under continuous and periodic illumination. They found that a variation in the duty cycles also meant a variation in photon flux; however, previous studies did not account for that. For instance, in the study by Sczechowski et al. [69] utilizing a light time of 72 milliseconds and a dark time of 1.45 seconds meant a photon flux 21 times lower when compared continuous illumination. The results by Buechler et al. [77] and Cornu et al. [78] gave the first indication that photonic efficiency under a sufficiently high-frequency periodic illumination approached the photonic efficiency under continuous illumination at the same average absorbed photon flux. They attributed the previously reported photonic efficiency enhancement by CPI to be due to either mass transport limitations or weak adsorption in the reaction steps. Later, Cornu et al. [79] investigated the time scales of redox intermediates at different pH under periodic illumination of the degradation of methyl orange. Their results revealed two rate-determining intermediates that had different lifetimes with opposite dependence on the pH. They assumed these intermediates were the reducing and oxidizing species. At high pH, the reducing species became more reactive, while at low pH the oxidizing species became the most reactive as a result of the shift in the electrical potential of TiO_2.

The effect of pH was further investigated by Tokode et al. [80] where they showed that both pH and duty cycle affect the photodegradation of methyl orange. At low duty cycle, the photonic efficiency was greater at an acidic pH since the electrostatic attraction is higher at low pH with surface $Ti^{IV}OH^{\bullet+}$ mediated oxidation. In contrast, the photonic efficiency was lower at high pH, as the TiO_2 becomes negatively charged, giving rise to a coulombic repulsion between the adsorbed species and the catalyst surface preventing the adsorption of the species.

Chen et al. [81] were the first to study the effect of controlled periodic illumination using LEDs. LEDs present an advantage over other radiation sources for controlled periodic illumination experiments as they can be alternatively turned on and off on a millisecond scale using electronic controllers instead of complex mechanical shutters [42]. The authors studied the photodecomposition of *o*-cresol and reached a similar conclusion than Cornu et al. [79]: at equivalent average photon rates, the photonic efficiency achieved under CPI at sufficient intermittence was lower but approached those under continuous illumination.

UV LEDs were also used by Tokode et al. [82] who investigated the effect of CPI on the photonic efficiency of the degradation of methyl orange. Their results showed an increase in photonic efficiency with reducing duty cycle. They also investigated the individual effect of light and dark times. For their reactor model, the increase in photonic efficiency was mainly due to the duty cycle rather than the light or dark time, which indicated that the reaction was not limited by mass diffusion or by the adsorption or desorption of chemical species. Additionally, they reached the same conclusion as Chen et al [81] and Cornu et al. [79]: no photonic efficiency enhancement due to CPI at an average intensity equal to the maximum intensity under continuous illumination.

Hou et al. [83] investigated the decomposition of gaseous isopropanol in a tubular optical fiber reactor by UV LED under CPI conditions. Their results showed that at equivalent duty cycle, both the removal efficiency and apparent quantum yield increase with increasing frequency of periodic illumination. They concluded that the application of periodic illumination provided the opportunity to renew the active sites on the surface of the catalyst, which subsequently enhanced the decomposition rate and the overall removal efficiency and photonic efficiency.

Based on the mathematical modeling of Upadhya et al. [74], Tokode et al. [84] reproduced the results of their previous experimental study [80] theoretically. Even though they found good agreement between the experimental and modeled quantum efficiency, the modified Langmuir-Hinshelwood rate equation did not accurately predict the experimental decomposition of the dye under CPI. The modified Langmuir-Hinshelwood rate equation model was developed by Chen et al. [81], who reported good agreement between experimental and modeled reaction rates. However, the experiments by Chen et al. [81] monitored reaction rates at several concentrations but a single duty cycle, whereas the experiments from Tokode et al. [80] monitored reaction rates at a single concentration but several duty cycles. As the dependence of the adsorption and reaction constants on the UV illumination intensity is not accounted for in the modified Langmuir-Hinshelwood, it makes the model just suitable for single duty cycle data.

In 2015, Korovin et al. [85] investigated the effect of high frequency controlled periodic illumination in the photodegradation of acetone vapor. This was only the third study involving a gas phase reaction after that of Buechler et al. [76] and Hou et al. [83]. They demonstrated that photonic efficiency augments with the increase of light pulses frequency and decrease of the duty cycle. Moreover, they also reached the conclusion that photonic efficiency under CPI is always lower than that of continuous illumination at equivalent average UV light intensities and equals it when the reaction becomes photon-limited.

Xiong et al. [86] studied the decomposition of acetaminophen under controlled periodic illumination by controlling both the duty cycle and the period. By changing the period at a fixed duty cycle of 0.5, they found that the reaction rate constant decreases drastically with the increase of the period. The highest rate constant was at 20 milliseconds, whereas at periods larger than 400 milliseconds no effect was observed on either the reaction rate constant or the photonic efficiency. To explain this behavior, they suggested that the dark time could be divided into two domains. The first time domain corresponds to the time starting right from the point where the LEDs are turned off to where most of the residual hydroxyl radicals have been consumed. The second time domain corresponds to the rest of the dark time until the LEDs are turned on again. If the concentration of hydroxyl radicals is high under the first time domain, organic pollutants can still undergo a series of oxidation reactions. Hence, if the first time domain dominates the dark time, the overall reaction will be faster than if the second time domain dominates the dark time.

Zhou et al. [87] studied the photocatalytic reduction of fumarate to succinate under controlled periodic illumination on ZnS mineral surfaces. They used a 1 kW high-pressure Hg(Xe) arc lamp in combination with a mechanical shutter and optical chopper to generate illumination periods as low as 0.208 milliseconds and as high as 25 seconds. Their study suggested that for fast illumination time intervals, the photonic efficiency under periodic illumination is practically identical to the one at continuous illumination. However, as the illumination time increases, the photonic efficiency decreases. Moreover, during this time lapse, they found two inflection points associated with redox carriers with different reactivity. The first inflection point represented the overall time needed to transfer conduction band electrons to reduce fumarate to succinate, while the second inflection point characterized the loss of oxidizing valence-band holes.

In the most recent work, Ku et al. [88] studied the decomposition of dimethyl phthalate (DMP) in aqueous solution under CPI. Their results showed that at a constant irradiation time of 60 minutes, both the decomposition of DMP and photonic efficiency under periodic illumination

increased with increasing dark times. For instance, more than 80% DMC was degraded when the illumination time was 0.1 seconds and the dark time was 5 seconds, compared to 19% under continuous illumination. They associated this behavior to the enhancement of surface replenishment and the inhibition of electron-hole recombination.

Table 1.3 presents a summary of the work involving controlled periodic illumination in heterogeneous photocatalysis in chronological order. From the experimental studies presented in Table 1.3, just the work by Cornu et al. [78] and Cornu et al. [79] reported the quantum yield by measuring the absorbed photon flux. All the other investigations reported photonic efficiencies and no study reported relative photonic efficiencies. Besides reporting photonic efficiencies, the work by Chen et al. [81] and Ku et al. [88] also reported the Electric Energy per Order as a means to compare the energy saving at the same UV irradiance with continuous illumination.

Table 1.3: Bibliography of work involving CPI in heterogeneous photocatalysis

Author	Year	Study	Type/Phase
Sczechowski et al. [69]	1993	CPI hypothesis and its effect on photonic efficiency and degradation of formate	Experimental/Aqueous
Sczechowski et al. [71]	1995	CPI effect on photonic efficiency and degradation of formate	Experimental/Aqueous
Stewart et al. [72]	1995	Effect of dark recovery time on photonic efficiency	Experimental/Aqueous
Foster et al. [73]	1996	Effect of CPI on photonic efficiency and degradation of 2-methyl-1,4-hydroquinone	Experimental/Aqueous
Upadhya et al. [74]	1997	CPI transient kinetic modelling	Theoretical-modelling
Buechler et al. [76]	1999	CPI effect on photonic efficiency and degradation of trichloroethylene	Experimental/Gaseous
Buechler et al. [77]	2001	Mechanism of CPI and degradation of formate	Experimental/Aqueous
Cornu et al. [78]	2001	CPI effect on quantum yield and degradation of formate	Experimental/Aqueous
Cornu et al. [79]	2003	Effect of pH on CPI and degradation of methyl orange	Experimental/Aqueous
Wang et al. [89]	2006	Effect of CPI on photonic efficiency and formation of HCHO from methanol	Experimental/Aqueous
Chen et al. [81]	2007	CPI effect on photonic efficiency and degradation of o-cresol	Experimental/Aqueous
Tokode et al. [82]	2012	CPI effect on photonic efficiency and degradation of methyl orange	Experimental/Aqueous
Hou et al. [83]	2013	CPI effect on photonic efficiency and degradation of isopropanol	Experimental/Gaseous
Xiong et al. [90]	2013	Residual disinfection effect of CPI	Experimental/Aqueous
Tokode et al. [80]	2014	Effect of pH on photonic efficiency and degradation of methyl orange	Experimental/Aqueous
Tokode et al. [84]	2014	CPI modelling	Theoretical-modelling
Korovin et al. [85]	2015	High frequency CPI and its effect on photonic efficiency and degradation of acetone	Experimental/Gaseous
Tokode et al. [70]	2015	CPI review	Theoretical
Zhou et al. [87]	2016	Effect of high frequency on the photonic efficiency of the photocatalytic reduction of fumarate to succinate	Experimental/Aqueous
Xiong et al. [86]	2017	Effect of duty cycle and period on the photonic efficiency and decomposition of acetaminophen	Experimental/Aqueous
Ku et al. [88]	2017	Effect of light and dark time on the photonic efficiency and temporal decomposition of dimethyl phtalate	Experimental/Aqueous

1.2.2. CPI in other fields

The concept of periodic illumination has also been investigated for different purposes in other fields. For example, it has been applied to control the formation of Turing structures. Turing structures are concentration patterns formed from the instability of chemical reaction-diffusion systems [91]. For instance, Horvath et al. [92] studied the illumination of Turing structures in the chlorine-dioxide-iodine-malonic acid reaction-diffusion system. Their results showed a more effective elimination of the Turing structures under periodic illumination compared to continuous illumination with the same average light intensity.

Controlled periodic illumination has also been applied in the investigation of the individual steps and mechanism reaction in photolysis. For example, Haden et al. [93] investigated the individual steps in the chain mechanism of acetaldehyde using intermittent light in a rotating reactor at 200°C and 300°C. Based on their experiments they estimated individual rate constants and calculated the activation energies.

Finally, Xiong et al. [90] investigated the residual disinfection effect under CPI. In their work, the photocatalytic disinfection performance of an antibiotic-resistant bacteria, *Escherichia coli ATCC* 700891 was studied under different light intensities and illumination modes. Their results showed that a residual disinfecting effect was present and could kill almost all bacteria within 240 minutes of dark time after being periodically illuminated for 90 minutes. They also reported that with the same UV dosage, the log-removal of antibiotic bacteria increased with increasing frequency. To date, this is the only study aiming at investigating the effect of CPI in the inactivation of bacteria; nevertheless, this work is of high significance since it presents similar results as the initial work in heterogeneous photocatalysis under CPI.

1.3. Photocatalytic degradation of volatile organic contaminants

Volatile organic compounds (VOCs) are among the most common and harmful contaminants emitted by anthropogenic sources [94], which can be found in both urban and industrial environments. VOCs can be emitted from industrial processes such as oil and gas, paints and solvents, agriculture, firewood burning, and transportation. In addition, they can also be released from the utilization of organic-based goods such as cleaning products, furniture, paints, and building materials [94].

VOCs are primarily composed of BTEX (benzene, toluene, ethylbenzene, and *o*-xylene) and halogenated hydrocarbons [95]. Many VOCs are toxic, and some can be considered carcinogenic, mutagenic, or teratogenic [96]. Their most significant environmental problem, however, is related to the possible production of photochemical oxidants such as ozone [97]. Tropospheric ozone damages forests and crops, injures or destroys living tissue, and is implicated in the formation of acid rain [98].

In indoor spaces, VOCs have been found to be at much higher concentrations than in outdoor spaces [99]. Since people spend between 70 and 90% of their life inside, exposure to VOCs is one of the most significant risk factors for respiratory and heart diseases according to the World Health Organization (WHO) [100]. The increasing number of regulations with respect to VOCs emissions has led to increasing research to develop new efficient and sustainable air cleaning processes. Among these processes, membrane separation, adsorption, and condensation have been utilized. Although removing air pollutants efficiently, these processes just transfer the pollutants from one phase to another phase and consequently, the pollutants are not degraded.

Heterogeneous photocatalysis is regarded as one of the most attractive methods since it can completely mineralize organic pollutants to carbon dioxide and water at low temperatures. While most of the research efforts have dealt with photocatalytic reactions in the liquid phase, degradation of gaseous organic compounds has recently gained more interest, especially for

air purification applications [101]. Gas phase photocatalysis was first investigated by Dibble et al. [102] in 1992 by studying the TiO_2 photocatalytic degradation of trichloroethylene (TCE). Nonetheless, it was only until the last decade that the photocatalytic degradation of gas phase contaminants has been explored to larger extents.

In addition to the light irradiance, which effect was described previously, two of the main experimental parameters that have a significant effect in the gas-phase photocatalytic degradation of organic contaminants are the inlet concentration and relative humidity. For instance, Hennezel et al. [103] and Ao et al. [104] have reported that the reaction efficiency of BTEX compounds depends on the amount of adsorbed species on the catalyst. At higher concentrations, the ratio between available active sites and pollutant molecules is smaller, and consequently, more molecules can leave the reactor without being degraded. Additionally, the conversion of aromatic compounds, such as toluene, is more difficult than that of chlorinated hydrocarbons or alcohols [105].

The effect of water vapor in the gas phase photocatalytic degradation reaction is two-fold. In the presence of water vapor, hydroxyl radicals are formed. These hydroxyl radicals can both directly attack the VOC molecules and suppress electron-hole recombination by behaving as hole traps. However, under high concentrations of water vapor, the water molecules might compete with the contaminant on the catalyst surface sites during adsorption [106], which consequently diminishes the photocatalytic degradation rate.

Moreover, deactivation of the catalyst during the degradation of aromatic compounds is one of the major disadvantages of the photocatalytic process. Here, reaction intermediates are strongly adsorbed on the surface of the catalyst and diminish the photocatalytic activity by blocking reaction sites [107].

1.4. Gaps and Thesis objectives

As outlined in Table 1.2, LEDs possess multiple advantages compared to other radiation devices, such as having an almost instant response time and being easy to integrate in the reactor design. Therefore, the main objective of this thesis is to further explore the advantages of LED-based photocatalytic reactors to improve the energetic efficiency of the process.

For over two decades, the mechanism and the effect of controlled periodic illumination on the photonic efficiency have been a controversial subject of research. The original hypothesis by Sczechowski et al. [69] for the enhancement of photonic efficiency through CPI has been both proved by initial studies [72–74] and challenged by subsequent studies [77, 78, 81, 89]. Subsequent studies concluded that the enhancement in photonic efficiency was due to mass transfer limitations and not necessarily to a decrease in electron-hole recombination.

Moreover, the effect of controlled periodic illumination has mainly been studied in liquid-phase systems, where mass transfer limitations may be present to a higher extent when compared to gas-phase reactions. In contrast, the effect of controlled periodic illumination in gas-phase systems has rarely been reported [76, 83, 85]. Therefore, the first specific objective of this thesis is to explore the effect that controlled periodic illumination has on the photocatalytic degradation of gaseous toluene. Several questions arise when trying to determine the effect of controlled periodic illumination, such as:

1. What is the effect of the duty cycle on the degradation of toluene? And what is its effect on the photonic efficiency?
2. What is the effect of the period on the degradation of toluene? And what is its effect on the photonic efficiency?
3. How does the effect of controlled periodic illumination compare to the effect of

continuous illumination under equivalent light irradiance?

4. How does the effect of controlled periodic illumination under a kinetic-limited reaction compare to the effect under a mass transfer-limited reaction?

In addition to having almost immediate response time, thus, allowing for periodic illumination experiments without the need of complex designs, LEDs can be easily incorporated in the reactor design. Even though the optimization of LED-based reactors has received little attention, a previous study by Khodadadian et al. [51] illustrated how LEDs can be flexibly positioned along the reactor length to control the reaction rate locally. Hence, the second specific objective of this work further elaborates on the study by Khodadadian et al. [51] by exploring the effect of different illumination profiles along the photoreactor length to optimize the light irradiance for a determined goal. The LED array within the photoreactor in this experimental work is evenly divided into five sections, each one of which controlled with a different power supply. Thus, allowing to have different light irradiance in each section. To determine the effect of different irradiance profiles along the reactor, the following questions are proposed:

1. What is the effect of varying the irradiance in a step-wise increase from the inlet to the outlet of the reactor when compared to uniform illumination?
2. What is the effect of varying the irradiance in a step-wise decrease from the inlet to the outlet of the reactor when compared to uniform illumination?
3. How is the effect of following a step-wise increase or decrease illumination profile compared to uniform illumination at the same average irradiance?
4. What is the optimal illumination profile for a determined toluene conversion?

Finally, the third specific objective of this thesis is to develop the process control of the system. Among the BTEX compounds, toluene is one of eight representative indoor VOCs by a proposed ASHRAE (American Society of Heating, Refrigerating and Air-Conditioning Engineers) test method for determining the effectiveness of gas-phase air filtration equipment [108]. Nevertheless, catalyst deactivation is a common observed phenomena in the photocatalytic degradation of toluene [105, 109]. Catalyst deactivation is mainly a function of the catalyst used [110] and the experimental conditions, such as relative humidity and toluene inlet concentration [111–114]. Changes in the experimental conditions may have either a positive or negative effect in the overall toluene conversion. Therefore, the development of the process control is of two-fold importance: (1) to meet the environmental regulations in case there is a disturbance that has a negative effect in the conversion; and (2) to save energy in case there is a disturbance that has a positive effect in the conversion. Furthermore, to the best knowledge of the author, there has not been any previous studies about the process control of photocatalytic reactors. To develop the process control, the following research questions need to be answered:

1. How is the dynamic response of the system to changes in the light irradiance?
2. How is the dynamic response of the system to perturbations, such as relative humidity and toluene inlet concentration?
3. How is the process behavior when a controller is implemented with and without perturbations?

1.5. Thesis Outline

This thesis consists of four Chapters and four Appendixes. Chapter 2 presents the experimental procedures and the reactor modelling. Here, both the photoreactor and the experimental set-up are first described in detail. Afterward, the experimental settings for the controlled periodic illumination, radiation profile, and process control are shown. Chapter 2 ends with the description of the reactor model and efficiency parameters.

Chapter 3 presents and discusses the results for the controlled periodic illumination, radiation profile, and process control experiments. In the controlled periodic illumination results, the effect of the duty cycle and the frequency are presented. Afterward, the effect of following different radiation profiles is shown both experimentally and mathematically. In the process control, first a sensitivity analysis regarding light irradiance, relative humidity, and toluene inlet concentration are presented. Later, the controller is designed and further validated experimentally. Finally, in Chapter 4, the most important outcomes and possible future work regarding this thesis are presented.

Appendix A describes the notation used throughout this thesis. Appendix B shows some photos regarding the experimental set-up. Appendix C presents the Matlab code used to model the system by following different radiation profiles. Appendix D builds up on the model shown in Appendix C to optimize the irradiance within the reactor. Finally, Appendix E illustrates an example of the Simulink block diagram used to simulate the process controller.

2

Experimental procedures and Reactor Modelling

2.1. Photoreactor configuration

Figure 2.1 presents a schematic representation of the LED-based annular photoreactor used in this study. The photoreactor consists of three concentric tubes. The first tube, with radius r_2 of 2.5cm, is the external tube where the TiO_2 photocatalyst (Degussa Evonik P25) is deposited on its inner wall.

The second tube, with radius r_1 of 2cm, is a transparent tube which allows the gases to flow without reaching the LED array. The last tube, with radius r_0 of 0.8cm, is where the LED array is allocated. The LED array is composed by a matrix of 40 axial by 6 radial LEDs evenly distributed over a 60-centimeter long reactor, to give a total of 240 LEDs.

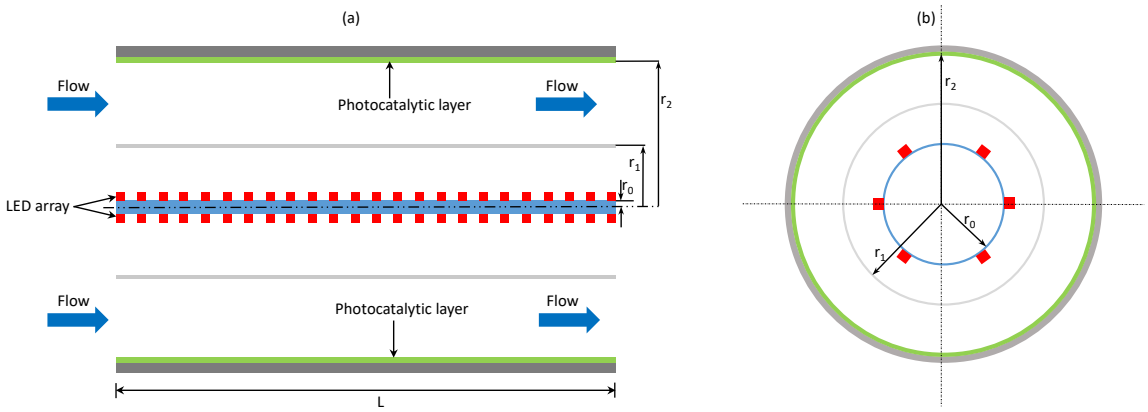

Figure 2.1: Schematic representation of the LED photocatalytic annular reactor: (a) Side view; (b) Cross-sectional view

2.2. UV-LED control unit

The irradiance of the LEDs (Nichia NSSU100CT) was controlled with LabView 2015 with five different power supplies (Aim TTi model PLH120-P), each one of which controlling a matrix of 8 axial by 6 radial LEDs. Having an independent power supply for each reactor section allows not only to have different irradiation per section but also gives more flexibility to vary the volumetric flow rate while maintaining similar residence time. Figure 2.2 illustrates the LEDs radiation spectrum, which has a peak wavelength at 365 nm.

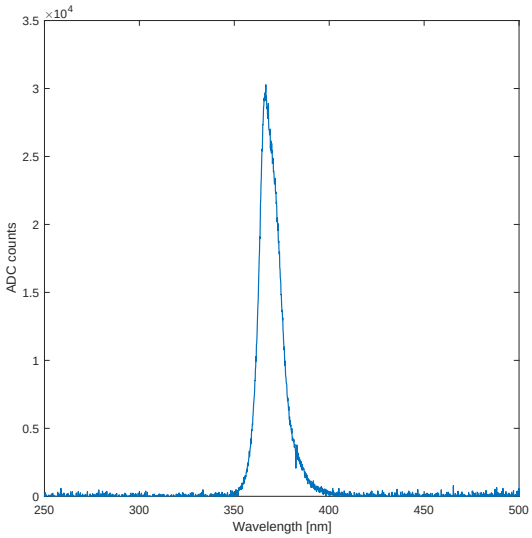

Figure 2.2: LEDs spectrum obtained with the spectrometer ULS-2048 Avantes Starline

The initial setup of the power supplies could not achieve fast switching on and off since the power supplies had an output capacitor which needed to be drained. Therefore, a short-circuit box was required to diminish the relaxation time of the LEDs. This short-circuit box when switched on, connected a 10 Ohm resistor in parallel with the LEDs and the switching on and off was controlled through the NI DAQ (National Instruments). Moreover, the current was measured through a 1 Ohm resistor over which the voltage was measured using a voltage divider circuit. Figure 2.3 compares the pulses achieved under the initial system and under the modified system.

(a) (b)

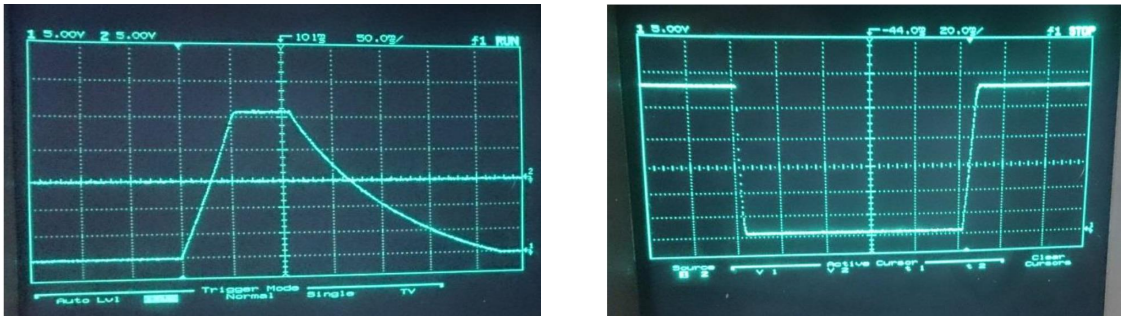

Figure 2.3: Comparison of the light pulses at: (a) Initial setup; and (b) System with short-circuit box

2.3. Experimental Operation

2.3.1. Experimental Setup

Figure 2.4 presents a schematic of the experimental system, which was controlled with Labview 2015. Here, MFC stands for mass flow controller, CEM for controlled evaporator mixer, GC for gas chromatograph, and MFM for mass flow meter. The mass flow controllers used to control the flow of toluene (MFC-18) and water (MFC-11) were Bronkhorst μFLOW series L01, whereas the ones used to control the flows of nitrogen (MFC-12, MFC-13, MFC-14) and oxygen (MFC-15, MFC-16, MFC-17) were Bronkhorst EL-FLOW Model F-201 CV.

The flow of water was directed towards CEM-1 (Bronkhorst CEM Model W202-A), set at a temperature of 50°C, where it was evaporated and mixed with nitrogen (MFC-12) and oxygen (MFC-16). Both the flow of nitrogen from MFC-14 and of oxygen from MFC-15 represent dilution lines. The flow of toluene (Sigma Aldrich anhydrous 99.8%) was directed towards CEM-2 (Bronkhorst CEM Model W202-A), set at a temperature of 40°C, where it was evaporated and mixed with nitrogen from MFC-13. The flow of oxygen from MFC-14 was always set to zero for safety reasons. The flows coming from both CEM-1 and CEM-2 were mixed before entering the photocatalytic reactor. The back-pressure regulator (Bronkhorst EL PRESS P-602CV) was always set at a pressure of 1.1 bar.

Furthermore, relative humidity, pressure, and temperature were monitored before the reactor. Both relative humidity and temperature were monitored with a transmitter (E+E Elektronik model EE210), whereas the pressure was monitored with a pressure meter (Bronkhorst EL PRESS P-602CV). The reactor was maintained isothermally at 30°C with a water jacket (Lauda ECO Silver RE 415) and compressed air was used as cooling fluid to prevent the LEDs from overheating. Finally, the concentrations were analyzed with a gas chromatograph system (Agilent Technologies model 7890B). The gas chromatograph was equipped with two flame ionization detectors (FID) and two thermal conductivity detectors (TCD). The role of the TCD detectors was to measure inert gasses (i.e. nitrogen and oxygen) and carbon dioxide, while the FID detectors measured the hydrocarbons.

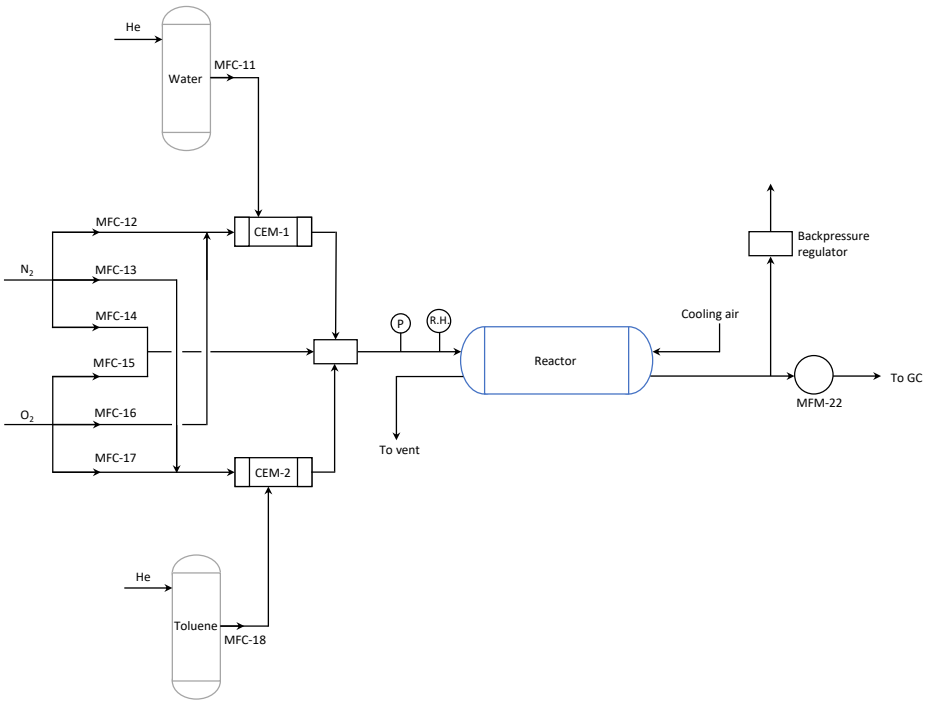

Figure 2.4: Schematic representation of the experimental system

2.3.2. Degradation under continuous illumination and controlled periodic illumination

For all experiments, the flow was first bypassed from the reactor to reach stable concentrations. Once stable concentrations were achieved, the reactor was purged allowing time for the dark reaction to take place and for the concentration of toluene to remain stable between 40 and 60 minutes. After the reactor was purged, the photocatalytic degradation was performed for two hours with the first GC analysis at a time of 6 minutes. Once the photocatalytic degradation was performed, the catalyst was regenerated by setting the flow of toluene to zero and irradiating the catalyst until the concentration of carbon dioxide was minimal.

Multiple experiments were performed to determine the effect of controlled periodic illumination under a kinetic-limited regime. Table 2.1 presents the operational conditions.

Table 2.1: Settings for the continuous and controlled periodic illumination experimental conditions under a volumetric flow rate of 1411 ml/min

Settings	Value
Toluene [mg/h] - MFC-18	10
Toluene concentration [ppmv]	29.3
Nitrogen [mln/min] - MFC-12	610
Nitrogen [mln/min] - MFC-13	50
Nitrogen [mln/min] - MFC-14	425
Oxygen [mln/min] - MFC-16	303
Water [mg/h] - MFC-11	1100
Relative humidity [%]	42.8
Volumetric flow rate [ml/min]	1144
Residence time [s]	18.03
Reynolds [-]	17.03

In the first set of experiments, the effect of duty cycle on the degradation of toluene and photonic efficiency was explored. The effect of the duty cycle was explored at two different periods: 0.5 and 1 second; where the illumination and dark times were varied accordingly with increasing duty cycle from 0.2 to 0.8. Afterward, a series of experiments under continuous illumination at equal average light irradiance were performed to compare the effect of controlled periodic illumination with continuous illumination. Figure 2.5 presents the average power consumption at each light irradiance under continuous illumination.

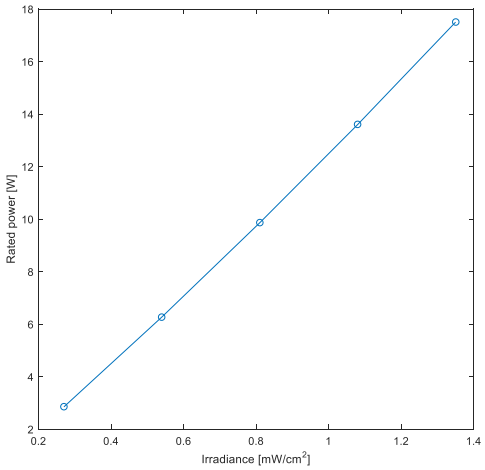

Figure 2.5: Power consumption under continuous illumination based on incident irradiance. Voltage set-point: 30V

Finally, the effect of period was explored at a fixed duty cycle of 0.5. Figure 2.6 illustrates a comparison of the illumination pulses at four different periods generated under a maximum power output of 17.5 Watts. From Figure 2.6, it is clear that there is a relaxation time for the LEDs to turn on and reach the maximum power and to turn off again. It is noted that for high periods (low frequency), the pulses are almost rectangular, whereas at for low periods (high frequency), the error is higher. In addition, at a period of 40 milliseconds, the pulse is no longer rectangular. Therefore, the final set of experiments were performed at three low periods: 50, 100, and 200 milliseconds, and one high period of 10 seconds.

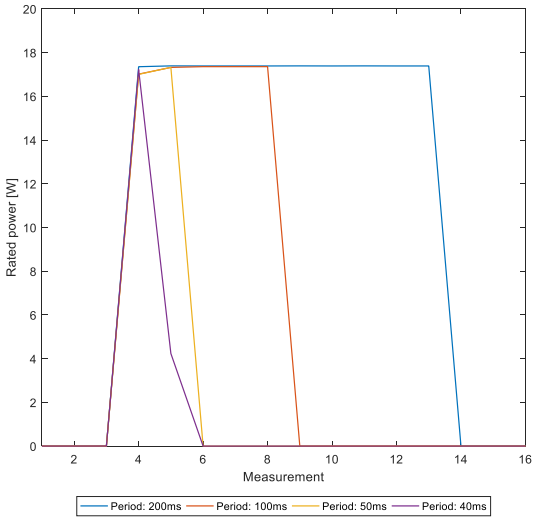

Figure 2.6: Comparison of the light pulses at different periods. All light pulses were generated at a duty cycle of 0.5 and at a maximum power of 17.5 Watts. The power output was measured every 10 milliseconds.

The photocatalytic degradation of toluene was also performed at two different lower volumetric flow rates to determine the diffusion-limited regime. Table 2.2 presents the operational settings for each experiment. For all volumetric flow rates, the concentration of toluene was maintained around 30 ppmv, the relative humidity around 43% and the residence time around 18 seconds. To avoid having higher residence time due to a lower volumetric flow rate, for the flow of 1134 ml/min, just four out of five parts of the reactor were irradiated. Likewise, for the flow of 854 ml/min, just three out of five parts of the reactor

were irradiated.

Table 2.2: Settings for the experimental conditions to achieve volumetric flow rates of 1134 and 854 ml/min

Settings	Value	
Toluene [mg/h] - MFC-18	8	6
Toluene concentration [ppmv]	29.2	29.1
Nitrogen [mln/min] - MFC-12	610	600
Nitrogen [mln/min] - MFC-13	50	50
Nitrogen [mln/min] - MFC-14	200	0
Oxygen [mln/min] - MFC-16	255	190
Water [mg/h] - MFC-11	850	660
Relative humidity [%]	42.6	41.8
Volumetric flow rate [ml/min]	1133	854
Residence time [s]	18.04	18.00
Reynolds [-]	13.69	10.32

2.3.3. Degradation under different radiation profiles

Two different radiation profiles were experimentally tested at three different average irradiance. In the first radiation profile, a step-wise increase in the irradiance was followed from inlet to outlet of the reactor, whereas in the second profile, a step-wise decrease was followed. Table 2.3 presents the radiation conditions for these experiments, where Section 1 represents the inlet of the reactor and Section 5 represents the outlet of the reactor.

Table 2.3: Illumination conditions per section of reactor following different radiation profiles. Section 1 represents the inlet of the reactor, whereas Section 5 represents the outlet

	Irradiance [mW/cm^2]					
Case	Section 1	Section 2	Section 3	Section 4	Section 5	Average
A	0.27	0.54	0.81	1.08	1.35	0.81
	0.675	0.844	1.012	1.181	1.35	1.012
	1.08	1.147	1.215	1.282	1.35	1.21
B	1.35	1.08	0.81	0.54	0.27	0.81
	1.35	1.18	1.012	0.844	0.675	1.012
	1.35	1.282	1.215	1.147	1.08	1.21

In addition to the experiments presented in Table 2.3, the mathematical modelling of the reactor divided in five sections was performed. Five reactors in series were modelled where the outlet concentration of the previous reactor was the inlet concentration of the next reactor. The mathematical modelling of the reactor is further elaborated in Section 2.4.

2.3.4. Process Control

The final goal of this thesis was to develop the process control system for the incident irradiation with disturbances in relative humidity and inlet toluene concentration in order to maintain a determined conversion set-point. To achieve this, an irradiation step, a relative humidity step, and an toluene concentration step were introduced to the system and the dynamic response was analyzed. Since the concentrations are analyzed with a gas chromatograph and the retention time of toluene is around 12 minutes, the dynamic response of the system cannot be monitored in-line. Hence, multiple experiments were performed at the same step input with different injection times to the gas chromatograph. In addition,

the experimental conditions were chosen so that there would be a certain degree of catalyst deactivation as perturbation in the system. Table 2.4 presents the experimental conditions for the process control experiments.

Table 2.4: Process control experimental conditions and settings

Settings	Value
Toluene [mg/h] - MFC-18	10
Toluene concentration [ppmv]	40.3
Nitrogen [mln/min] - MFC-12	610
Nitrogen [mln/min] - MFC-13	50
Nitrogen [mln/min] - MFC-14	120
Oxygen [mln/min] - MFC-16	230
Water [mg/h] - MFC-11	750
Relative humidity [%]	40
Volumetric flow rate [ml/min]	1026
Residence time [s]	24.8
Reynolds [-]	12.4

For the irradiance step, the irradiance was changed from 50% of the maximum value (13.5 W/m^2) to 75% and from 50% to 100%. For the relative humidity step, the water flow was changed from 750 mg/h (40.3% relative humidity) to 1100 mg/h (58.4% relative humidity). Finally, for the inlet concentration step, the toluene mass flow was changed from 10 mg/h (40.3 ppm) to 13 mg/h (52.5 ppm). All steps were made at 146 minutes of photocatalytic reaction.

2.4. Reactor Model

2.4.1. Transport and Kinetics Model

The material balance for the concentration of toluene in cylindrical coordinates along the photoreactor assuming steady state and that convection in the axial direction and diffusion in the radial direction are the dominant mass transfer mechanisms is given by Equation 2.1:

$$D\frac{1}{r}\frac{\partial}{\partial r}\left(r\frac{\partial C\,(r,z)}{\partial r}\right)-u\,(r)\left(\frac{\partial C\,(r,z)}{\partial z}\right)=0 \tag{2.1}$$

Where C is the concentration of toluene (mol/m^3), D is the diffusion coefficient of toluene in the gas mixture (m^2/s), and $u(r)$ is the fully developed laminar flow velocity profile in an annulus (m/s).

By solving the continuity equation and momentum balance for a fully developed laminar flow in an annulus, the velocity profile in Equation 2.1 is described by [51]:

$$u\,(r)=2\frac{Q}{\pi {r_2}^2}\frac{\ln\left(\frac{r_1}{r_2}\right)}{\left[\left(1-\left(\frac{r_1}{r_2}\right)^4\right)\ln\left(\frac{r_1}{r_2}\right)+\left(1-\left(\frac{r_1}{r_2}\right)^2\right)^2\right]}\left(1-\left(\frac{r}{r_2}\right)^2-\frac{\left[1-\left(\frac{r_1}{r_2}\right)^2\right]}{\ln\left(\frac{r_1}{r_2}\right)}\right)\ln\left(\frac{r}{r_2}\right) \tag{2.2}$$

Where $u(r)$ is the velocity of the gas (m/s), Q is the volumetric flow rate (m^3/s), and r_1 and r_2 are the middle transparent tube and outer tube radius (m), respectively.

Considering that the chemical reaction occurs only at the catalyst surface, the boundary conditions to solve Equation 2.1 are:

$$D\left(\frac{\partial C\,(r_2,z)}{\partial r}\right) = -R \tag{2.3}$$

$$\frac{\partial C\,(r_1,z)}{\partial r} = 0 \tag{2.4}$$

while the initial condition is:

$$C\,(r,0) = C_{in} \tag{2.5}$$

where R is the degradation rate of toluene (mol/(m^{2}s)) and C_{in} is the concentration of toluene at the inlet of the reactor (mol/m^3).

The heterogeneous photocatalytic reactions often follow Langmuir Hinshelwood kinetics [42, 70]. Assuming constant water vapor composition, the reaction rate can be described by Equation 2.6 [51]:

$$-R\,(r_2,z) = I^{\beta}\frac{kKC\,(r_2,z)}{1+KC\,(r_2,z)} \tag{2.6}$$

where I is the incident irradiance (W/m^2), β is the reaction order with respect to UV light, k is the reaction rate constant, and K is the adsorption constant of toluene.

The average concentration of toluene at the reactor outlet and the average conversion are given by Equations 2.7 and 2.8, respectively [51, 115]:

$$C_{out} = \frac{\int_{r_1}^{r_2} C\,(r,L)\,u\,(r)\,r dr}{\int_{r_1}^{r_2} u\,(r)\,r dr} \tag{2.7}$$

$$X = 1 - \frac{C_{out}}{C_{in}} \tag{2.8}$$

where C_{out} is the average concentration at the outlet (mol/m^3), X is the average toluene conversion, and L is the reactor length (m).

Based on the full degradation reaction of toluene to carbon dioxide and water:

$$C_7H_{8(g)} + 9O_{2(g)} \rightarrow 4H_2O_{(l)} + 7CO_{2(g)} \tag{2.9}$$

the mineralization of toluene can be calculated as the ratio of carbon dioxide detected by the gas chromatograph and the theoretical carbon dioxide given by Equation 2.9:

$$Mineralization = \frac{[CO_2]_{measured}}{[CO_2]_{theoretical}} = \frac{[CO_2]_{measured}}{7\,(X)\,(C_{in})} \tag{2.10}$$

For controlled periodic illumination, Equation 2.6 may be expressed by [81]:

$$-R\left(r_2,z\right)=\left(\gamma I_{\max}\right)^{\beta}\frac{kKC\left(r_2,z\right)}{1+KC\left(r_2,z\right)} \tag{2.11}$$

where γ is the duty cycle and $I_{\max}$ is the maximum incident irradiance (W/m^2).

Table 2.5 presents the kinetic parameters for the photocatalytic degradation of toluene estimated in a previous study by Khodadadian et al. [51].

Table 2.5: Estimated kinetic parameters for the photocatalytic degradation of toluene

Parameter	Value	Units
k	1.64E-7	mol m s^{-1} $W^{-0.5}$
K	692	m^3 mol^{-1}
β	0.5	-

2.4.2. Photonic Efficiency

The photonic efficiency is the ratio between the reaction rate and the incident photon flux [83]:

$$\zeta=\frac{-R}{d[hv]_{inc}/dt} \tag{2.12}$$

where $d[hv]_{inc}/dt$ represents the incident molar flow of photons (mol/s).

The reaction rate term in Equation 2.12 was calculated based on the mass balance of toluene [81]:

$$-R=Q\left(C_{in}-C_{out}\right) \tag{2.13}$$

Considering the good monochromaticity of the UV LEDs, the molar flow of photons was estimated based on 365 nm irradiation (see Figure 2.2). Thus, the energy of one photon at 365nm is given by Equation 2.14:

$$E=\frac{hc}{\lambda} \tag{2.14}$$

where E is the energy of a photon in J, h is Planck's constant with a value of 6.626×10^{-34} J s, c is the speed of light with a value of 2.998×10^{8} m/s, and λ is the peak wavelength in m.

The number of photons per second incident on the catalyst film is then computed as:

$$N_{photons}=\frac{I_{avg}A_s}{E} \tag{2.15}$$

where A_s is the catalyst area (m^2).

Finally, multiplying the result from Equation 2.15 by Avogadro's number gives the molar flow of photons:

$$\frac{d[hv]_{inc}}{dt} = 6.022 \times 10^{23} \cdot N_{photons} \tag{2.16}$$

2.4.3. Electric Energy per Order

In Chapter 1.1.4, it was described how Bolton et al. [57] suggested the use of two Figures of Merit to determine the efficiency and economic feasibility of photocatalytic processes. Since the photocatalytic degradation of toluene is performed on a diluted system (concentration of toluene around 30 ppmv), the proper Figure of Merit to compare the energy consumption under continuous and controlled periodic illumination is Electric Energy per Order E_{EO}.

The E_{EO} is therefore defined as the electrical energy required to degrade the concentration of toluene in the inlet volumetric flow rate by one order of magnitude, which can be calculated with Equation 2.17:

$$E_{EO} = \frac{P}{F \ln\left(\frac{C_{in}}{C_{out}}\right)} \tag{2.17}$$

where P is the rated power (W), F is the flow rate (L/h), and C_{in} and C_{out} are the initial and final concentrations of toluene (ppmv), respectively.

2.4.4. Five-Section Reactor Model

The reactor model was developed in a previous investigation [51] in Matlab; hence, the model was adapted to satisfy the conditions of five different irradiation values within the reactor length. The system was modeled as five different reactors in series, each one of them having a length of 0.12 meters, and where the outlet concentration of the previous reactor is the inlet concentration of the following reactor. Figure 2.7 illustrates a schematic representation of the model.

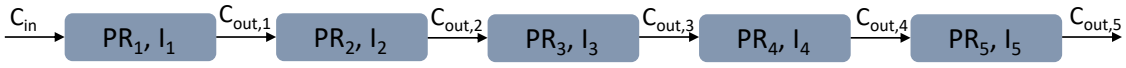

Figure 2.7: Schematic representation of the system of five photocatalytic reactors in series. PR_i stands for each photocatalytic reactor and I_i stands for the irradiance in each reactor.

Just the outlet concentration of reactor 5 was averaged along the radius to compute the final conversion. The Matlab code to model the system of five photocatalytic reactors in series is presented in Appendix C.

Moreover, one optimization case (P_1) was performed to further look at the effect of following different irradiation profiles along the reactor length. The optimization problem was a multiobjective optimization, where both the average outlet concentration of toluene and the sum of the irradiance of all the five reactors were to be minimized.

$$P_1 = \begin{cases} \min \bar{C}_{out,5}\,(I_i) \\ \min \sum_{i=1}^{5} I_i \\ 0 \leqslant I_i \leqslant 13.5 \end{cases} \tag{2.18}$$

The optimization problem was solved using Matlab 2016b. P_1 is subject to the minimization of two objective functions; thus, a genetic algorithm approach was followed since it supports multiple objectives. A genetic algorithm is a method to solve constrained and unconstrained optimization problems based on a natural selection process that mimics biological evolution. A Pareto plot of both objective functions was generated with a function tolerance stopping criteria of 1E-4. The Matlab code for the optimization problem is presented in Appendix D.

3

Results and Discussion

3.1. Effect of controlled periodic illumination

3.1.1. Effect of duty cycle

Figure 3.1 illustrates the average degradation of toluene under both continuous and periodic illumination. Here, it is clearly seen that for controlled periodic illumination, as the duty cycle increases, so does the degradation of toluene since the incident irradiance increases as well. For instance, for a period of 1 second, the average degradation at a duty cycle of 0.2 is 16%, whereas under continuous illumination at an incident irradiance of 1.35 mW/cm^2, the average degradation is of 46%. It is also noted that under these flow conditions, the degradation of toluene is statistically the same for both periods under controlled periodic illumination and for continuous illumination.

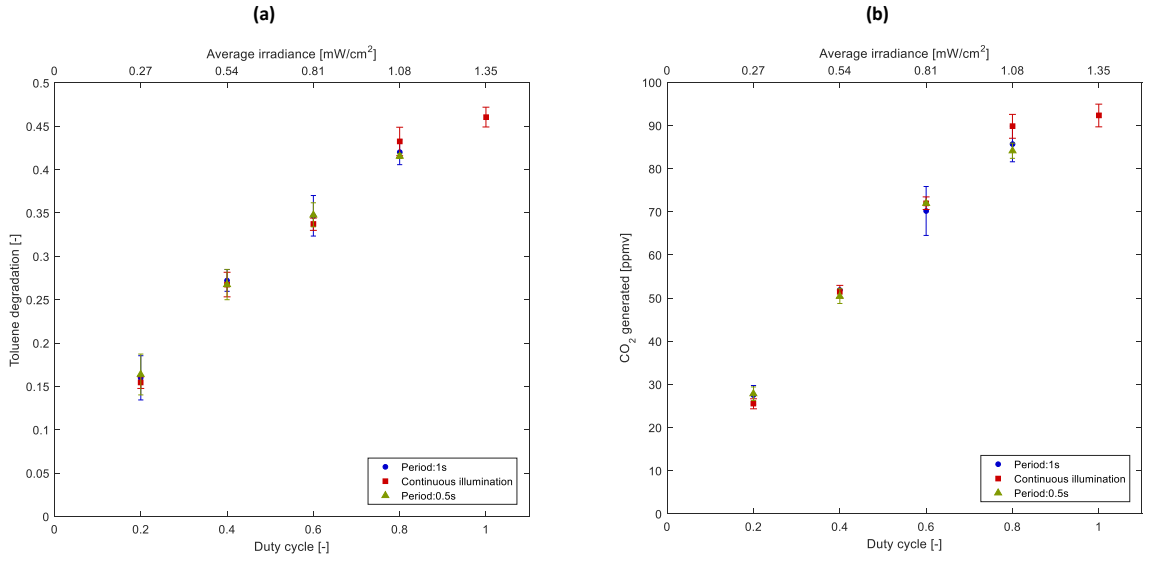

Figure 3.1: Effect of duty cycle on (a) Photodegradation of toluene under continuous and periodic illumination; and (b) Generation of carbon dioxide. Volumetric flow rate: 1411 ml/min; Initial concentration of toluene: 29.5 ± 2 ppmv; Relative humidity: 43%; Maximum incident irradiance: 1.35 mW/cm^2; Maximum average power consumption: 17.5 W; Error bars: confidence interval of 95%

Figure 3.2 presents the parity plot between the toluene degradation values obtained experimentally under controlled periodic illumination and continuous illumination and the predicted values obtained with the mathematical model described in Chapter 2.4. Even though there is a slightly higher deviation at lower irradiance, the experimental values are in good agreement with those predicted by the model. Since there is good agreement between the predicted and experimental values, it can thus be concluded that the reaction rate model proposed by Chen et al. [81] describes accurately the degradation of toluene under controlled periodic illumination conditions. In the aforementioned reaction rate model, the average incident irradiance is correlated to the duty cycle and the maximum incident as described with Equation 2.4.1.

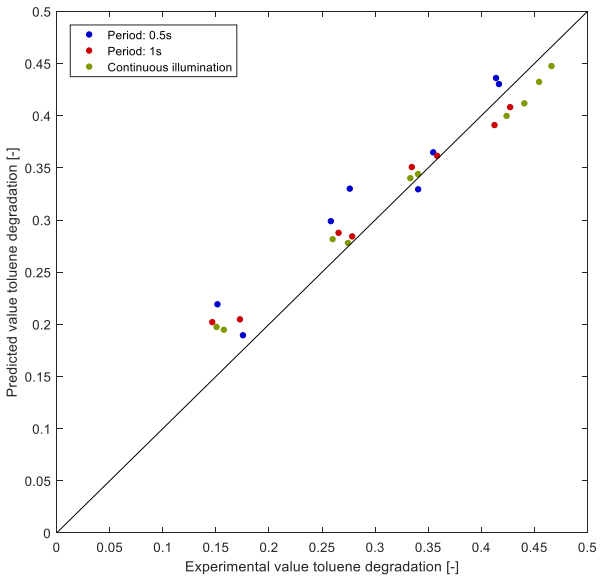

Figure 3.2: Parity plot for all experimental and predicted toluene degradation values for controlled periodic illumination and continuous illumination. No error bars are shown since the duplicate is also plotted.

Furthermore, Figure 3.3 illustrates three different efficiency curves comparing the degradation of toluene under continuous illumination and controlled periodic illumination at both periods. Figure 3.3(a) shows the degradation of toluene normalized by the rated power, Figure 3.3(b) presents the photonic efficiency computed with Equation 2.12, and Figure 3.3(c) illustrates the Electric Energy per Order of Magnitude computed with Equation 2.17.

Both Figures 3.3(a) and (b) present a similar profile since the incident photon flux has a linear relationship with the rated power. Since the illumination conditions had no significant effect on the degradation of toluene, there is also no significant difference in the results between continuous illumination and periodic illumination in Figure 3.3. Both the degradation normalized by the rated power and the photonic efficiency have a significant decrease with increasing average incident irradiance. For instance, for an incident irradiance of 0.27 mW/cm^2 under continuous illumination, the photonic efficiency was 0.65%, whereas it was 0.35% at the maximum incident irradiance. This corresponds to almost a two-fold increase in the photonic efficiency.

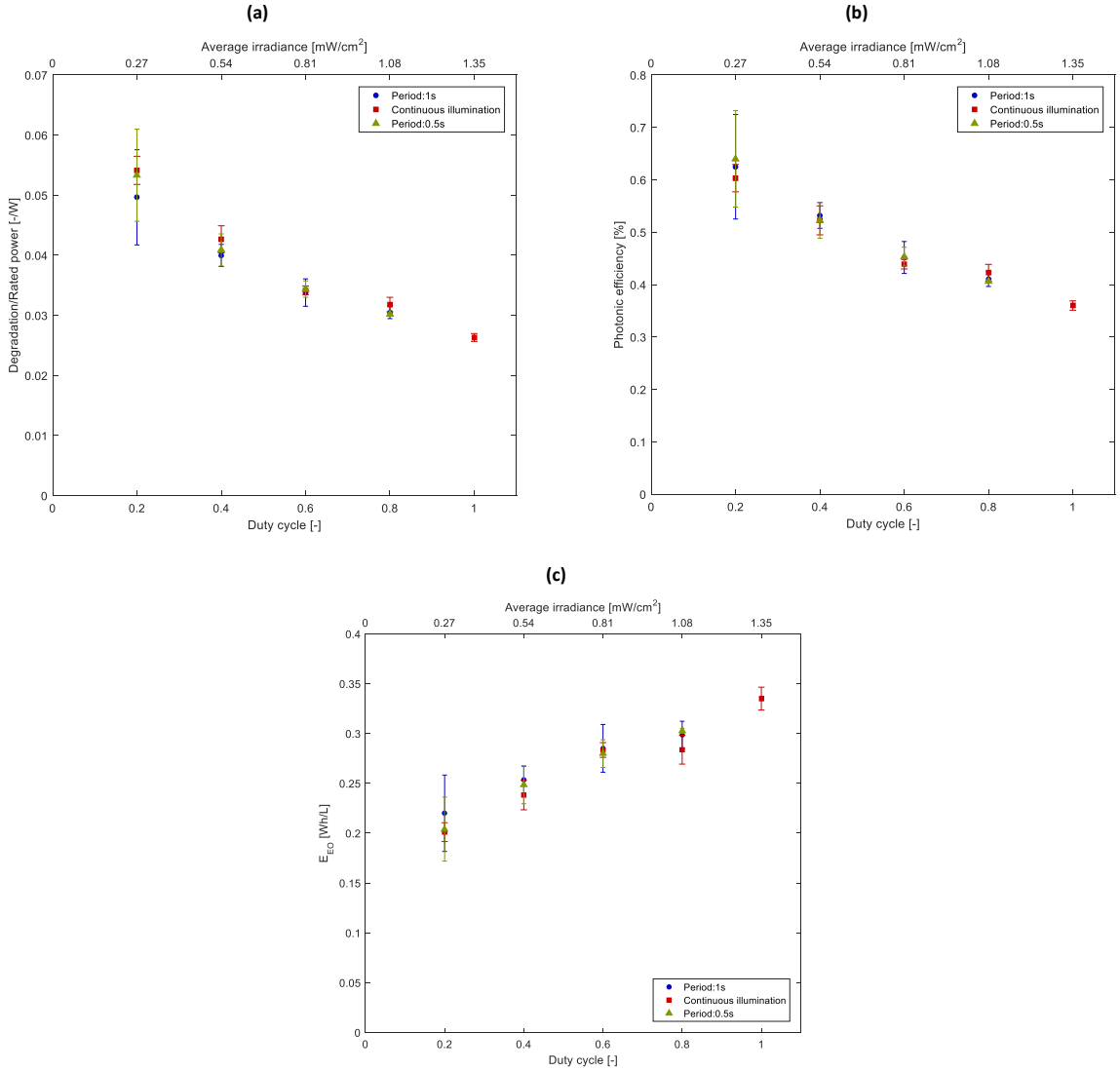

Figure 3.3: Effect of duty cycle on (a) Photodegradation of toluene normalized by the average rated power; (b) Photonic efficiency; and (c) Electric Energy per Order of Magnitude under continuous and periodic illumination. Volumetric flow rate: 1411 ml/min; Initial concentration of toluene: 29.5 ± 2 ppmv; Relative humidity: 43%; Maximum incident irradiance: 1.35 mW/cm^2; Maximum average power consumption: 17.5 W; Error bars: confidence interval of 95%

The enhancement in the photonic efficiency seen in Figure 3.3(b) is ascribed to the decreasing of electron-hole recombination, not due to the illumination conditions since there is no difference between periodic illumination and continuous illumination, but rather to the irradiance-reaction rate dependency. The reaction rate has a linear dependence with the photon flux at low irradiance, whereas at high irradiance, the dependence becomes square-root. These results are consistent with those of Buechler et al. [76], Buechler et al. [75], and Tokode et al. [82], which showed that under a kinetically-controlled regime, controlled periodic illumination did not enhance the photonic efficiency when compared to continuous illumination.

Additionally, Figure 3.3(c) illustrates the inverse profile from (a) and (b): as the incident irradiance increases, the energy required to degrade one order of magnitude the concentration of toluene increases as well. For example, under continuous illumination at an incident irradiance of 0.27 mW/cm^2, the E_{EO} is 0.2 Wh/L, whereas it is 0.33 Wh/L at the maximum light irradiance.

The investigations by Buechler et al. [75] and Buechler et al. [76] reported that under a diffusion-limited regime, controlled periodic illumination enhances the photonic efficiency. In principle, illuminating periodically the catalyst under a diffusion-limited regime would give the reactant more time to reach the active surface. In a diffusion-limited regime, as the volumetric flow rate increases, the reaction rate should become independent of fluid velocity, indicating that the reaction is no longer limited by the transport of reactants from the bulk fluid to the active catalyst and is dominated by surface reactions. The dominant regime depends on both the flow behavior of the gas mixture and the experimental conditions [96].

Figure 3.4 illustrates the average conversion of toluene at three different volumetric flow rates. There is no significant difference on the degradation of toluene when decreasing the volumetric flow rate. For instance, the average degradation was 46% for a volumetric flow rate of 1411 ml/min, 49% for a volumetric flow rate of 1133 ml/min, and 47% for a volumetric flow rate of 854 ml/min. The lack of significant effect of decreasing the volumetric flow rate on the degradation of toluene means that under these experimental conditions, the reaction rate is limited by surface kinetics and not by the mass transfer of toluene from the bulk fluid to the catalyst surface. Since there are no mass transfer limitations in the system, the effect of controlled periodic illumination could only be investigated under a kinetic-limited regime. Unfortunately, operating at lower volumetric flow rates was not possible under the current experimental set-up. Hence, the effect of controlled periodic illumination under a diffusion-limited regime was not explored.

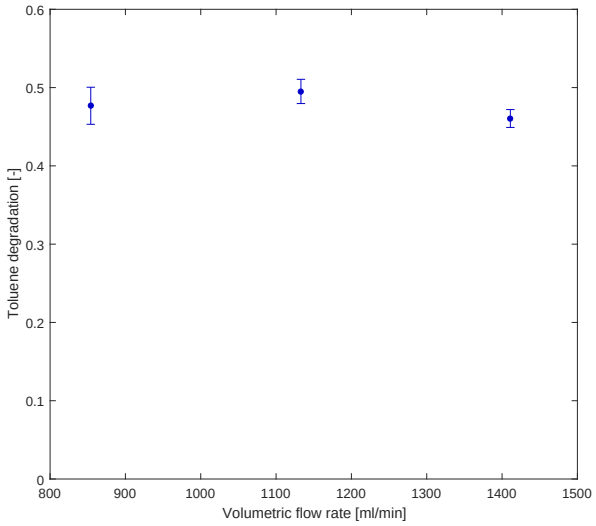

Figure 3.4: Average degradation of toluene at different volumetric flow rates. Initial concentration of toluene: 29.5 ± 2 ppmv; Relative humidity: 43%; Maximum incident irradiance: 1.35 mW/cm^2; Residence time: 18s; Error bars: confidence interval of 95%

3.1.2. Effect of frequency

Figure 3.5 presents the effect of the period at a fixed duty cycle of 0.5. From Figure 3.5(a), which presents the effect of the period on the degradation of toluene, it is noted that at lower periods (higher frequencies) the degradation of toluene is also lower. For instance, for a period of 50 milliseconds, the average degradation was 24%, whereas for a period of 10 seconds, the average degradation was 30%. However, at lower periods the rated power was also lower; meaning that although working at the same duty cycle, the incident photon flux was not the same.

For example, for a period of 50 milliseconds, the average rated power was 6.86W, whereas for a period of 200 milliseconds, the average rated power was 7.92W. This difference is mainly

due to the relaxation times of the LEDs since at higher frequencies, the error due to the time it takes for the LEDs to switch on and to switch off becomes larger relatively to the illumination time as it was illustrated in Figure 2.6. Therefore, in Figure 3.5(b), when the degradation is normalized by the rated power, it is clearly seen that working at higher frequencies has no significant difference when compared to lower frequencies.

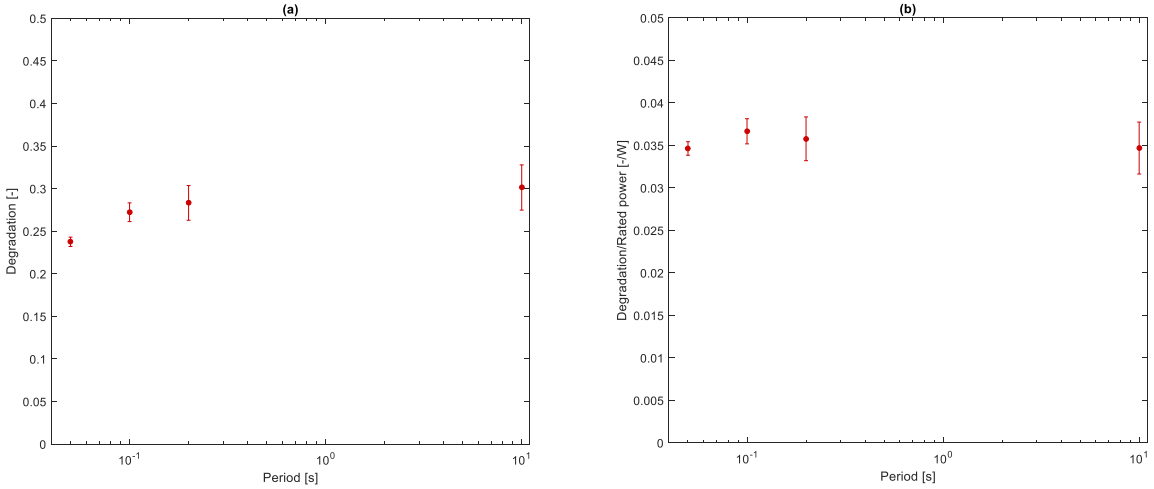

Figure 3.5: Effect of the period at fixed duty cycle of 0.5 on: (a) Toluene degradation; and (b) Toluene degradation normalized by the power consumption. Volumetric flow rate: 1411 ml/min; Initial concentration of toluene: 29.5 ± 2 ppmv; Relative humidity: 43%; Maximum incident irradiance: 1.35 mW/cm^2; Maximum average power consumption: 17.5 W; Error bars: confidence interval of 95%

Studies regarding the effect of the period at fixed duty cycle have remained limited and have mainly focused on the determination of the lifetime of active species. Cornu et al. [78], Korovin et al. [85], and Zhou et al. [87] reported a maximum value of photonic efficiency at their lowest working period, which was also equal to the value obtained under continuous illumination at the same average irradiance. In addition, with increasing period, the authors found two different inflection points associated with the lifetime of active species. These two inflection points cannot be appreciated in Figure 3.5 possibly because in this experiment an average reaction rate rather than an initial rate of oxidation is determined.

3.2. Radiation profile

The photocatalytic reactor under investigation in this study has the LED array divided into five independent sections. Each section of the LED array is then controlled with a different power supply, which allows to test different illumination profiles to further optimize the required energy input. Two different illumination profiles were experimentally tested: Case A and Case B. Case A follows a step-wise increase in the irradiance along the reactor length, while Case B follows a step-wise decrease in the irradiance. Two situations may be possible:

1. At the inlet of the reactor the driving force for the diffusion of toluene from the bulk fluid to the catalyst is higher than at the outlet; hence, a lower irradiance at the inlet of the reactor would be more energetically optimal.

2. At the inlet of the reactor there is a high concentration of toluene; thus, a higher irradiance at the inlet of the reactor may yield a higher toluene conversion due to an increase in the charge carriers.

Figure 3.6 illustrates the degradation of toluene under a step-wise increase (Case A) and a step-wise decrease (Case B) irradiation profile as presented in Table 2.3, together with the degradation of toluene under a uniform illumination along the reactor length at three different average irradiance. It is noted that aside from the result obtained for Case B at an irradiance of 0.81 mW/cm^2, there is no significant difference among the illumination methods. Nevertheless, for Case A, where the higher irradiance was at the outlet of the reactor, the degradation of toluene seems to be slightly higher than under uniform illumination. In contrast, for Case B, where the higher irradiance was at the inlet of the reactor, the degradation of toluene seems to be slightly lower. For instance, at an irradiance of 1.01 mW/cm^2, the degradation of toluene was 38.9% for Case A, 37.9% for Case B and 38.2% for uniform illumination.

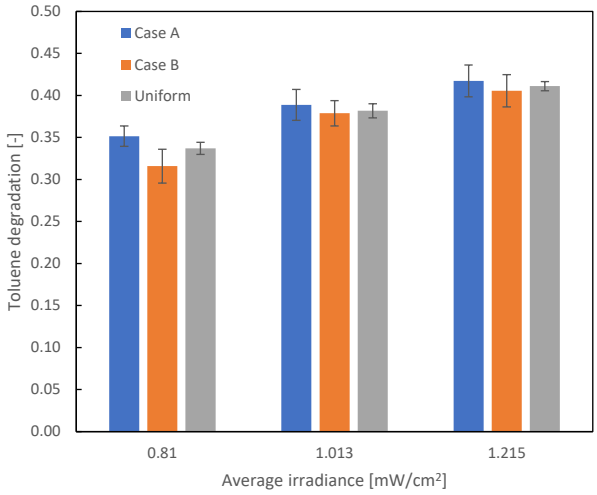

Figure 3.6: Effect of different radiation profiles on the degradation of toluene. Volumetric flow rate: 1411 ml/min; Initial concentration of toluene: 29.5 ± 2 ppmv; Relative humidity: 43%; Maximum incident irradiance: 1.35 mW/cm^2; Maximum average power consumption: 17.5 W; Error bars: confidence interval of 95%

Since the results illustrated in Figure 3.6 for all three cases were similar, a mathematical model of five photocatalytic reactors in series was developed (see Appendix C). Figure 3.7 illustrates the results obtained for the conditions presented in Figure 3.6. For all three different average irradiance, the uniform illumination profile achieved a higher conversion, while Case B showed the lowest conversion. It is also noted that the difference between the three cases is the highest for an irradiance of 0.81 mW/cm^2 and it is the lowest for the irradiance of 1.215 mW/cm^2. For instance, at an irradiance of 0.81 mW/cm^2, the conversion under a uniform illumination profile was 35.09%, whereas it was 34.04% and 33.98% for Case A and Case B, respectively. In contrast, at an irradiance of 1.215 mW/cm^2, the conversion of toluene was 42.42%, 42.39%, and 42.38% for a uniform illumination profile, Case A, and Case B, respectively.

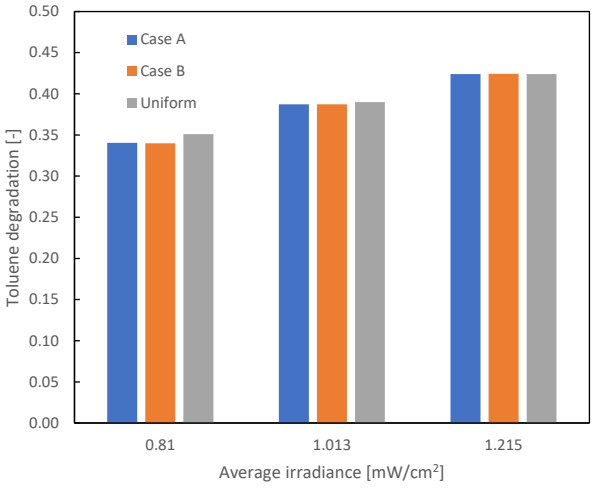

Figure 3.7: Effect of different radiation profiles on the degradation of toluene. Volumetric flow rate: 1411 ml/min; Initial concentration of toluene: 30 ± 2 ppmv; Relative humidity: 43%; Maximum incident irradiance: 1.35 mW/cm^2; Maximum average power consumption: 17.5 W

Experimentally, the degradation of toluene under Case A was slightly higher than under Case B or under a uniform profile as presented in Figure 3.6. Nevertheless, the experimental results among all three different irradiation profiles is not statistical different and hence, the difference between the results obtained with the mathematical model and the experimental results may be just due to the experimental error. In addition, it is worth noting that the conversion of toluene presented in Figure 3.7 are very similar to those obtained from the experiments, which means that the Five Reactors in Series can model the system adequately.

From the model results illustrated in Figure 3.7 it is then concluded that a uniform illumination profile yields a better degradation of toluene whereas a step-wise decrease profile gives the worst degradation of toluene. A step-wise increase in irradiance yields a better conversion of toluene than a step-wise decrease because at the inlet of the reactor the driving force for the diffusion of toluene towards the active catalyst is higher.

To further explore the effect of having different irradiance in each reactor section, an optimization model was developed in Matlab (see Appendix D). Figure 3.8 presents the Pareto front for optimization problem P_1, relating both objective functions in Equation 3.8. The Pareto front clearly shows that there is a trade-off between the conversion of toluene and the incident irradiance. There are no two different values of irradiance that correspond to a same toluene conversion. In fact, as it is presented in Figure 3.8, a uniform profile always yields the highest toluene conversion.

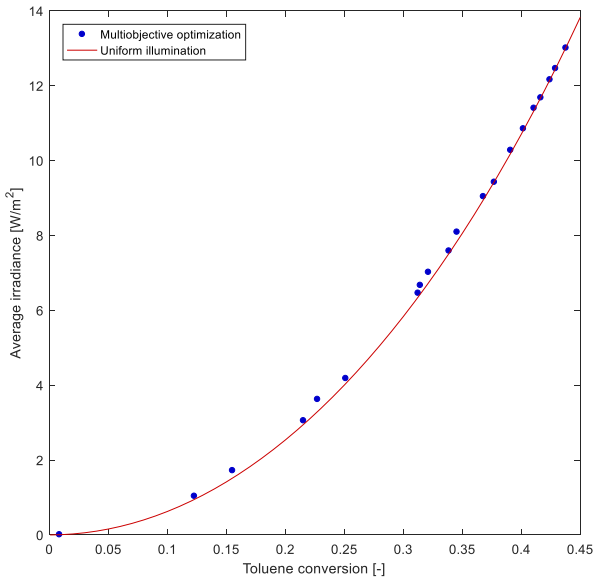

Figure 3.8: Toluene conversion under the multiobjective optimization and under uniform illumination. Initial concentration: 1.28164E-3 mol/m^3; Volumetric flow rate: 1411 ml/min; Maximum irradiance: 13.5 W/m^2.

Therefore, two things can be concluded: (a) a uniform illumination profile yields a slightly higher toluene conversion throughout the whole average irradiance spectrum; and (2) the conversion of toluene under these conditions is a stronger function of the average incident irradiance rather than by how it is illuminated. This was further corroborated with an experiment comparing the conversion of toluene when one section of the reactor was illuminated at 13.5 W/m^2 and when the whole reactor was illuminated at an irradiance of 2.7 W/m^2, to have the same average irradiance. The conversion of toluene was 15% when the whole reactor was illuminated and 13% when just one section of the reactor was illuminated. This difference can be ascribed to many factors, such as mass transfer, available active sites on the catalyst, etc.; nonetheless, the difference is not significant and is within the experimental error of the system. Hence, for this system, there was no gain in efficiency or energy saving by following an illumination profile. Nevertheless, it is possible that for a system with mass transfer limitations, following an illumination profile will yield a better result. In a system with mass transfer limitations, the reaction order with respect to the UV irradiation will tend to zero; thus, the penalty for having a high irradiance along the reactor may be significant. However, since in this system there are no mass transfer limitations, it is not possible to determine whether this will be the case experimentally.

3.3. Process Control

Sensitivity Analysis

3.3.1. Irradiation

Figure 3.9 illustrates the time on stream profile for both the degradation of toluene (Figure 3.9(a)) and the carbon dioxide production (Figure 3.9(b)) for an irradiance of 0.675 mW/cm^2 and 1.35 mW/cm^2. It is clearly noted that there is a certain delay time between the turning on of the LEDs and the time when the gas chromatograph can note a change in the concentration of toluene due to its degradation. The delay time is associated with the time it takes for the outlet flow of the reactor to reach the gas chromatograph and is a function of the volumetric flow rate. For these flow conditions, the delay time is approximately 1.5 minutes.

Moreover, from Figure 3.9(a) it is noted that the highest toluene degradation happens as soon as the LEDs are turned on and then decreases rapidly during the first 10 minutes of reaction. After approximately 10 minutes, though decreasing due to the catalyst deactivation, the slope becomes less steep and reaches a stable value between 100 and 140 minutes of reaction. A similar behaviour is noted in Figure 3.9(b), where the maximum carbon dioxide production for both irradiation values happens at approximately 20 minutes and then decreases due to the catalyst deactivation.

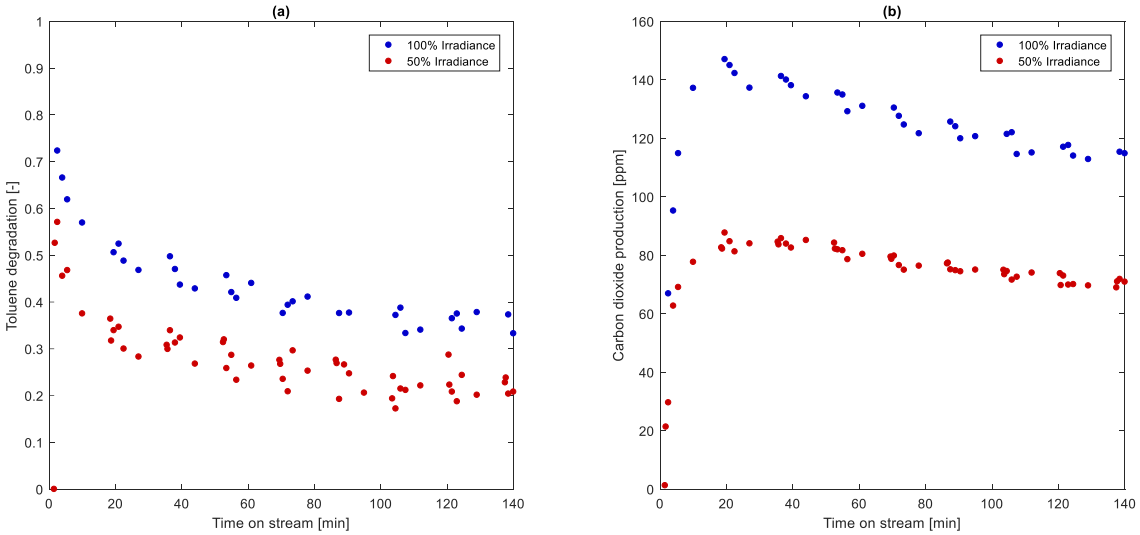

Figure 3.9: (a) Toluene degradation dynamic response; and (b) Carbon dioxide generation dynamic response. Inlet toluene concentration: 40ppmv; Maximum irradiance: 13.5 W/m^2; Relative humidity: 40%; Volumetric flow rate: 1026 ml/min; Residence time: 24.8s

Jovic et al. [110] obtained similar results as those illustrated in Figure 3.9(a). The authors observed three characteristic periods in the time-dependent conversion of toluene: (1) a very short (i.e. less than 10 minutes) initiation period where the conversion of toluene rapidly increased and reached a maximum value; (2) a period of constant toluene conversion; and (3) a period where the conversion started to decrease due to the catalyst deactivation.

Figure 3.9 also illustrates three different periods. In the initiation period, the maximum toluene conversion is obtained almost as soon as the LEDs are turned on. This behavior can be attributed to the formation of hydroxyl radicals [110]. It is important to note that during this period there is almost no carbon dioxide formation (see Figure 3.9(b)). Thus, although toluene is degraded, it is mainly degraded to intermediates. In the second period, there is a rapid decrease in toluene conversion, possibly due to the active site competition between toluene, water, and intermediates formed. During the second period, there is also an increase in carbon dioxide formation; hence, the intermediates start being mineralized into carbon dioxide. Lastly, the third period comprises the catalyst deactivation, where both the conversion of toluene and carbon dioxide formation decrease in a gradual fashion.

To compare the time-on-stream behaviour between the conditions for the process control experiments and the controlled periodic illumination experiments, Figure 3.10 illustrates the time-on-stream degradation of toluene and carbon dioxide production under an irradiance of 0.675 mW/cm^2 for the experimental conditions at which the controlled periodic illumination experiments were performed. Just as in Figure 3.9, Figure 3.10 also presents three periods: a really fast initiation period, followed by a fast decrease in toluene conversion and increase in carbon dioxide formation, followed by a relatively constant toluene conversion and carbon dioxide generation. In general, no catalyst deactivation was observed during the controlled periodic illumination experimental conditions.

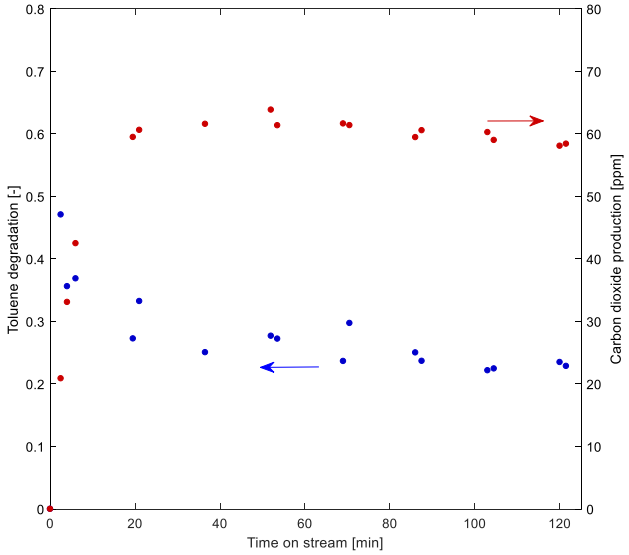

Figure 3.10: Toluene degradation and carbon dioxide generation time on stream characteristic behaviour at an average irradiance of 0.675 mW/cm^2. Initial concentration of toluene: 29.5 ± 2 ppmv; Relative humidity: 43%; Maximum incident irradiance: 1.35 mW/cm^2; Residence time: 18s;

Catalyst deactivation has been widely reported in the literature in studies with toluene as target compound, where the strong adsorption of intermediates or side products on the catalyst surface has been linked to its deactivation [105, 109, 113]. Consequently, a change in color to brown has been observed [116]. Specifically, benzaldehyde has been widely reported as one of the main intermediates that cause catalyst deactivation during the degradation of toluene [110, 113, 117]. Benzaldehyde is more strongly bound to TiO_2 than toluene, which is also probably the reason why benzaldehyde was not detected in the outlet stream of the reactor during the photocatalytic experiments.

Figure 3.11 illustrates the dynamic response of the system when a 25% step increase in irradiance is introduced. Additionally, Figure 3.12 presents the dynamic response of the system when a 50% step increase in irradiance is performed. In both Figures, it can be clearly seen that both the conversion of toluene and the generation of carbon dioxide have an almost immediate response when the irradiance is increased. As mentioned before, there is a time delay of approximately 1.5 minutes, which considers the time it takes for the outlet flow to reach the gas chromatograph. Nonetheless, after such time, both the toluene conversion and carbon dioxide generation are the maximum, followed by a gradual decrease due to the catalyst deactivation.

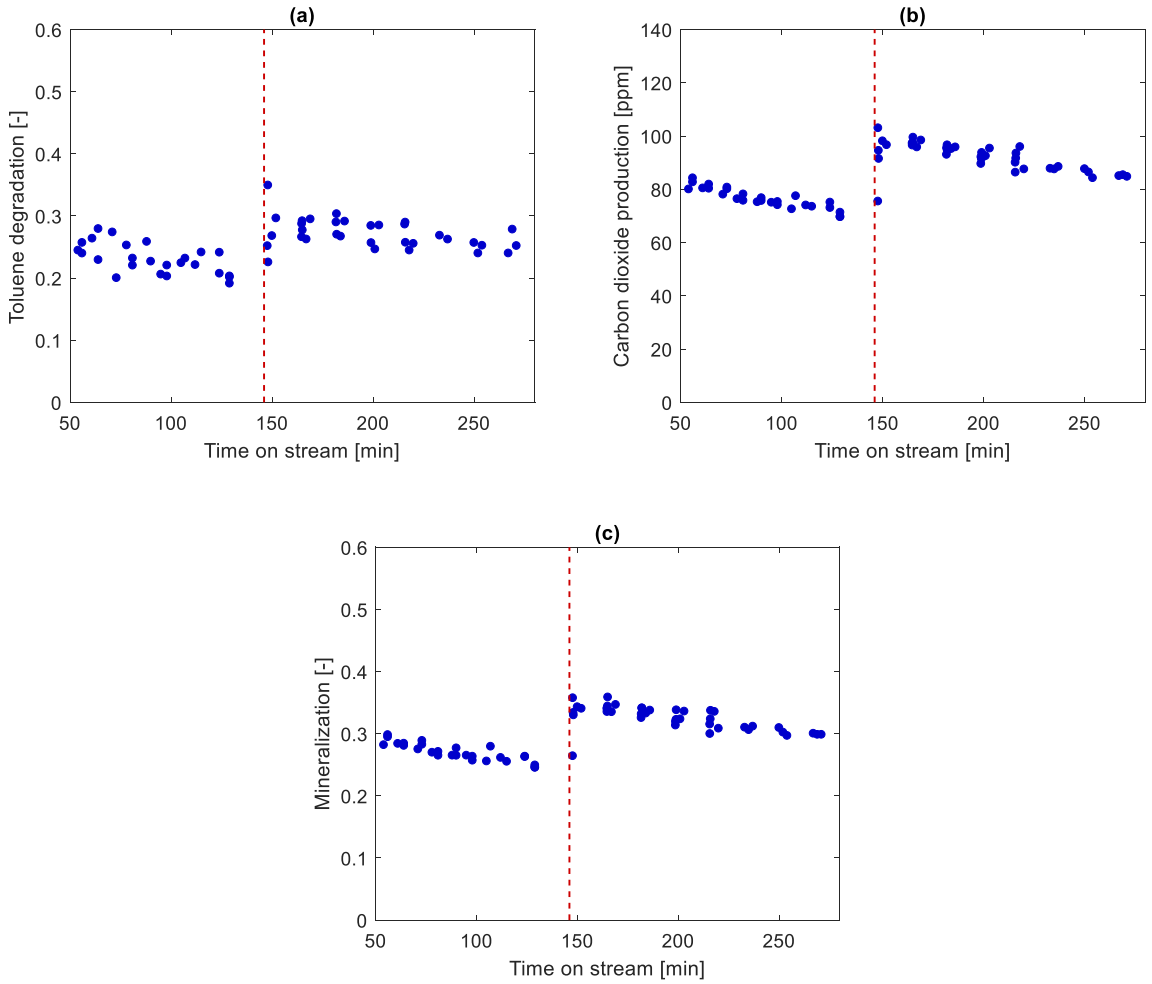

Figure 3.11: Dynamic response to an irradiance step input from 50% to 75% for (a) Toluene degradation; (b) Carbon dioxide generation; and (c) Toluene mineralization. Inlet toluene concentration: 40ppmv; Maximum irradiance: 13.5 W/m^2; Relative humidity: 40%; Volumetric flow rate: 1026 ml/min; Residence time: 24.8s. The red dotted lines represent the time at which the step input was performed: 146 min.

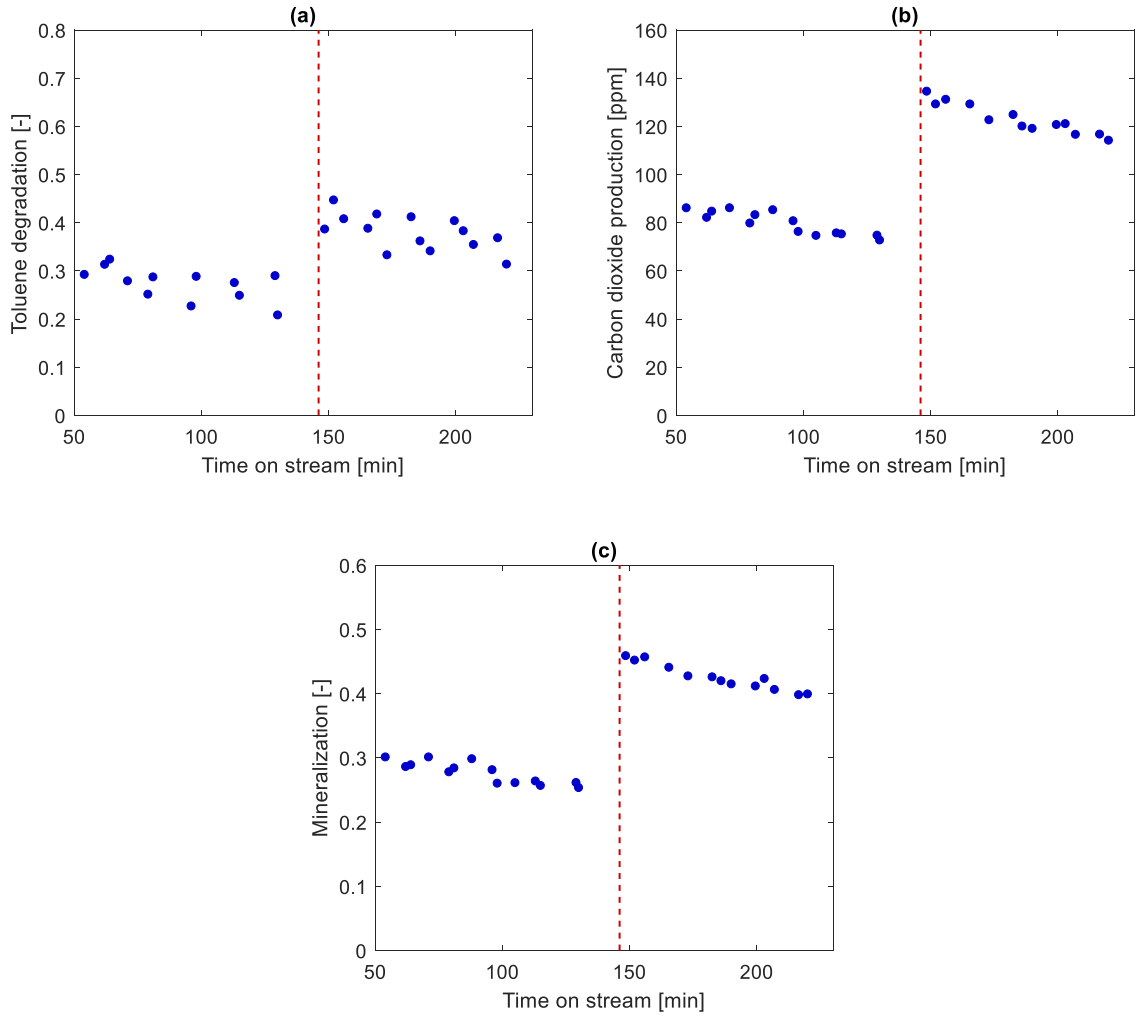

Figure 3.12: Toluene mineralization dynamic response to an irradiance step input from 50% to 100%. Inlet toluene concentration: 40ppmv; Maximum irradiance: 13.5 W/m^2; Relative humidity: 40%; Volumetric flow rate: 1026 ml/min; Residence time: 24.8s. The red dotted lines represent the time at which the step input was performed: 146 min.

3.3.2. Relative humidity

Figure 3.13 illustrates the dynamic response of the system to a step increase of 19.3% in relative humidity. From Figure 3.13(a) it is noted that after the relative humidity is increased, no increase or decrease in the conversion of toluene is observed. Since the conversion of toluene remained constant, increasing the relative humidity prevented further catalyst deactivation. However, there is a significant increase in the generation of carbon dioxide (see Figure 3.13(b)), which subsequently augments the mineralization of toluene (see Figure 3.13(c)). Furthermore, the increase in mineralization of toluene happens in a gradual fashion rather than in an almost instant manner as in the irradiation step. These results are in good agreement with those obtained by Jeong et al. [111] who noted that at higher relative humidity, the selectivity to carbon dioxide increases, while the toluene removal efficiency diminishes.

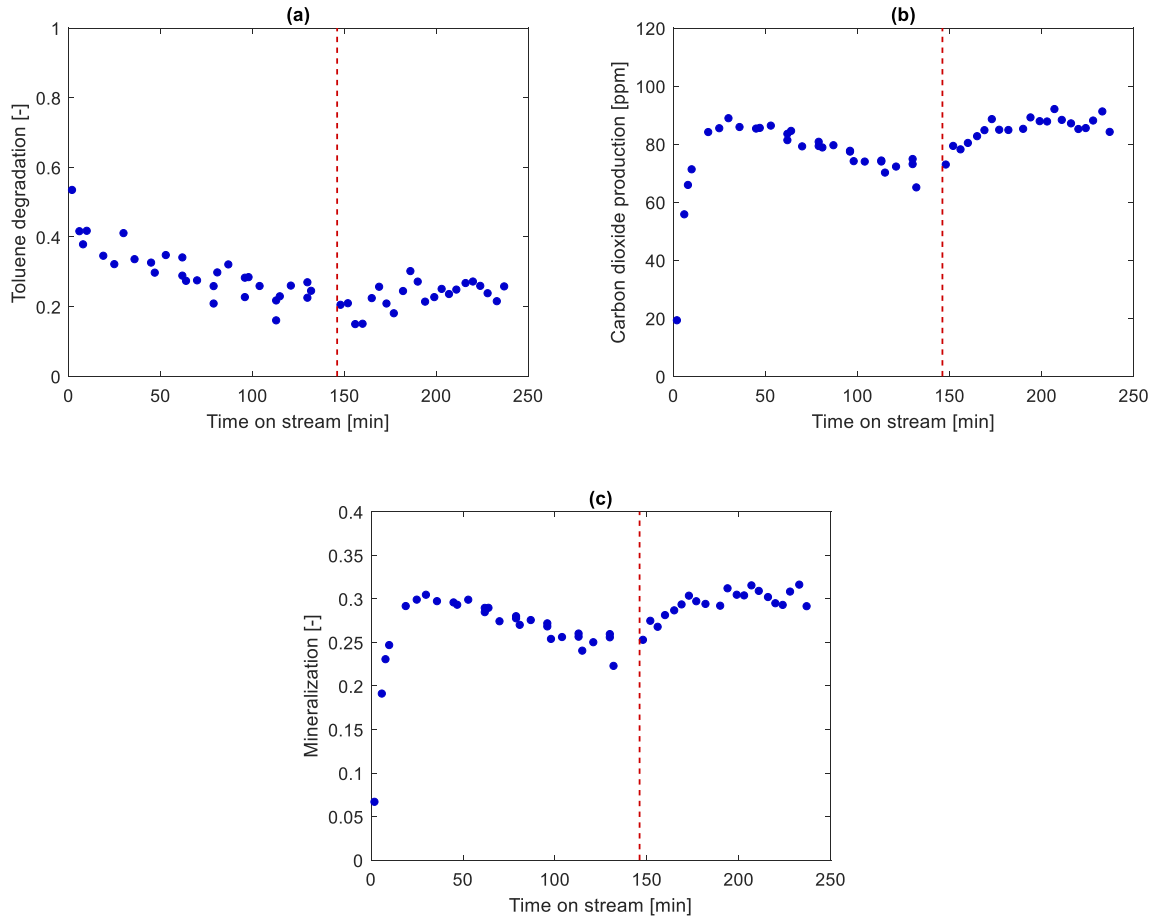

Figure 3.13: Dynamic response to a relative humidity step input from 40.3% to 58.4% for (a) Toluene degradation; (b) Carbon dioxide generation; and (c) Toluene mineralization. Inlet toluene concentration: 40ppmv; Irradiance: 6.75 W/m^2; Volumetric flow rate: 1026 ml/min; Residence time: 24.8s. The red dotted lines represent the time at which the step input was performed: 146 min.

Furthermore, according to Guo et al. [112], Martra et al. [114], and Duan et al. [116], the increase of relative humidity has a twofold effect: (1) it produces hydroxyl radicals which help oxidize pollutants together with the photogenerated holes in gaseous systems; and (2) it improves the elimination of accumulated benzaldehyde. Overall, even though the presence of water vapor has a positive effect to avoid catalyst deactivation, at high relative humidity it also has a competitive effect for active sites; hence, diminishing the conversion of toluene.

3.3.3. Toluene concentration

Figure 3.14 illustrates the dynamic response of the system when a step increase in the inlet concentration of toluene from approximately 40 ppm to 52.5 ppm is performed.

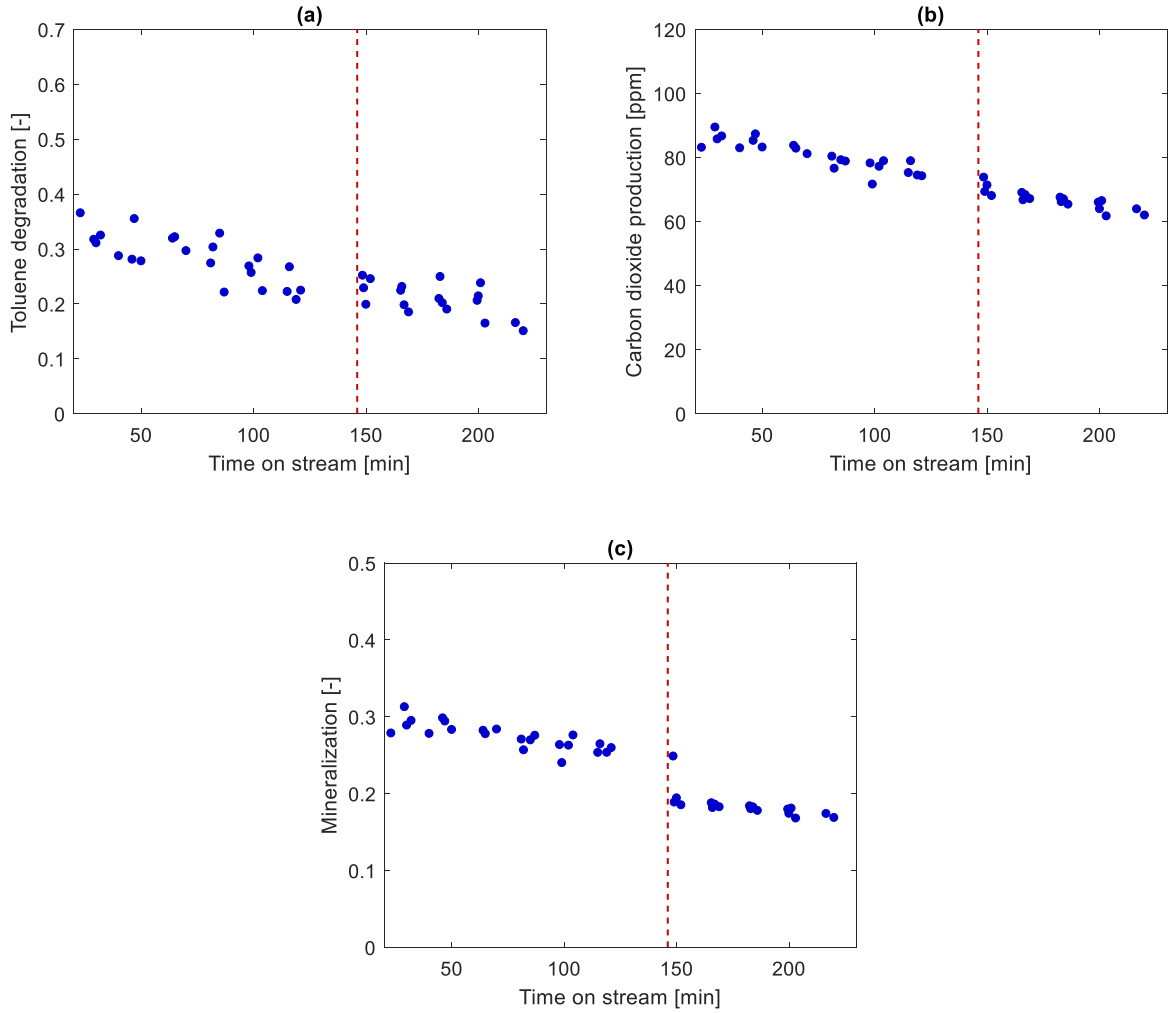

Figure 3.14: Dynamic response to a toluene concentration step input from 40 ppm to 52.5 ppm for (a) Toluene degradation; (b) Carbon dioxide generation; and (c) Toluene mineralization. Inlet toluene concentration: 40ppmv; Irradiance: 6.75 W/m^2; Volumetric flow rate: 1026 ml/min; Residence time: 24.8s. The red dotted lines represent the time at which the step input was performed: 146 min.

In contrast to Figure 3.13(a), where the degradation of toluene remained at a relatively constant value of around 25% after a step in relative humidity was introduced, the degradation of toluene presented in Figure 3.14(a) decreases further with time and reaches a value of approximately 15% after 200 minutes. In addition, the generation of carbon dioxide (see Figure 3.14(b)), continues to decrease with relatively the same steepness once the step in concentration is made. The aforementioned behavior is possibly due to the saturation of active sites; thus, an increase in the inlet concentration has no positive effect in the degradation of toluene or carbon dioxide production. Consequently, the decrease in the mineralization of toluene, illustrated in Figure 3.14(c), is further exacerbated and almost immediate once the step in the concentration is made.

3.3.4. Controller design

Based on the experimental results presented in Figures 3.11, 3.12, 3.13, and 3.14 the transfer functions of the process and the disturbances were estimated with Equation 3.1. To simplify the system, both the plant and the disturbances were approximated with a first order transfer function:

$$G_i(s) = \frac{K_i}{\tau_i s + 1} \tag{3.1}$$

where: K_i is the process gain, τ_i is the process time constant, G_i is the transfer function, and $_i$ represents respectively the irradiance, relative humidity, or toluene inlet concentration. The process gain was computed with Equation 3.2:

$$K_i = \frac{y_i(2) - y_i(1)}{u_i(2) - u_i(1)} \tag{3.2}$$

where: $y_i(1)$ and $y_i(2)$ are the output variable at the first and second steady states, respectively, and $u_i(1)$ and $u_i(2)$ are the input variable before and after the step is made. In addition, the time constant was computed as 63% of the time required to reach to the steady state [118].

The values of the gains and time constants for the process and the perturbations are shown in Table 3.1. Since the gains for the 25% and 50% step in irradiation were similar, just one gain is reported. Moreover, the irradiance gain for both degradation and mineralization of toluene is estimated to be the same.

Table 3.1: Gains and time constants for the process variables: irradiance, relative humidity, and toluene inlet concentration.

Variable	K (degradation)	K (mineralization)	τ
Irradiance [W/m^2]	0.02915	0.02915	122
Relative humidity [%]	-	0.00375	952
Toluene inlet concentration [ppm]	-	-0.0065	151

Figure 3.15 presents the estimated transfer function together with the experimental data for the conversion of toluene (Figure 3.15(a)) and the mineralization of toluene (Figure 3.15(b)). Likewise, Figure 3.16 illustrates the estimated mineralization transfer functions for the relative humidity (3.16(a)) and the inlet concentration of toluene (3.16(b)).

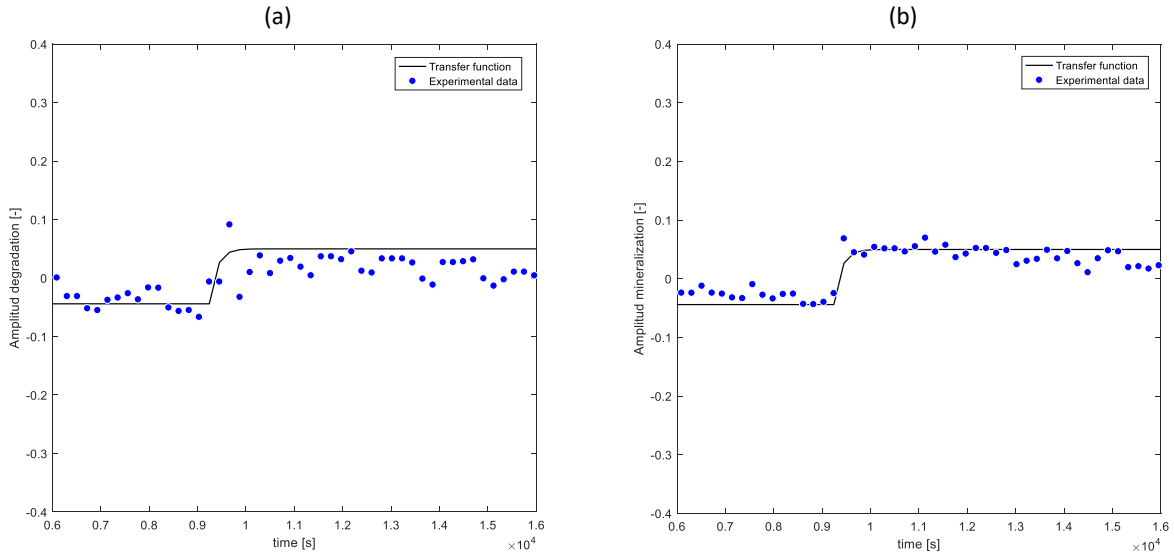

Figure 3.15: Irradiance transfer functions together with the experimental data for (a) toluene degradation; and (b) toluene mineralization

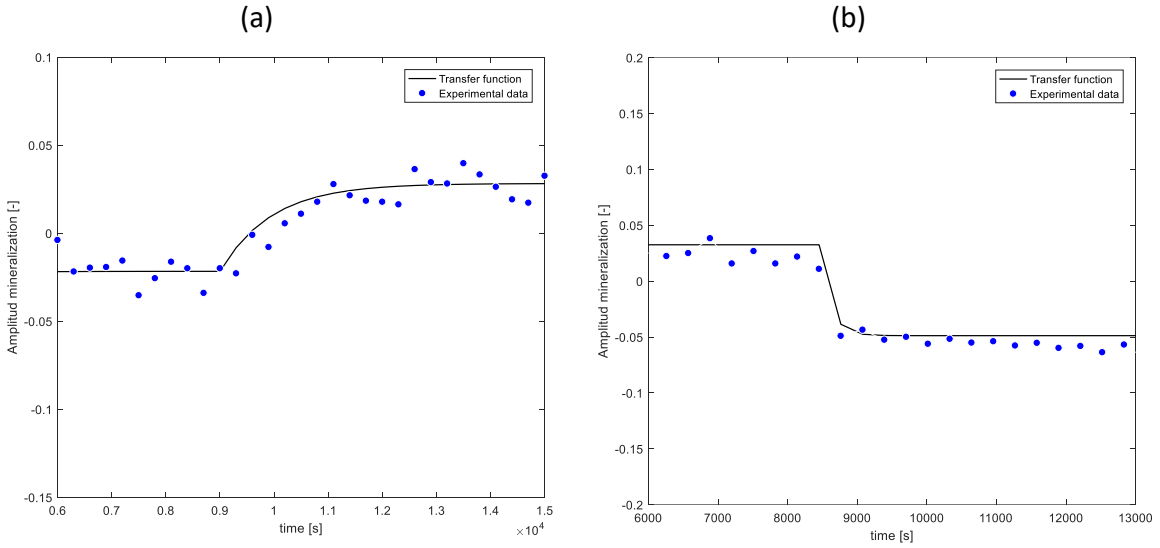

Figure 3.16: Toluene mineralization transfer functions together with the experimental data for (a) Relative humidity; and (b) Toluene inlet concentration

Based on the irradiance gain and time constant presented in Table 3.1, the PI controller was tuned following the IMC tuning rules [118]:

$$K_C = \frac{0.588}{K_{Irr}}\left(\frac{\tau_{Irr} + \frac{\theta}{2}}{\theta}\right) \tag{3.3}$$

$$\tau_I = \tau_{Irr} + \frac{\theta}{2} \tag{3.4}$$

where: K_C is the controller gain, K_{Irr} is the irradiance process gain, τ_{Irr} is the irradiance time constant, θ is the time delay, and τ_I is the controller integral time. The time delay was

assumed as 17 minutes, corresponding to the time the gas chromatograph takes to analyse each sample.

Appendix E illustrates a Simulink model where the PI controller was simulated. The PI tuning parameters computed with Equations 3.3 and 3.4 are 12.8 and 660 seconds, respectively. Figure 3.17 illustrates the simulations performed with the tuned settings, as well as the response of the system to relative humidity and inlet concentration perturbations.

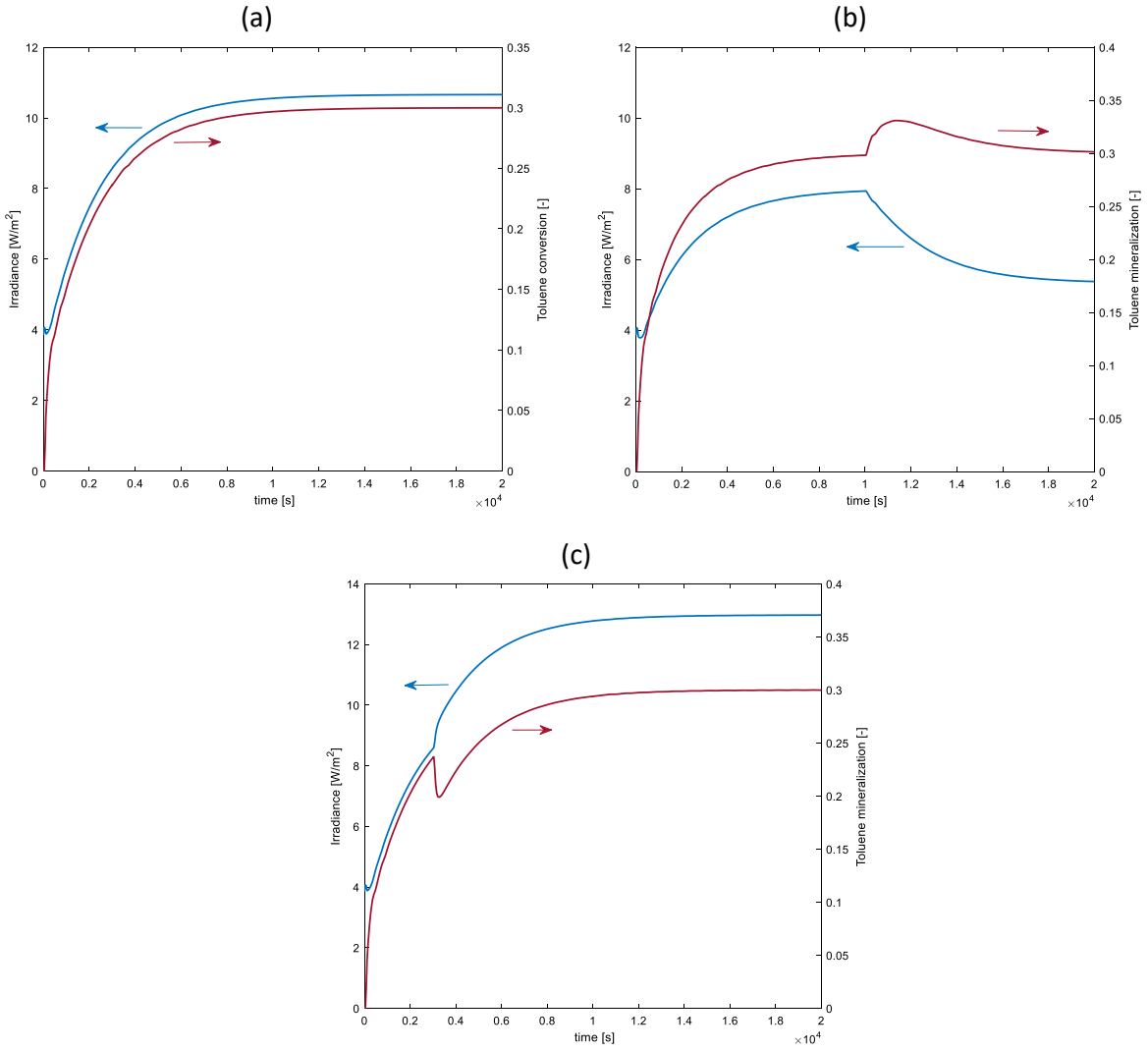

Figure 3.17: Simulink PI controller simulations for (a) Degradation of toluene, (b) Mineralization of toluene with a step change in relative humidity of 20%, and (c) Mineralization of toluene with a step change in toluene concentration of 5 ppm. The setpoint was maintained at 0.3 for all cases; PI tuned parameters: K_C = 12.15 and τ_I = 632s.

From Figure 3.17, it can be seen that the PI controller settings used give a good and smooth response to both achieve the set-point (Figure 3.17(a)) and reject the disturbances (Figure 3.17(b) and (c)). As illustrated in the experiments from Figure 3.13(c), 3.17(b) shows that to reject the effect that an increase in relative humidity has in toluene mineralization, the irradiance would have to diminish to achieve the set-point. In contrast, to reject the effect that an increase in toluene inlet concentration has in toluene mineralization and maintain the set-point, the irradiance would have to increase as it is shown in Figure 3.17(c).

3.3.5. Control validation

The control of the photocatalytic reactor was performed manually using Equation 3.5 [119]. In Equation 3.5, p_k represents the output of the controller at the kth sampling instant (W/m^2), K_C the gain of the controller, e_k is the error at the kth sampling instant, e_{k-1} is the error at the previous sampling, p_{k-1} is the output of the controller at the previous sampling, Δt is the time between successive measurements of the controlled variable, and τ_I is the integral time of the controller.

$$p_k = p_{k-1} + K_C \left[e_k - e_{k-1} + \frac{\Delta t}{\tau_I} e_k \right] \tag{3.5}$$

Figure 3.18 illustrates two different validation experiments using feedback control. In the first experiment, presented in Figure 3.18(a), different toluene conversion set-points were given to the controller under experimental conditions with no catalyst deactivation present: relative humidity of 55% and toluene inlet concentration of 30 ppm. Here, it is noted that the controller can reach the different set-points relatively fast. In the second experiment, illustrated in Figure 3.18(b), the toluene conversion was fixed at a set-point of 0.3 at conditions where catalyst deactivation occurs: toluene inlet concentration of 40 ppm and relative humidity of 40%. Even though catalyst deactivation was present, the controller could maintain the conversion close to the set-point throughout the photocatalytic reaction.

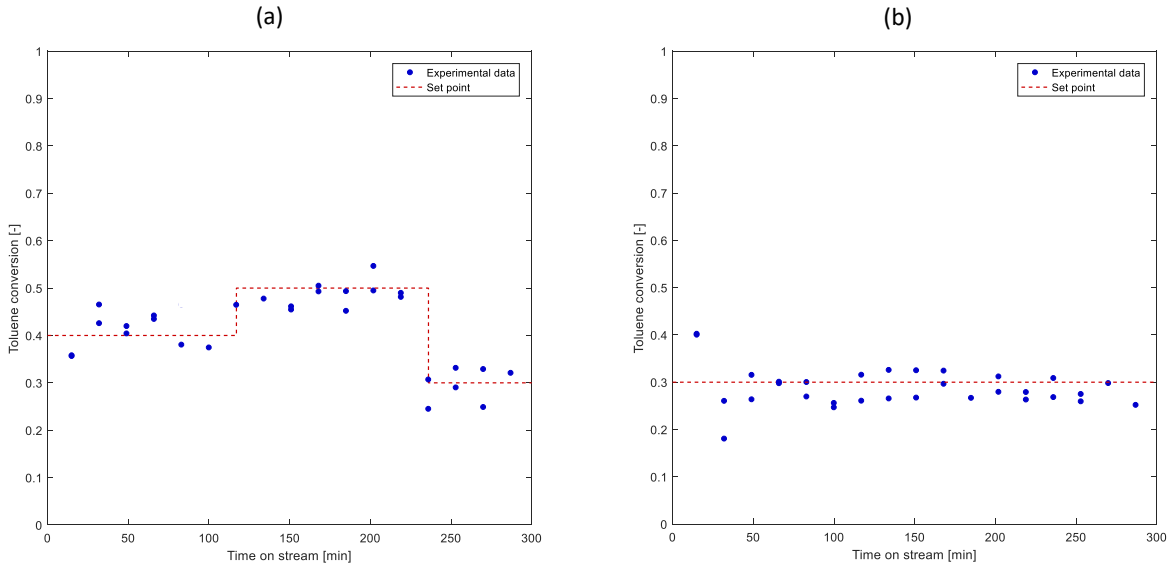

Figure 3.18: (a) Toluene conversion using feedback PI control at different set points with no catalyst deactivation; Toluene inlet concentration: 30 ppm, Relative humidity: 55%, Volumetric flow rate: 897 ml/min. (b) Toluene conversion using feedback PI control with catalyst deactivation. Relative humidity: 40.15%, Toluene inlet concentration: 40 ppm, Volumetric flow rate: 1026 ml/min.

Nonetheless, it is important to note that when catalyst deactivation is present to a higher extend, it is likely that feedback control will not be sufficient to maintain the set-point throughout the photocatalytic reaction. One possibility to overcome this is to implement feedforward control, which will require either an empirical or theoretical model relating toluene inlet concentration, relative humidity, and irradiance to catalyst deactivation through time. However, increasing the irradiance to reach the set-point while experiencing catalyst deactivation is a temporary solution and not the optimal solution in terms of energy. The irradiance will continuously increase throughout the photocatalytic reaction and the regeneration of the catalyst will take more time. Catalyst deactivation can be avoided by

operating at conditions where the catalyst does not deactivate with time, such as higher relative humidity and lower toluene inlet concentration, by doping the catalyst [120], by recirculating the outflow of the reactor [110], or by using ultrasound to promote the desorption of the reaction products from the catalyst [8].

Furthermore, Figure 3.19 illustrates a process control experiment with relative humidity and toluene inlet concentration disturbances in addition to the catalyst deactivation disturbance. From Figure 3.19(a), it is seen that the toluene conversion is maintained close to the set-point of 0.3 even when there is a change in relative humidity or toluene inlet concentration. Moreover, Figure 3.19(b) illustrates the output irradiance of the controller. Here, it is clearly seen that before the relative humidity changes from a value of 40.1% to 53.2%, the irradiance required to maintain the toluene conversion at the set-point continuously increases due to catalyst deactivation. However, when working at a relative humidity of 50.3%, the irradiance required to maintain the set-point stabilizes at a constant value of around 9 W/m^2, meaning there is no catalyst deactivation under these conditions.

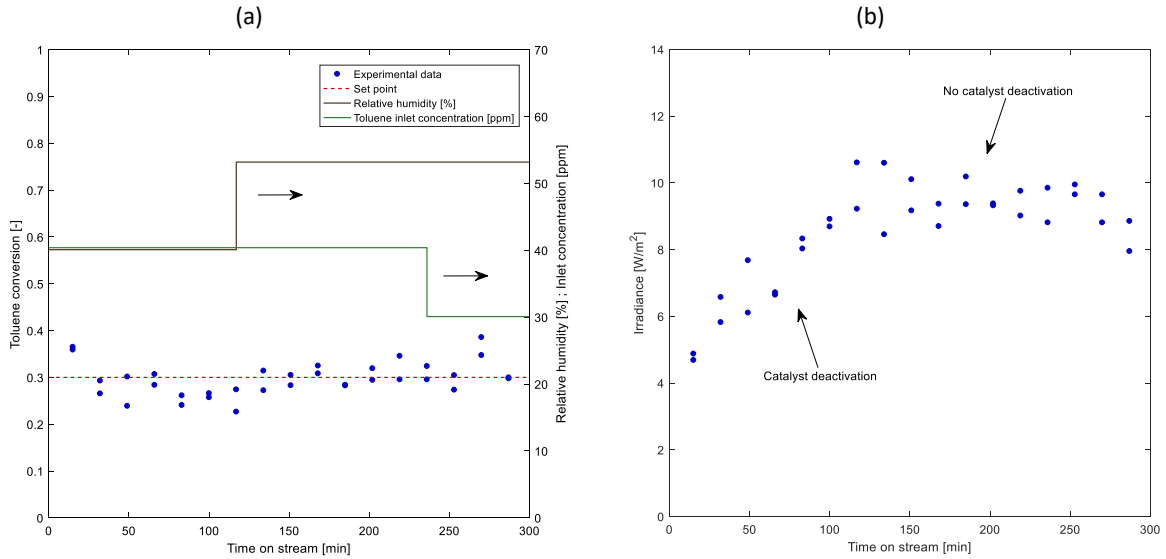

Figure 3.19: (a) Toluene conversion using feedback PI control with relative humidity and toluene inlet concentration perturbances; and (b) Irradiance controller output throughout the photocatalytic reaction. Conversion set-point: 0.3; Volumetric flow rate: 1020 ml/min; Initial toluene inlet concentration: 40.4 ppm; Final toluene inlet concentration: 30.1 ppm; Initial relative humidity: 40.1%; Final relative humidity: 53.2%.

4

Conclusions and Further Work

4.1. Controlled periodic illumination

Multiple experiments were performed to determine the effect of controlled periodic illumination in the degradation of gas-phase toluene in an annular LED-based photocatalytic reactor. Both the effect of the duty cycle and the period were explored and the results were compared with continuous illumination at equivalent incident irradiance to answer the four research questions presented in Chapter 1.4. By increasing the duty cycle, the conversion of toluene increased as well since the average irradiance was higher. The photonic efficiency decreased with increasing duty cycle and incident irradiance. Nevertheless, the conversion of toluene under controlled periodic illumination was no different when compared with continuous illumination at equivalent incident irradiance. Therefore, illuminating the catalyst periodically did not enhance the photonic efficiency when compared to continuous illumination.

In addition, the effect of the period was explored at a fixed duty cycle of 0.5. Relatively rectangular periods were maintained until periods as low as 50 milliseconds. However, even though the duty cycle remained fixed at 0.5, the lower the period, the higher error due to the relaxation times of the LEDs. Since the rated power was not the same for all the periods, the conversion of toluene had to be normalized by the power consumption to be able to compare all periods under the same irradiance, which remained constant regardless of the period. Hence, the photonic efficiency was not enhanced by increasing the frequency of controlled periodic illumination.

Overall, it was noted that under a kinetic-limited regime, the conversion of toluene at equal irradiance under controlled periodic illumination and continuous illumination was the same. Unfortunately, the effect of controlled periodic illumination under a diffusion-limited regime could not be investigated since a decrease in the volumetric flow rate while maintaining a similar residence time yielded a similar toluene conversion. Future work should aim at exploring the effect of controlled periodic illumination under a diffusion-limited regime and in trying to achieve higher frequencies.

4.2. Radiation profile

Three different illumination profiles were compared experimentally to determine whether following a stepwise increase or a stepwise decrease in the irradiance had an advantage when compared to a uniform irradiance along the reactor length. Even though experimentally a stepwise increase yielded a slightly higher conversion in toluene than a stepwise decrease or uniform illumination, it was not statistically significant. Therefore, a mathematical model of five photocatalytic reactors in series was developed. Mathematically, although the three illumination profiles had a very similar toluene conversion, the toluene conversion was always higher under uniform illumination and was always lower under a stepwise decrease in irradiance.

To further explore if an illumination profile could decrease the energy consumption for a specific toluene conversion, a two-objective optimization was performed to try to achieve a maximum possible toluene conversion with the lower irradiation possible. The best toluene conversion was always achieved under uniform illumination. Future work should try to explore the effect of following an illumination profile under a diffusion-limited regime. Under a diffusion-limited regime, the penalty due to electron-hole recombination is higher; thus, following an illumination profile may help reduce the energy consumption for a given toluene conversion.

4.3. Process Control

The process control was developed by first exploring the sensitivity that changes in irradiance, toluene inlet concentration, and relative humidity had in the conversion and mineralization of toluene. When the irradiance and toluene inlet concentration were increased, the system responded almost immediately; whereas a change in relative humidity had a slower response. The sensitivity analysis results showed that increasing the relative humidity to a certain value stopped catalyst deactivation and augmented the mineralization of toluene. In contrast, an increase in toluene inlet concentration diminished the mineralization of toluene. A PI feedback controller was then designed assuming a first order transfer function for the process and the disturbances and tuned using the IMC tuning rules. The feedback controller successfully maintained the conversion of toluene at the established set-point under experimental conditions with no perturbations and under experimental conditions with perturbations such as catalyst deactivation, and changes in relative humidity and toluene inlet concentration.

Future work should aim at developing a more complex control scheme, including broader changes in the volumetric flow rate and in relative humidity. It is expected that at a certain value of relative humidity, the conversion of toluene will drop due to the competition of active sites between the toluene molecules and the water molecules. However, under the experimental conditions tested in this work, just the positive effect of diminishing catalyst deactivation was observed. Developing a more complex control scheme may lead to large operational and energy savings when the operating conditions vary. Moreover, a mathematical model for catalyst deactivation that integrates the effect of relative humidity, toluene inlet concentration, and irradiance should be developed to further optimize the photocatalytic reaction conditions.

Bibliography

[1] A. M. Omer. Energy, environment and sustainable development. *Renewable and Sustainable Energy Reviews*, 12(9):2265–2300, 2008.

[2] A. Stankiewicz. Energy Matters. *Chemical Engineering Research and Design*, 84(7):511–521, 2006.

[3] O. Carp, C. L. Huisman, and A. Reller. Photoinduced reactivity of titanium dioxide. *Progress in Solid State Chemistry*, 32(1-2):33–177, 2004.

[4] D. W. Chen, F. M. Li, and A. K. Ray. Effect of mass transfer and catalyst layer thickness on photocatalytic reaction. *Aiche Journal*, 46(5):1034–1045, 2000.

[5] D. M. Blake, P. Maness, Z. Huang, E. J. Wolfrum, J. Huang, and W. A. Jacoby. Application of the Photocatalytic Chemistry of Titanium Dioxide to Disinfection and the Killing of Cancer Cells. *Separation & Purification Reviews*, 28(1):1–50, jan 1999.

[6] J. M. Herrmann. Heterogeneous photocatalysis: state of the art and present applications In honor of Pr. R.L. Burwell Jr. (1912–2003), Former Head of Ipatieff Laboratories, Northwestern University, Evanston (Ill). *Topics in Catalysis*, 34(1-4):49–65, may 2005.

[7] M. Motegh. *Design of Photocatalytic Reactors*. PhD thesis, Delft University of Technology, 2013.

[8] T. Van Gerven, G. Mul, and J. Moulijn. A review of intensification of photocatalytic processes. *Chemical Engineering and Processing: Process Intensification*, 46(9):781–789, 2007.

[9] N. Zhang, Y. Zhang, and Y.J. Xu. Recent progress on graphene-based photocatalysts: current status and future perspectives. *Nanoscale*, 4(19):5792, 2012.

[10] N.P. Huang, X. Min-hua, C.W Yuan, and Y. Rui-rong. The study of the photokilling effect and mechanism of ultrafine TiO2 particles on U937 cells. *Journal of Photochemistry and Photobiology A: Chemistry*, 108(2):229–233, 1997.

[11] D. Bennett. University of California at Davis: Catalysis, 2015.

[12] M. N. Chong, B. Jin, C. W.K. Chow, and C. Saint. Recent developments in photocatalytic water treatment technology: A review. *Water Research*, 44(10):2997–3027, 2010.

[13] R. W. Matthews. Hydroxylation Reactions Induced by Near-ultraviolet Photolysis of Aqueous Titanium Dioxide Suspensions. *J. Chem. SOC. Faraday Trans. I*, 80, 1984.

[14] C. D. Jaeger and A. J. Bard. Spin trapping and electron spin resonance detection of radical intermediates in the photodecomposition of water at titanium dioxide particulate systems. *The Journal of Physical Chemistry*, 83(24):3146–3152, nov 1979.

[15] M. R. Hoffmann, S. T. Martin, W. Y. Choi, and D. W. Bahnemann. Environmental Applications of Semiconductor Photocatalysis. *Chemical Reviews*, 95(1):69–96, 1995.

[16] A. J. Hoffman, E. R. Carraway, and M. R. Hoffmann. Photocatalytic Production of Semiconductor Collolds and Organic Peroxides on Quantum-Sized. *Environmental science & technology*, 28(5):776–785, 1994.

[17] S. T. Martin, A. T. Lee, and M. R. Hoffmann. Chemical mechanism of inorganic oxidants in the TiO2/UV process: increased rates of degradation of chlorinated hydrocarbons. *Environmental Science & Technology*, 29(10):2567–2573, oct 1995.

[18] S. Parsons. *Advanced oxidation processes for water and wastewater treatment*. IWA, London :, 2004.

[19] O. Ola, M. Maroto-Valer, D. Liu, S. MacKintosh, C. W. Lee, and J. C. S. Wu. Performance comparison of CO 2 conversion in slurry and monolith photoreactors using Pd and Rh-TiO 2 catalyst under ultraviolet irradiation. *Applied Catalysis B: Environmental*, 126:172–179, 2012.

[20] M.F.J Dijkstra, A. Michorius, H. Buwalda, H.J. Panneman, J.G.M Winkelman, and A.A.C.M Beenackers. Comparison of the efficiency of immobilized and suspended systems in photocatalytic degradation. *Catalysis Today*, 66(2):487–494, 2001.

[21] S. Gelover, L. A. Gomez, K. Reyes, M. T. Leal, and S. Tio. A practical demonstration of water disinfection using TiO 2 films and sunlight Coliforms Bacterial regrowth. 2006.

[22] T.T. Lim, P.S. Yap, M. Srinivasan, and An. G. Fane. TiO2 AC Composites for Synergistic Adsorption-Photocatalysis Processes: Present Challenges and Further Developments for Water Treatment and Reclamation. *Critical Reviews in Environmental Science and Technology*, 41(13):1173–1230, may 2011.

[23] R. K. Upadhyay, N. Soin, and S. S. Roy. Role of graphene/metal oxide composites as photocatalysts, adsorbents and disinfectants in water treatment: a review. *RSC Advances*, 4(8):3823, 2014.

[24] U. I. Gaya and A. H. Abdullah. Heterogeneous photocatalytic degradation of organic contaminants over titanium dioxide: A review of fundamentals, progress and problems. *Journal of Photochemistry and Photobiology C: Photochemistry Reviews*, 9(1):1–12, 2008.

[25] S. Pehkonen, R. Slefert, Y. Erel, S. Webb, and M. R. Hoffmann. Photoreduction of Iron Oxyhydroxides in the Presence of Important Atmospheric Organic Compounds. *Environmental science & technology*, 27:2056–2062, 1993.

[26] T. Shiragami, C. Pac, and S. Yanagida. Visible-light-induced two-electron-transfer photoreductions on cadmium sulfide: effects of morphology. *The Journal of Physical Chemistry*, 94(2):504–506, 1990.

[27] T. Shiragami, H. Ankyu, S. Fukami, C. Pac, S. Yanaglda, H. Mori, and H. Fujita. Semiconductor photocatalysis: visible light induced photoreduction of aromatic ketones and electron-deficient alkenes catalysed by quantised cadmium sulfide. *Journal of the Chemical Society, Faraday Transactions*, 88(7):1055, 1992.

[28] J. Herrmann. Heterogeneous photocatalysis: fundamentals and applications to the removal of various types of aqueous pollutants. *Catalysis Today*, 53(1):115–129, 1999.

[29] T. N. Obee and R. T. Brown. TiO2 Photocatalysis for Indoor Air Applications: Effects of Humidity and Trace Contaminant Levels on the Oxidation Rates of Formaldehyde, Toluene, and 1,3-Butadiene. *Environmental Science & Technology*, 29(5):1223–1231, 1995.

[30] H.W. Brandhorst. Terrestrial photovoltaic measurement procedures. NASA TM, 73702. pages 1022–77, 1977.

[31] D. F. Ollis, E. Pelizzetti, and N. Serpone. Photocatalyzed destruction of water contaminants. *Environmental Science & Technology*, 25(9):1522–1529, 1991.

[32] D. F. Ollis and A. E. Hussain. *Photocatalytic purification and treatment of water and air: proceedings of the 1st international conference on TiO2 photocatalytic purification and treatment of water and air, London, Ontario, Canada*. Amsterdam, 1993.

[33] A. V. Emeline, V. Ryabchuk, and N. Serpone. Factors affecting the efficiency of a photocatalyzed process in aqueous metal-oxide dispersions. *Journal of Photochemistry and Photobiology A: Chemistry*, 133(1-2):89–97, 2000.

[34] H. de Lasa, B. Serrano, and M. Salaices. *Photocatalytic Reaction Engineering*. Springer US, Boston, MA, 2005.

[35] W. S. Kuo and P. H. Ho. Solar photocatalytic decolorization of methylene blue in water. *Chemosphere*, 45(1):77–83, 2001.

[36] I. Muñoz, J. Rieradevall, F. Torrades, J. Peral, and X. Domenech. Environmental assessment of different advanced oxidation processes applied to a bleaching Kraft mill effluent. *Chemosphere*, 62(1):9–16, 2006.

[37] M. Litter, P. Boule, D. Bahnemann, and P. Robertson. *Environmental Photochemistry Part II*, volume 2M. 2005.

[38] W. Jo and R. J. Tayade. New Generation Energy-E ffi cient Light Source for Photocatalysis : LEDs for Environmental Applications. *Industrial and Engineering Chemistry Research*, 53:2073–2084, 2014.

[39] D. S. Bhatkhande, S. P. Kamble, S. B. Sawant, and V. G. Pangarkar. Photocatalytic and photochemical degradation of nitrobenzene using artificial ultraviolet light. *Chemical Engineering Journal*, 102(3):283–290, 2004.

[40] M. A. Gondal, M. N. Sayeed, and Z. Seddigi. Laser enhanced photo-catalytic removal of phenol from water using p-type NiO semiconductor catalyst. *Journal of Hazardous Materials*, 155(1-2):83–89, 2008.

[41] A. H. Yahaya, M. A. Gondal, and A. Hameed. Selective laser enhanced photocatalytic conversion of CO 2 into methanol. *Chemical Physics Letters*, 400(1-3):206–212, 2004.

[42] D. H. Chen, X. Ye, and K. Li. Oxidation of PCE with a UV LED photocatalytic reactor. *Chemical Engineering and Technology*, 28(1):95–97, 2005.

[43] A. A. Bergh and P. J. Dean. *Light-emitting diodes*. Clarendon Press, 1976.

[44] T. Bettles, S. Schujman, J.A. Smart, W. Liu, and L. Schowalter. UV Light Emitting Diodes; Their Applications and Benefits. *IUVA News*, (June):11–15, 2007.

[45] J. R. Bolton, K. G. Bircher, W. Tumas, and C. A. Tolman. Figures-of-merit for the technical development and application of advanced oxidation technologies for both electric- and solar-driven systems (IUPAC Technical Report). *Pure and Applied Chemistry*, 73(4):627–637, 2001.

[46] R. Haitz and J. Y. Tsao. Solid-state lighting: 'The case' 10 years after and future prospects. *Physica Status Solidi (A) Applications and Materials Science*, 208(1):17–29, 2011.

[47] A. Bergh, G. Craford, A. Duggal, and R. Haitz. The Promise and Challenge of Solid-State Lighting. *Physics Today*, 54(12):42, 2001.

[48] E. F. Schubert and J. K. Kim. Solid-state light sources getting smart. *Science*, 308(5726):1274–8, 2005.

[49] J. Y. Tsao. Solid state lightning: lamps, chips, and materials of tomorrow. (IEEE Circuits Devices Magazine 20:28), 2004.

[50] O Tokode, R Prabhu, L Lawton, and P Robertson. UV LED Sources for Heterogeneous Photocatalysis. *Hdb Env Chem*, 35:159–180, 2015.

[51] F. Khodadadian, A. Poursaeidesfahani, Z. Li, J. R. van Ommen, A. I. Stankiewicz, and R. Lakerveld. Model-Based Optimization of a Photocatalytic Reactor with Light-Emitting Diodes. *Chemical Engineering and Technology*, 39(10):1946–1954, 2016.

[52] Z. Wang, J. Liu, Y. Dai, W. Dong, S. Zhang, and J. Chen. CFD modeling of a UV-LED photocatalytic odor abatement process in a continuous reactor. *Journal of Hazardous Materials*, 215-216:25–31, 2012.

[53] N. Serpone, R. Terzian, D. Lawless, P. Kennepohl, and G. Sauve. On the usage of turnover numbers heterogeneous photocatalysis ' and quantum yields in. 73:11–16, 1993.

[54] A. L. Linsebigler, G. Lu, and J. T Yates. Photocatalysis on TiO2 Surfaces: Principles, Mechanisms, and Selected Results. *Chemical Reviews*, 95(3):735–758, 1995.

[55] N. Serpone. Relative photonic efficiencies and quantum yields in heterogeneous photocatalysis. *Journal of Photochemistry and Photobiology A: Chemistry*, 104(1-3):1–12, 1997.

[56] N. Serpone and A. Salinaro. Terminology, relative photonic efficiencies and quantum yields in heterogeneous photocatalysis. Part I: Suggested protocol. *Pure and Applied Chemistry*, 71(2):303–320, 1999.

[57] J. Bolton, K. Bircher, W. Tumas, and C. Tolman. Figures of Merit for the Technical Development and Application of Advanced Oxidation Process. *Journal of Advanced Oxidation Technologies*, 1996.

[58] T. S. Natarajan, K. Natarajan, H. C. Bajaj, and R. J. Tayade. Energy efficient UV-LED source and TiO2 nanotube array-based reactor for photocatalytic application. *Industrial and Engineering Chemistry Research*, 50(13):7753–7762, 2011.

[59] J. Disdier, J. M. Herrmann, and P. Pichat. Platinum / Titanium Dioxide Catalysts. *Journal of Chemical Society, Faraday Transactions*, 79:651–660, 1983.

[60] T. Xu, L. Zhang, H. Cheng, and Y. Zhu. Significantly enhanced photocatalytic performance of ZnO via graphene hybridization and the mechanism study. *Applied Catalysis B: Environmental*, 101(3-4):382–387, 2011.

[61] K. R. Gopidas, M. Bohorquez, and P. V. Kamat. Photophysical and Photochemical Aspects of Coupled Semiconductors. Charge-Transfer Processes In Colloidal CdS-TiO, and CdS-AgI Systems. *J. Phys. Chem.*, 94(12):6435–6440, 1990.

[62] N. Vlachopoulos, P. Liska, J. Augustynski, and M. Grätzel. Very efficient visible light energy harvesting and conversion by spectral sensitization of high surface area polycrystalline titanium dioxide films. *Journal of the American Chemical Society*, 110(4):1216–1220, 1988.

[63] C. Butler and A. P. Davis. Photocatalytic oxidation in aqueous titanium dioxide suspensions: the influence of dissolved transition metals. *J. Photochem. Photobiol. A: Chem*, 70(3):273–283, 1993.

[64] V. Etacheri, C. Di, J. Schneider, D. Bahnemann, and S. C. Pillai. Visible-light activation of TiO 2 photocatalysts : Advances in theory and experiments. *JJournal of Photochemistry and Photobiology C: Photochemistry Reviews*, 25:1–29, 2015.

[65] T. Cao, D. Wang, D. S. Geng, L.M. Liu, and J. Zhao. A strain or electric field induced direct bandgap in ultrathin silicon film and its application in photovoltaics or photocatalysis. *Phys. Chem. Chem. Phys.*, 18(10):7156–7162, 2016.

[66] K. Vinodgopal and P. V. Kamat. Electrochemically assisted photocatalysis using nanocrystalline semiconductor thin films. *Solar Energy Materials and Solar Cells*, 38(1-4):401–410, 1995.

[67] Z. Li. *LED-Based Photocatalytic Reactor Design*. PhD thesis, Delft University of Technology, 2016.

[68] Z. Jiang, H. Wang, H. Huang, and C. Cao. Photocatalysis enhancement by electric field: TiO2 thin film for degradation of dye X-3B. *Chemosphere*, 56(5):503–508, 2004.

[69] J. G. Sczechowski, Carl A. Koval, and R. D. Noble. Evidence of critical illumination and dark recovery times for increasing the photoefficiency of aqueous heterogeneous photocatalysis. *Journal of Photochemistry and Photobiology A: Chemistry*, 74(2-3):273–278, sep 1993.

[70] O. Tokode, R. Prabhu, L. A. Lawton, and P. K. J. Robertson. Journal of Photochemistry and Photobiology A : Chemistry Controlled periodic illumination in semiconductor photocatalysis. 2015.

[71] J. G. Sczechowski, C. A. Koval, and R. D. Noble. A Taylor vortex reactor for heterogeneous photocatalysis. *Chemical Engineering Science*, 50(20):3163–3173, 1995.

[72] G. Stewart and M. A. Fox. The effect of dark recovery time on the photoefficiency of heterogeneous photocatalysis by TiO2 suspended in non-aqueous media. *Research on Chemical Intermediates*, 21(8-9):933–938, aug 1995.

[73] N. S. Foster, C. A. Koval, J. G. Sczechowski, and R. D. Noble. Investigation of controlled periodic illumination effects on photo-oxidation processes at titanium dioxide films using rotating ring disk photoelectrochemistry. 406:213–217, 1996.

[74] S. Upadhya and D. F. Ollis. Simple Photocatalysis Model for Photoefficiency Enhancement via Controlled, Periodic Illumination. *The Journal of Physical Chemistry B*, 101(14):2625–2631, 1997.

[75] K. J. Buechler, C. H. Nam, and T. M. Zawistowski. Design and Evaluation of a Novel-Controlled Periodic Illumination Reactor To Study Photocatalysis. *Industrial & Engineering Chemistry Research*, 38(4):1258–1263, 1999.

[76] K.J. Buechler and R.D. Noble. Investigation of the effects of controlled periodic illumination on the oxidation of gaseous trichloroethylene using a thin film of TiO2. *Ind. Eng. Chem. Res.*, 38:892–896, 1999.

[77] K. Buechler and T. Zawistowski. Investigation of the mechanism for the controlled periodic illumination effect in TiO2 photocatalysis. *Ind. Eng. Chem. Res.*, 40:1097–1102, 2001.

[78] C. J. G. Cornu, A. J. Colussi, and M. R. Hoffmann. Quantum Yields of the Photocatalytic Oxidation of Formate in Aqueous TiO2 Suspensions under Continuous and Periodic Illumination. *J. Phys. Chem. B*, 105(7):1351–1354, 2001.

[79] C. J. G. Cornu, A. J. Colussi, and M. R. Hoffmann. Time scales and pH dependences of the redox processes determining the photocatalytic efficiency of TiO2 nanoparticles from periodic illumination experiments in the stochastic regime. *Journal of Physical Chemistry B*, 107(14):3156–3160, 2003.

[80] O. Tokode, R. Prabhu, Linda A. Lawton, and P. K. J. Robertson. The effect of pH on the photonic efficiency of the destruction of methyl orange under controlled periodic illumination with UV-LED sources. *Chemical Engineering Journal*, 246:337–342, 2014.

[81] H. W. Chen, Y. Ku, and A. Irawan. Photodecomposition of o-cresol by UV-LED/TiO2 process with controlled periodic illumination. *Chemosphere*, 69(2):184–190, 2007.

[82] O. I. Tokode, R. Prabhu, L. A. Lawton, and P. K. J. Robertson. Effect of controlled periodic-based illumination on the photonic efficiency of photocatalytic degradation of methyl orange. *Journal of Catalysis*, 290:138–142, 2012.

[83] W. M. Hou and Y. Ku. Photocatalytic decomposition of gaseous isopropanol in a tubular optical fiber reactor under periodic UV-LED illumination. *Journal of Molecular Catalysis A: Chemical*, 374-375:7–11, 2013.

[84] O. Tokode, R. Prabhu, L. A. Lawton, and P. K.J. Robertson. Mathematical modelling of quantum yield enhancements of methyl orange photooxidation in aqueous TiO2 suspensions under controlled periodic UV LED illumination. *Applied Catalysis B: Environmental*, 156-157:398–403, 2014.

[85] E. Korovin, D. Selishchev, A. Besov, and D. Kozlov. UV-LED TiO2 photocatalytic oxidation of acetone vapor: Effect of high frequency controlled periodic illumination. *Applied Catalysis B: Environmental*, 163:143–149, 2015.

[86] P. Xiong and J. Hu. Decomposition of acetaminophen (Ace) using TiO2 / UVA / LED system. 282:48–56, 2017.

[87] R. Zhou and M. I. Guzman. Photocatalytic Reduction of Fumarate to Succinate on ZnS Mineral Surfaces. *Journal of Physical Chemistry C*, 120(13):7349–7357, 2016.

[88] Y. Ku, S.J. Shiu, and H.C. Wu. Decomposition of dimethyl phthalate in aqueous solution by UV–LED/TiO2 process under periodic illumination. *Journal of Photochemistry and Photobiology A: Chemistry*, 332:299–305, 2017.

[89] C. Y. Wang, R. Pagel, J. K. Dohrmann, and D. W. Bahnemann. Antenna mechanism and deaggregation concept: novel mechanistic principles for photocatalysis. *Comptes Rendus Chimie*, 9(5-6):761–773, 2006.

[90] P. Xiong and J. Hu. Inactivation/reactivation of antibiotic-resistant bacteria by a novel UVA/LED/TiO2 system. *Water Research*, 47(13):4547–4555, 2013.

[91] A. M. Turing. The chemical basis of morphogenesis. *Bulletin of Mathematical Biology*, 52(1-2):153–197, 1990.

[92] A. Horváth, M. Dolnik, A. Muñuzuri, A. Zhabotinsky, and I. Epstein. Control of Turing Structures by Periodic Illumination. *Physical Review Letters*, 83(15):2950–2952, 1999.

[93] W. L. Haden. The Chain Photolysis of Acetaldehyde in Intermittent Light. *The Journal of Chemical Physics*, 10(7):445, 1942.

[94] C. S. Lugo-Vega, B. Serrano-Rosales, and H. de Lasa. Immobilized particle coating for optimum photon and TiO2 utilization in scaled air treatment photo reactors. *Applied Catalysis B: Environmental*, 198:211–223, 2016.

[95] F. B. Li, X. Z. Li, C. H. Ao, S. C. Lee, and M. F. Hou. Enhanced photocatalytic degradation of VOCs using Ln3+-TiO2 catalysts for indoor air purification. *Chemosphere*, 59(6):787–800, 2005.

[96] A. Bouzaza, C. Vallet, and A. Laplanche. Photocatalytic degradation of some VOCs in the gas phase using an annular flow reactor: Determination of the contribution of mass transfer and chemical reaction steps in the photodegradation process. *Journal of Photochemistry and Photobiology A: Chemistry*, 177(2-3):212–217, 2006.

[97] S. B. Kim, H. T. Hwang, and S. C. Hong. Photocatalytic degradation of volatile organic compounds at the gas-solid interface of a TiO2 photocatalyst. *Chemosphere*, 48(4):437–444, 2002.

[98] J. Fishman. The global consequences of increasing tropospheric ozone concentrations. *Chemosphere*, 22(7):685–695, 1991.

[99] L. Wallace, E. Pellizzari, and C. Wendel. Total Volatile Organic Concentrations in 2700 Personal, Indoor; and Outdoor Air Samples collected in the US EPA Team Studies. *Indoor Air*, 1(4):465–477, 1991.

[100] World Health Organization. WHO Air quality guidelines for particulate matter, ozone, nitrogen dioxide and sulfur dioxide: global update 2005: summary of risk assessment. *Geneva: World Health Organization*, pages 1–22, 2006.

[101] G. B. Raupp, A. Alexiadis, M. M. Hossain, and R. Changrani. First-Principles Modeling, Scaling Laws and Design of Structured Photocatalytic Oxidation Reactors for Air Purification. *Catalysis Today*, 69(1-4):41–49, 2001.

[102] L. Dibble and G. B. Raupp. Fluidized-bed photocatalytic oxidation of trichloroethylene in contaminated air streams. *Environmental Science & Technology*, 26(3):492–495, 1992.

[103] O. Hennezel and D. F. Ollis. Trichloroethylene-promoted photocatalytic oxidation of air contaminants. *Journal of Catalysis*, 167(1):118–126, 1997.

[104] C. H. Ao, S. C. Lee, C. L. Mak, and L. Y. Chan. Photodegradation of volatile organic compounds (VOCs) and NO for indoor air purification using TiO2: Promotion versus inhibition effect of NO. *Applied Catalysis B: Environmental*, 42(2):119–129, 2003.

[105] R. M. Alberici and W. F. Jardim. Photocatalytic destruction of VOCS in the gas-phase using titanium dioxide. *Applied Catalysis B: Environmental*, 14(1-2):55–68, 1997.

[106] J. Peral and D. F. Ollis. Heterogeneous Photocatalytic Oxidation of Gas-Phase Organics for Air Purification: Acetone, 1-Butanol, Butyraldehyde, Formaldehyde, and m-Xylene Oxidation. *JOURNAL OF CATALYSIS*, 136:554–565, 1992.

[107] J. Jeong, K. Sekiguchi, and K. Sakamoto. Photochemical and photocatalytic degradation of gaseous toluene using short-wavelength UV irradiation with TiO 2 catalyst: Comparison of three UV sources. *Chemosphere*, 57(7):663–671, 2004.

[108] Z. Pengyi, L. Fuyan, Y. Gang, C. Qing, and Z. Wanpeng. A comparative study on decomposition of gaseous toluene by O3/UV, TiO2/UV and O3/TiO2/UV. *Journal of Photochemistry and Photobiology A: Chemistry*, 156(1-3):189–194, 2003.

[109] R. Mendez-Roman and N. Cardona-Martinez. Relationship between the formation of surface species and catalyst deactivation during the gas-phase photocatalytic oxidation of toluene. *Catalysis Today*, 40(4):353–365, 1998.

[110] F. Jovic, V. Tomasic, A. Davidson, J. P. P. Nogier, and V. Kosar. Photocatalytic Treatment of Air: How to deal with the problem of TiO2 deactivation. *Chemical and Biochemical Engineering Quarterly*, 27(1):37–42, 2013.

[111] M. G. Jeong, E. J. Park, H. O. Seo, K. D. Kim, Y. D. Kim, and D. C. Lim. Humidity effect on photocatalytic activity of TiO2 and regeneration of deactivated photocatalysts. *Applied Surface Science*, 271:164–170, 2013.

[112] T. Guo, Z. Bai, C. Wu, and T. Zhu. Influence of relative humidity on the photocatalytic oxidation (PCO) of toluene by TiO2 loaded on activated carbon fibers: PCO rate and intermediates accumulation. *Applied Catalysis B: Environmental*, 79(2):171–178, 2008.

[113] A. J. Maira, K. L. Yeung, J. Soria, J. M. Coronado, C. Belver, C. Y. Lee, and V. Augugliaro. Gas-phase photo-oxidation of toluene using nanometer-size TiO2 catalysts. *Applied Catalysis B: Environmental*, 29(4):327–336, 2001.

[114] G. Martra, S. Coluccia, L. Marchese, V. Augugliaro, V. Loddo, L. Palmisano, and M. Schiavello. The role of H2O in the photocatalytic oxidation of toluene in vapour phase on anatase TiO2 catalyst. *Catalysis Today*, 53(4):695–702, 1999.

[115] G. E. Imoberdorf, A. E. Cassano, H. A. Irazoqui, and O. M. Alfano. Optimal design and modeling of annular photocatalytic wall reactors. *Catalysis Today*, 129(1-2 SPEC. ISS.):118–126, 2007.

[116] X. Duan, D. Sun, Z. Zhu, X. Chen, and P. Shi. Photocatalytic decomposition of toluene by TiO2 film as photocatalyst. *Journal of Environmental Science and Health, Part A*, 37(4):679–692, 2002.

[117] S. Ardizzone, C. L. Bianchi, G. Cappelletti, A. Naldoni, and C. Pirola. Photocatalytic degradation of toluene in the gas phase: Relationship between surface species and catalyst features. *Environmental Science and Technology*, 42(17):6671–6676, 2008.

[118] S. Skogestad. Simple analytic rules for model reduction and PID controller tuning. *Modeling, Identification and Control*, 25(2):85–120, 2004.

[119] D. E. Seborg, D. Mellichamp, T. F. Edgar, and F. J. Doyle. Process Dynamics and Control. *Process Dynamics and Control*, page 2010, 2010.

[120] T. H. Xie and J. Lin. Origin of photocatalytic deactivation of TiO2 film coated on ceramic substrate. *Journal of Physical Chemistry C*, 111(27):9968–9974, 2007.

List of Tables

List of Figures

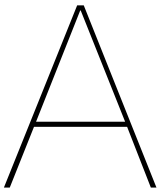

Notation

c	speed of light constant [2.998E8 m/s]
C	concentration [mol/L, ppmv, mol/m^3]
C_f	final concentration [mol/L, ppmv, mol/m^3]
C_o	initial concentration [mol/L, ppmv, mol/m^3]
D	molecular diffusion coefficient toluene [8.6E-6 m^2/s]
E	energy of a photon [J]
E_{EM}	electric energy per unit mass [kWh/kg, Wh/kg]
E_{EO}	electric energy per order [kWh/m^3, Wh/L]
F	flow rate [m^3/h]]
h	Planck's constant [6.626E-34 Js]
I_{avg}	average intensity [W/m^2, mW/cm^2]
I_{max}	maximum intensity [W/m^2, mW/cm^2]
k	reaction rate constant [1.64E-7 molm/($W^{0.5}$s)]
K	adsorption constant [692 m^3/mol]
L	reactor length [0.6 m]
M	molecular weight [g/mol]
$N_{photons}$	Number of photons per second [Einstein/s]
P	rated power [W, kW]
Q	volumetric flow rate [m^3/s]
r_o	reactor tube 1 radius [0.8 cm]
r_1	reactor tube 2 radius [2 cm]
r_2	reactor tube 3 radius [2.5 cm]
R	reaction rate
t_{OFF}	dark time [s]
t_{ON}	light time [s]
u(r)	velocity profile [m/s]
V	volume [L]
X	toluene conversion [-]

Greek letters

β	reaction order with respect to UV light [0.5]
γ	duty cycle [-]
ζ	photonic efficiency [-]
ζ_r	relative photonic efficiency [-]
λ	wavelength [nm, m]
τ	period [s]
Φ	quantum yield [-]

Abbreviations

AOP	advanced oxidation process
CEM	controlled evaporator mixer
CPI	controlled periodic illumination
GC	gas chromatograph
LED	light emitting diodes
MFC	mass flow controller
MFM	mass flow meter
PR	photocatalytic reactor
R.H.	relative humidity
SSL	solid state lighting
TNA	TiO_2 nanotube array
UV	ultraviolet

B

Figures Experimental System

Figure B.1: Overview of the experimental system: (1) LED-based annular photoreactor; (2) Verborg reactor; (3) gas chromatograph

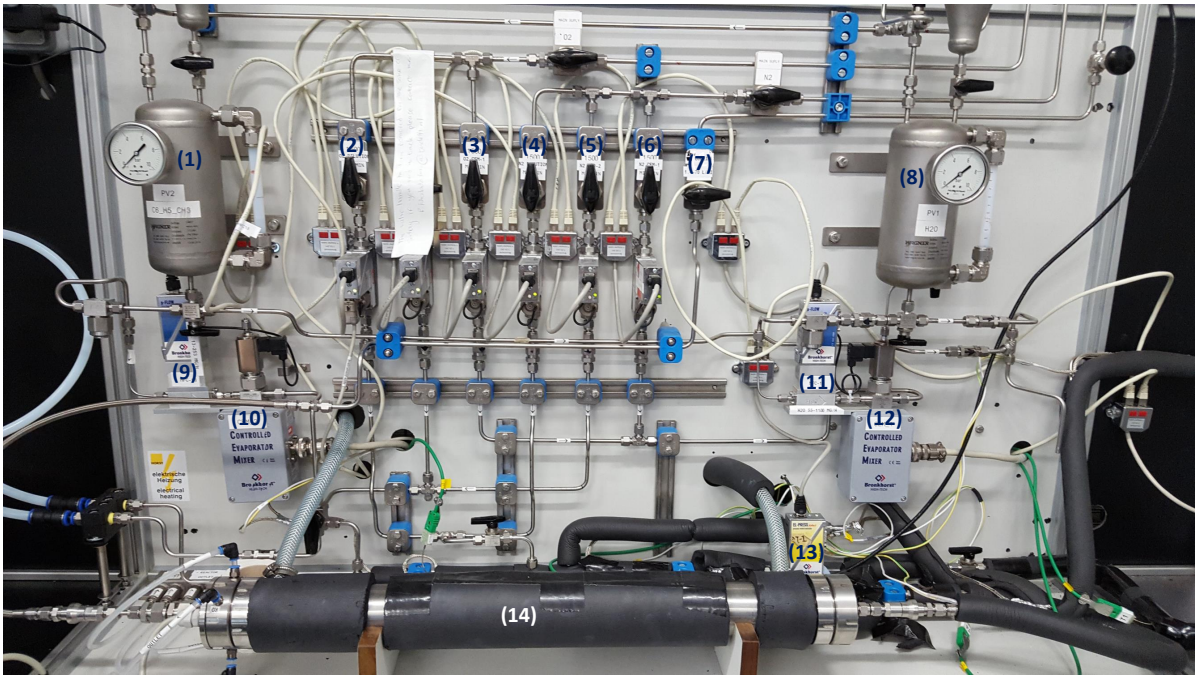

Figure B.2: Experimental system: (1) Toluene vessel; (2) Oxygen dilution line MFC-12; (3) Oxygen to CEM-2 MFC-16; (4) Nitrogen dilution line MFC-14; (5) Nitrogen to CEM-2 MFC-13; (6) Nitrogen to CEM-1 MFC-12; (7) Compressed air; (8) Water vessel; (9) Toluene MFC-18; (10) CEM-2; (11) Water MFC-11; (12) CEM-1; (13) Pressure meter; (14) LED-based annular photoreactor

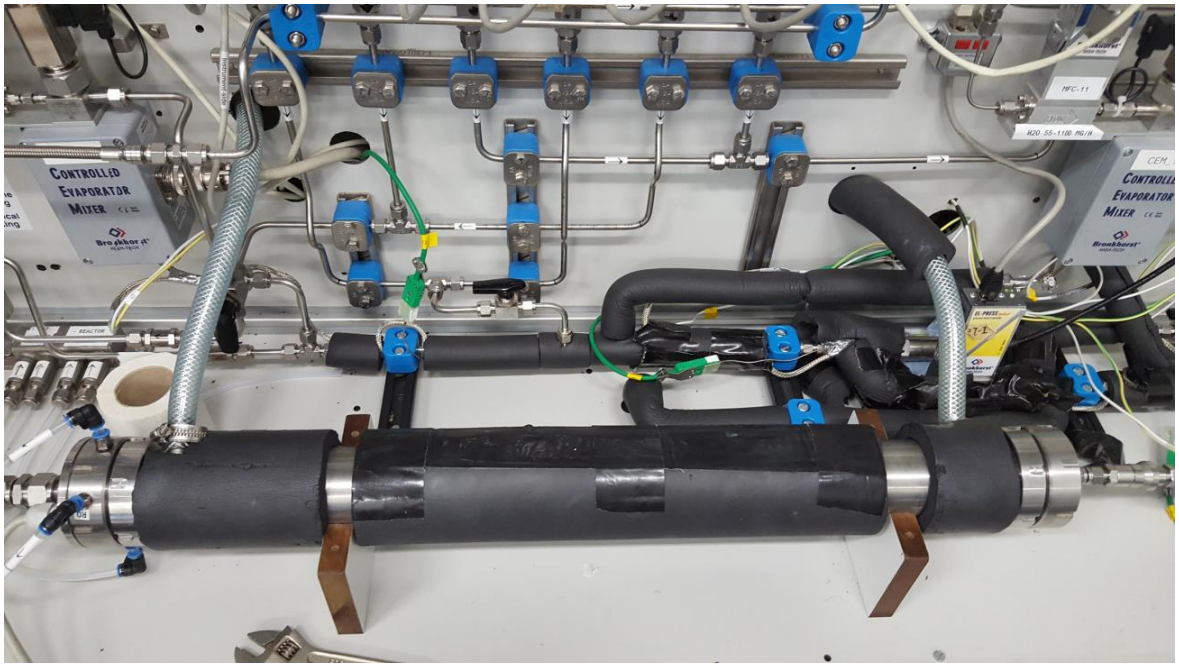

Figure B.3: LED-based annular photoreactor

Figure B.4: Gas chromatograph GC System 7890B Agilent Technologies

C

Matlab Code: Five Reactors in Series

```
%This program models five annular LED reactors in series, where the outlet
%concentration of the previous reactor is the inlet concentration of the
%next reactor.

function [cout,conv]=LED_reactor_2D_uni_LH_v3_nlfit_com_mult(P,x)

clear
clc
format shortEng

%% Initial data
cin=1.28164e-3;          % inlet concentration reactor 1, mol/m3
Q=23.522e-6;             % volumetric flow rate, m3/s
E1=13.5;                 % irradiance of each section of reactor, W/m2
E2=12.82;
E3=12.15;
E4=11.47;
E5=10.8;
Cin_w=0.721;             % concentration of water in this model
                         % doesn't matter since all
                         % experiments were performed at the
                         % same R.H.
%% Discretization
% number of nodes in axial direction
Grid.m=100000/5;
Grid.dz=1/(Grid.m-1);
Grid.z=linspace(0,1,Grid.m);
% number of nodes in radial direction
Grid.n=20;
Grid.dr=1/(Grid.n-1);
Grid.r=linspace(0,1,Grid.n);

%% Geometry
v.r0=0.008;              % radius of the tubes, m
v.r1=0.02;
v.r2=0.025;
v.L1=0.6/5;          % each section is one fifth of the total reactor length
```

```
%% Parameters
v.Q=Q;                  % [m3/s]
v.C_in1=cin;            % [mole/m3]
v.E1=E1;                % [W/m2]
v.E2=E2;
v.E3=E3;
v.E4=E4;
v.E5=E5;

v.Cin_w=Cin_w;

p.k= 1.64e-7;          % reaction rate constant
p.Kabs=692;            % adsorption constant
p.gama=0.5;            % rxn order with respect to UV radiation
p.D=8.6e-6;            % molecular diffusion [m2/s]
p.Kabs_w=0;

% required functions
u=velocity(v,Grid);

C=zeros(Grid.m,Grid.n);

%% for the first section
C(1,:)=v.C_in1;

for i=1:Grid.m-1

    for j=2:Grid.n-1

        C(i+1,j)=(v.L1*Grid.dz/u(j))*(p.D/((v.r2-v.r1)^2*Grid.dr^2)-...
        p.D/(Grid.r(j)*(v.r2-v.r1)+v.r1)*1/(Grid.dr*(v.r2-v.r1)))*C(i,j-1)+...
        (v.L1*Grid.dz/u(j))*(p.D/(Grid.r(j)*(v.r2-v.r1)+v.r1)*...
        1/(Grid.dr*(v.r2-v.r1))-2*p.D/(Grid.dr^2*(v.r2-v.r1)^2)+u(j)/...
        (v.L1*Grid.dz))*C(i,j)+(p.D/(Grid.dr^2*(v.r2-v.r1)^2))*...
        (v.L1*Grid.dz/u(j))*C(i,j+1);
    end
    C(i+1,1)=C(i+1,2);

     a=((v.r2-v.r1)*Grid.dr*(v.E1^p.gama)*p.k*p.Kabs)/p.D;
     aa=p.Kabs^2;
     bb=2*p.Kabs+2*p.Kabs*p.Kabs_w*v.Cin_w-C(i+1,Grid.n-1)*p.Kabs^2;

     cc=1+2*p.Kabs_w*v.Cin_w+p.Kabs_w^2*v.Cin_w^2-2*p.Kabs*C(i+1,Grid.n-1)-...
     2*C(i+1,Grid.n-1)*p.Kabs*p.Kabs_w*v.Cin_w+a;
     dd=-C(i+1,Grid.n-1)*(1+2*p.Kabs_w*v.Cin_w+p.Kabs_w^2*v.Cin_w^2);

     goh=roots([aa,bb,cc,dd]);

     C(i+1,Grid.n)=goh(real(goh) > 0 & imag(goh) == 0) ;


conv1=1-mean(C(Grid.m,:))/v.C_in1;
cout_1=mean(C(Grid.m,:));

end
```

```
disp(cout_1)
cout_m1=C(Grid.m,:);
v.C_in2=cout_m1;

%% for the second section
C(1,:)=v.C_in2;

for i=1:Grid.m-1

    for j=2:Grid.n-1

        C(i+1,j)=(v.L1*Grid.dz/u(j))*(p.D/((v.r2-v.r1)^2*Grid.dr^2)-...
        p.D/(Grid.r(j)*(v.r2-v.r1)+v.r1)*1/(Grid.dr*(v.r2-v.r1)))*C(i,j-1)+...
        (v.L1*Grid.dz/u(j))*(p.D/(Grid.r(j)*(v.r2-v.r1)+v.r1)*...
        1/(Grid.dr*(v.r2-v.r1))-2*p.D/...
        (Grid.dr^2*(v.r2-v.r1)^2)+u(j)/(v.L1*Grid.dz))*C(i,j)+...
        (p.D/(Grid.dr^2*(v.r2-v.r1)^2))*...
        (v.L1*Grid.dz/u(j))*C(i,j+1);
    end
    C(i+1,1)=C(i+1,2);

     a=((v.r2-v.r1)*Grid.dr*(v.E2^p.gama)*p.k*p.Kabs)/p.D;
     aa=p.Kabs^2;
     bb=2*p.Kabs+2*p.Kabs*p.Kabs_w*v.Cin_w-C(i+1,Grid.n-1)*p.Kabs^2;

     cc=1+2*p.Kabs_w*v.Cin_w+p.Kabs_w^2*v.Cin_w^2-...
     2*p.Kabs*C(i+1,Grid.n-1)-2*C(i+1,Grid.n-1)*p.Kabs*p.Kabs_w*v.Cin_w+a;
     dd=-C(i+1,Grid.n-1)*(1+2*p.Kabs_w*v.Cin_w+p.Kabs_w^2*v.Cin_w^2);

     goh=roots([aa,bb,cc,dd]);

     C(i+1,Grid.n)=goh(real(goh) > 0 & imag(goh) == 0) ;


conv2=1-mean(C(Grid.m,:))./v.C_in2;
cout_2=mean(C(Grid.m,:));

end
disp(cout_2)
cout_m2=C(Grid.m,:);
v.C_in3=cout_m2;

%% for the third section
C(1,:)=v.C_in3;

for i=1:Grid.m-1

    for j=2:Grid.n-1

        C(i+1,j)=(v.L1*Grid.dz/u(j))*(p.D/((v.r2-v.r1)^2*Grid.dr^2)-...
        p.D/(Grid.r(j)*(v.r2-v.r1)+v.r1)*1/(Grid.dr*(v.r2-v.r1)))*C(i,j-1)+...
        (v.L1*Grid.dz/u(j))*(p.D/(Grid.r(j)*(v.r2-v.r1)+v.r1)*...
        1/(Grid.dr*(v.r2-v.r1))-2*p.D/(Grid.dr^2*(v.r2-v.r1)^2)+...
        u(j)/(v.L1*Grid.dz))*C(i,j)+...
        (p.D/(Grid.dr^2*(v.r2-v.r1)^2))*...
        (v.L1*Grid.dz/u(j))*C(i,j+1);
```

```
    end
    C(i+1,1)=C(i+1,2);

     a=((v.r2-v.r1)*Grid.dr*(v.E3^p.gama)*p.k*p.Kabs)/p.D;
     aa=p.Kabs^2;
     bb=2*p.Kabs+2*p.Kabs*p.Kabs_w*v.Cin_w-C(i+1,Grid.n-1)*p.Kabs^2;

     cc=1+2*p.Kabs_w*v.Cin_w+p.Kabs_w^2*v.Cin_w^2-2*p.Kabs*C(i+1,Grid.n-1)-...
     2*C(i+1,Grid.n-1)*p.Kabs*p.Kabs_w*v.Cin_w+a;
     dd=-C(i+1,Grid.n-1)*(1+2*p.Kabs_w*v.Cin_w+p.Kabs_w^2*v.Cin_w^2);

     goh=roots([aa,bb,cc,dd]);

     C(i+1,Grid.n)=goh(real(goh) > 0 & imag(goh) == 0) ;


conv3=1-mean(C(Grid.m,:))./v.C_in3;
cout_3=mean(C(Grid.m,:));

end
disp(cout_3)
cout_m3=C(Grid.m,:);
v.C_in4=cout_m3;

%% for the fourth section
C(1,:)=v.C_in4;

for i=1:Grid.m-1

    for j=2:Grid.n-1

        C(i+1,j)=(v.L1*Grid.dz/u(j))*(p.D/((v.r2-v.r1)^2*Grid.dr^2)-...
        p.D/(Grid.r(j)*(v.r2-v.r1)+v.r1)*1/(Grid.dr*(v.r2-v.r1)))*C(i,j-1)+...
        (v.L1*Grid.dz/u(j))*(p.D/(Grid.r(j)*(v.r2-v.r1)+v.r1)*...
        1/(Grid.dr*(v.r2-v.r1))-2*p.D/(Grid.dr^2*(v.r2-v.r1)^2)+...
        u(j)/(v.L1*Grid.dz))*C(i,j)+(p.D/(Grid.dr^2*(v.r2-v.r1)^2))*...
        (v.L1*Grid.dz/u(j))*C(i,j+1);
    end
    C(i+1,1)=C(i+1,2);

     a=((v.r2-v.r1)*Grid.dr*(v.E4^p.gama)*p.k*p.Kabs)/p.D;
     aa=p.Kabs^2;
     bb=2*p.Kabs+2*p.Kabs*p.Kabs_w*v.Cin_w-C(i+1,Grid.n-1)*p.Kabs^2;

     cc=1+2*p.Kabs_w*v.Cin_w+p.Kabs_w^2*v.Cin_w^2-2*p.Kabs*C(i+1,Grid.n-1)-...
     2*C(i+1,Grid.n-1)*p.Kabs*p.Kabs_w*v.Cin_w+a;
     dd=-C(i+1,Grid.n-1)*(1+2*p.Kabs_w*v.Cin_w+p.Kabs_w^2*v.Cin_w^2);

     goh=roots([aa,bb,cc,dd]);

     C(i+1,Grid.n)=goh(real(goh) > 0 & imag(goh) == 0) ;


conv4=1-mean(C(Grid.m,:))./v.C_in4;
cout_4=mean(C(Grid.m,:));
```

```
end
disp(cout_4)
cout_m4=C(Grid.m,:);
v.C_in5=cout_m4;

%% for the fifth section
C(1,:)=v.C_in5;

for i=1:Grid.m-1

    for j=2:Grid.n-1

        C(i+1,j)=(v.L1*Grid.dz/u(j))*(p.D/((v.r2-v.r1)^2*Grid.dr^2)-...
        p.D/(Grid.r(j)*(v.r2-v.r1)+v.r1)*1/(Grid.dr*(v.r2-v.r1)))*C(i,j-1)+...
        (v.L1*Grid.dz/u(j))*(p.D/(Grid.r(j)*(v.r2-v.r1)+v.r1)*...
        1/(Grid.dr*(v.r2-v.r1))-2*p.D/(Grid.dr^2*(v.r2-v.r1)^2)+...
        u(j)/(v.L1*Grid.dz))*C(i,j)+(p.D/(Grid.dr^2*(v.r2-v.r1)^2))*...
        (v.L1*Grid.dz/u(j))*C(i,j+1);
    end
    C(i+1,1)=C(i+1,2);

     a=((v.r2-v.r1)*Grid.dr*(v.E5^p.gama)*p.k*p.Kabs)/p.D;
     aa=p.Kabs^2;
     bb=2*p.Kabs+2*p.Kabs*p.Kabs_w*v.Cin_w-C(i+1,Grid.n-1)*p.Kabs^2;

     cc=1+2*p.Kabs_w*v.Cin_w+p.Kabs_w^2*v.Cin_w^2-2*p.Kabs*C(i+1,Grid.n-1)-...
     2*C(i+1,Grid.n-1)*p.Kabs*p.Kabs_w*v.Cin_w+a;
     dd=-C(i+1,Grid.n-1)*(1+2*p.Kabs_w*v.Cin_w+p.Kabs_w^2*v.Cin_w^2);

     goh=roots([aa,bb,cc,dd]);

     C(i+1,Grid.n)=goh(real(goh) > 0 & imag(goh) == 0) ;


conv5=1-mean(C(Grid.m,:))./v.C_in5;
cout_5=mean(C(Grid.m,:));

end
disp(cout_5)

end

%% Velocity function
function u= velocity(v,Grid)

p_1=1/(3.14*v.r2^2)*(log(v.r1/v.r2)/((1-(v.r1/v.r2)^4)*log(v.r1/v.r2)+...
(1-(v.r1/v.r2)^2)^2));
p_2=(1-(v.r1/v.r2)^2)/log(v.r1/v.r2);

u=zeros(Grid.n,1);
for j=1:Grid.n
    u(j)=2*v.Q*p_1*(1-(((v.r2-v.r1)*Grid.r(j)+v.r1)/v.r2)^2-p_2*...
    log(((v.r2-v.r1)*Grid.r(j)+v.r1)/v.r2));
end

end
```

D

Matlab Code: Optimization

```
%This program finds the optimal irradiance per section
%of reactor along the whole irradiance spectrum to reach the
%maximum conversion using a genetic algorithm

%function multiobjective_genetic_algorithm_LED_thesis

FitFcn=@LED_reactor_2D_mult;
nvars=5;

LB=[0,0,0,0,0];
UB=[13.5,13.5,13.5,13.5,13.5];
options=optimoptions('gamultiobj','UseParallel',true,'PlotFcn',
@gaplotpareto,'FunctionTolerance',1e-4);

[x,fval]=gamultiobj(FitFcn,nvars,[],[],[],[],LB,UB,[],options);

function cout_5=LED_reactor_2D_GA(E)

format shortEng
%% Initial data
cin=1.28164e-3;          %inlet concentration reactor 1, mol/m3
Q=23.522e-6;             %volumetric flow rate, m3/s
Cin_w=0.721;

%% Discretization
% number of nodes in axial direction
Grid.m=100000/5;
Grid.dz=1/(Grid.m-1);
Grid.z=linspace(0,1,Grid.m);
% number of nodes in radial direction
Grid.n=20;
Grid.dr=1/(Grid.n-1);
Grid.r=linspace(0,1,Grid.n);

%% Geometry
v.r0=0.008;              % radius of the tubes, m
```

```
v.r1=0.02;
v.r2=0.025;
v.L1=0.6/5;                % length of each section, m

%% Parameters
v.Q=Q;                     % [m3/s]
v.C_in1=cin;               % [mole/m3]

v.Cin_w=Cin_w;

p.k= 1.64e-7;              % reaction rate constant
p.Kabs=692;                % adsorption constant
p.gama=0.5;                % rxn order with respect to UV radiation
p.D=8.6e-6;                % molecular diffusion [m2/s]
p.Kabs_w=0;

% required functions
u=velocity(v,Grid);

C=zeros(Grid.m,Grid.n);

%% for the first section
C(1,:)=v.C_in1;

for i=1:Grid.m-1

    for j=2:Grid.n-1

        C(i+1,j)=(v.L1*Grid.dz/u(j))*(p.D/((v.r2-v.r1)^2*Grid.dr^2)-...
        p.D/(Grid.r(j)*(v.r2-v.r1)+v.r1)*1/(Grid.dr*(v.r2-v.r1)))*C(i,j-1)+...
        (v.L1*Grid.dz/u(j))*(p.D/(Grid.r(j)*(v.r2-v.r1)+v.r1)*1/...
        (Grid.dr*(v.r2-v.r1))-2*p.D/(Grid.dr^2*(v.r2-v.r1)^2)+...
        u(j)/(v.L1*Grid.dz))*C(i,j)+(p.D/(Grid.dr^2*(v.r2-v.r1)^2))*...
        (v.L1*Grid.dz/u(j))*C(i,j+1);
    end
    C(i+1,1)=C(i+1,2);

     a=((v.r2-v.r1)*Grid.dr*(E(1)^p.gama)*p.k*p.Kabs)/p.D;
     aa=p.Kabs^2;
     bb=2*p.Kabs+2*p.Kabs*p.Kabs_w*v.Cin_w-C(i+1,Grid.n-1)*p.Kabs^2;

     cc=1+2*p.Kabs_w*v.Cin_w+p.Kabs_w^2*v.Cin_w^2-2*p.Kabs*C(i+1,Grid.n-1)-...
     2*C(i+1,Grid.n-1)*p.Kabs*p.Kabs_w*v.Cin_w+a;
     dd=-C(i+1,Grid.n-1)*(1+2*p.Kabs_w*v.Cin_w+p.Kabs_w^2*v.Cin_w^2);

     goh=roots([aa,bb,cc,dd]);

     C(i+1,Grid.n)=goh(real(goh) > 0 & imag(goh) == 0) ;


conv1=1-mean(C(Grid.m,:))/v.C_in1;
cout_1=mean(C(Grid.m,:));

end
disp(cout_1)
cout_m1=C(Grid.m,:);
```

```
v.C_in2=cout_m1;

%% for the second section
C(1,:)=v.C_in2;

for i=1:Grid.m-1

    for j=2:Grid.n-1

        C(i+1,j)=(v.L1*Grid.dz/u(j))*(p.D/((v.r2-v.r1)^2*Grid.dr^2)-...
        p.D/(Grid.r(j)*(v.r2-v.r1)+v.r1)*1/(Grid.dr*(v.r2-v.r1)))*C(i,j-1)+...
        (v.L1*Grid.dz/u(j))*(p.D/(Grid.r(j)*(v.r2-v.r1)+v.r1)*...
        1/(Grid.dr*(v.r2-v.r1))-2*p.D/(Grid.dr^2*(v.r2-v.r1)^2)+...
        u(j)/(v.L1*Grid.dz))*C(i,j)+(p.D/(Grid.dr^2*(v.r2-v.r1)^2))*...
        (v.L1*Grid.dz/u(j))*C(i,j+1);
    end
    C(i+1,1)=C(i+1,2);

     a=((v.r2-v.r1)*Grid.dr*(E(2)^p.gama)*p.k*p.Kabs)/p.D;
     aa=p.Kabs^2;
     bb=2*p.Kabs+2*p.Kabs*p.Kabs_w*v.Cin_w-C(i+1,Grid.n-1)*p.Kabs^2;

     cc=1+2*p.Kabs_w*v.Cin_w+p.Kabs_w^2*v.Cin_w^2-2*p.Kabs*C(i+1,Grid.n-1)-...
     2*C(i+1,Grid.n-1)*p.Kabs*p.Kabs_w*v.Cin_w+a;
     dd=-C(i+1,Grid.n-1)*(1+2*p.Kabs_w*v.Cin_w+p.Kabs_w^2*v.Cin_w^2);

     goh=roots([aa,bb,cc,dd]);

     C(i+1,Grid.n)=goh(real(goh) > 0 & imag(goh) == 0) ;

conv2=1-mean(C(Grid.m,:))./v.C_in2;
cout_2=mean(C(Grid.m,:));

end
disp(cout_2)
cout_m2=C(Grid.m,:);
v.C_in3=cout_m2;

%% for the third section
C(1,:)=v.C_in3;

for i=1:Grid.m-1

    for j=2:Grid.n-1

        C(i+1,j)=(v.L1*Grid.dz/u(j))*(p.D/((v.r2-v.r1)^2*Grid.dr^2)-...
        p.D/(Grid.r(j)*(v.r2-v.r1)+v.r1)*1/(Grid.dr*(v.r2-v.r1)))*C(i,j-1)+...
        (v.L1*Grid.dz/u(j))*(p.D/(Grid.r(j)*(v.r2-v.r1)+v.r1)*...
        1/(Grid.dr*(v.r2-v.r1))-2*p.D/(Grid.dr^2*(v.r2-v.r1)^2)+...
        u(j)/(v.L1*Grid.dz))*C(i,j)+(p.D/(Grid.dr^2*(v.r2-v.r1)^2))*...
        (v.L1*Grid.dz/u(j))*C(i,j+1);
    end
    C(i+1,1)=C(i+1,2);

     a=((v.r2-v.r1)*Grid.dr*(E(3)^p.gama)*p.k*p.Kabs)/p.D;
     aa=p.Kabs^2;
```

```
        bb=2*p.Kabs+2*p.Kabs*p.Kabs_w*v.Cin_w-C(i+1,Grid.n-1)*p.Kabs^2;

        cc=1+2*p.Kabs_w*v.Cin_w+p.Kabs_w^2*v.Cin_w^2-2*p.Kabs*C(i+1,Grid.n-1)-...
        2*C(i+1,Grid.n-1)*p.Kabs*p.Kabs_w*v.Cin_w+a;
        dd=-C(i+1,Grid.n-1)*(1+2*p.Kabs_w*v.Cin_w+p.Kabs_w^2*v.Cin_w^2);

        goh=roots([aa,bb,cc,dd]);

        C(i+1,Grid.n)=goh(real(goh) > 0 & imag(goh) == 0) ;

conv3=1-mean(C(Grid.m,:))./v.C_in3;
cout_3=mean(C(Grid.m,:));

end
disp(cout_3)
cout_m3=C(Grid.m,:);
v.C_in4=cout_m3;

%% for the fourth section
C(1,:)=v.C_in4;

for i=1:Grid.m-1

    for j=2:Grid.n-1

        C(i+1,j)=(v.L1*Grid.dz/u(j))*(p.D/((v.r2-v.r1)^2*Grid.dr^2)-...
        p.D/(Grid.r(j)*(v.r2-v.r1)+v.r1)*1/(Grid.dr*(v.r2-v.r1)))*C(i,j-1)+...
        (v.L1*Grid.dz/u(j))*(p.D/(Grid.r(j)*(v.r2-v.r1)+v.r1)*...
        1/(Grid.dr*(v.r2-v.r1))-2*p.D/(Grid.dr^2*(v.r2-v.r1)^2)+...
        u(j)/(v.L1*Grid.dz))*C(i,j)+(p.D/(Grid.dr^2*(v.r2-v.r1)^2))*...
        (v.L1*Grid.dz/u(j))*C(i,j+1);
    end
    C(i+1,1)=C(i+1,2);

     a=((v.r2-v.r1)*Grid.dr*(E(4)^p.gama)*p.k*p.Kabs)/p.D;
     aa=p.Kabs^2;
     bb=2*p.Kabs+2*p.Kabs*p.Kabs_w*v.Cin_w-C(i+1,Grid.n-1)*p.Kabs^2;

     cc=1+2*p.Kabs_w*v.Cin_w+p.Kabs_w^2*v.Cin_w^2-2*p.Kabs*C(i+1,Grid.n-1)-...
     2*C(i+1,Grid.n-1)*p.Kabs*p.Kabs_w*v.Cin_w+a;
     dd=-C(i+1,Grid.n-1)*(1+2*p.Kabs_w*v.Cin_w+p.Kabs_w^2*v.Cin_w^2);

     goh=roots([aa,bb,cc,dd]);

     C(i+1,Grid.n)=goh(real(goh) > 0 & imag(goh) == 0) ;


conv4=1-mean(C(Grid.m,:))./v.C_in4;
cout_4=mean(C(Grid.m,:));

end
disp(cout_4)
cout_m4=C(Grid.m,:);
v.C_in5=cout_m4;

%% for the fifth section
```

```
C(1,:)=v.C_in5;

for i=1:Grid.m-1

    for j=2:Grid.n-1

        C(i+1,j)=(v.L1*Grid.dz/u(j))*(p.D/((v.r2-v.r1)^2*Grid.dr^2)-...
        p.D/(Grid.r(j)*(v.r2-v.r1)+v.r1)*1/(Grid.dr*(v.r2-v.r1)))*C(i,j-1)+...
        (v.L1*Grid.dz/u(j))*(p.D/(Grid.r(j)*(v.r2-v.r1)+v.r1)*...
        1/(Grid.dr*(v.r2-v.r1))-2*p.D/(Grid.dr^2*(v.r2-v.r1)^2)+...
        u(j)/(v.L1*Grid.dz))*C(i,j)+(p.D/(Grid.dr^2*(v.r2-v.r1)^2))*...
        (v.L1*Grid.dz/u(j))*C(i,j+1);
    end
    C(i+1,1)=C(i+1,2);

     a=((v.r2-v.r1)*Grid.dr*(E(5)^p.gama)*p.k*p.Kabs)/p.D;
     aa=p.Kabs^2;
     bb=2*p.Kabs+2*p.Kabs*p.Kabs_w*v.Cin_w-C(i+1,Grid.n-1)*p.Kabs^2;

     cc=1+2*p.Kabs_w*v.Cin_w+p.Kabs_w^2*v.Cin_w^2-2*p.Kabs*C(i+1,Grid.n-1)-...
     2*C(i+1,Grid.n-1)*p.Kabs*p.Kabs_w*v.Cin_w+a;
     dd=-C(i+1,Grid.n-1)*(1+2*p.Kabs_w*v.Cin_w+p.Kabs_w^2*v.Cin_w^2);

     goh=roots([aa,bb,cc,dd]);

     C(i+1,Grid.n)=goh(real(goh) > 0 & imag(goh) == 0) ;

conv5=1-mean(C(Grid.m,:))./v.C_in5;
cout_5=mean(C(Grid.m,:));

end
disp(cout_5)

end

%% Velocity function
function u= velocity(v,Grid)

p_1=1/(3.14*v.r2^2)*(log(v.r1/v.r2)/((1-(v.r1/v.r2)^4)*...
log(v.r1/v.r2)+(1-(v.r1/v.r2)^2)^2));
p_2=(1-(v.r1/v.r2)^2)/log(v.r1/v.r2);

u=zeros(Grid.n,1);
for j=1:Grid.n
    u(j)=2*v.Q*p_1*(1-(((v.r2-v.r1)*Grid.r(j)+v.r1)/v.r2)^2-...
    p_2*log(((v.r2-v.r1)*Grid.r(j)+v.r1)/v.r2));
end

end
```

E

Simulink program: Process control

This Appendix presents two different figures. Figure E.1 illustrates an example of the Simulink block diagram to simulate the process control. When the gains of the concentration disturbance (Gain Co) and humidity disturbance (Gain RH) are set to 1, the system simulates the mineralization of toluene; otherwise the system simulates the conversion of toluene. The setpoint is set to 0.3 and is controlled via a PI controller. There is a saturation block that limits the irradiance of the controller to the working range of 0 to 13.5 W/m^2. A time delay of 1020 seconds (17 minutes) is assigned to the gas chromatograph. This time delay is the time required to analyze one sample. In addition, a time delay of 90 seconds is assigned to the disturbances. This time delay is the approximate time it takes to the flow to leave the reactor and reach the gas chromatograph.

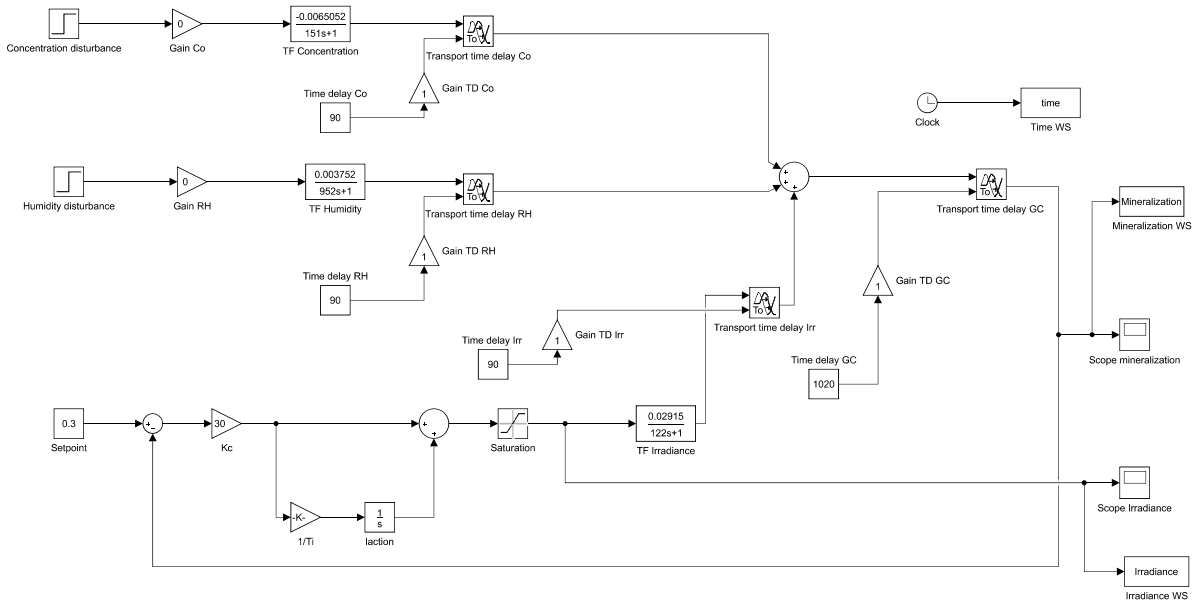

Figure E.1: Example of the Simulink block diagram to simulate the process control

Figure E.2 presents the system response to different values of the controller gain at a fixed time constant of 632 seconds (see also Table 3.1). It can be noted that increasing the controller gain to a value higher than the one computed with the IMC tuning rules has a two-fold negative effect: (1) there is a higher overshoot and undershoot in the irradiance, and (2) the system starts to fluctuate.

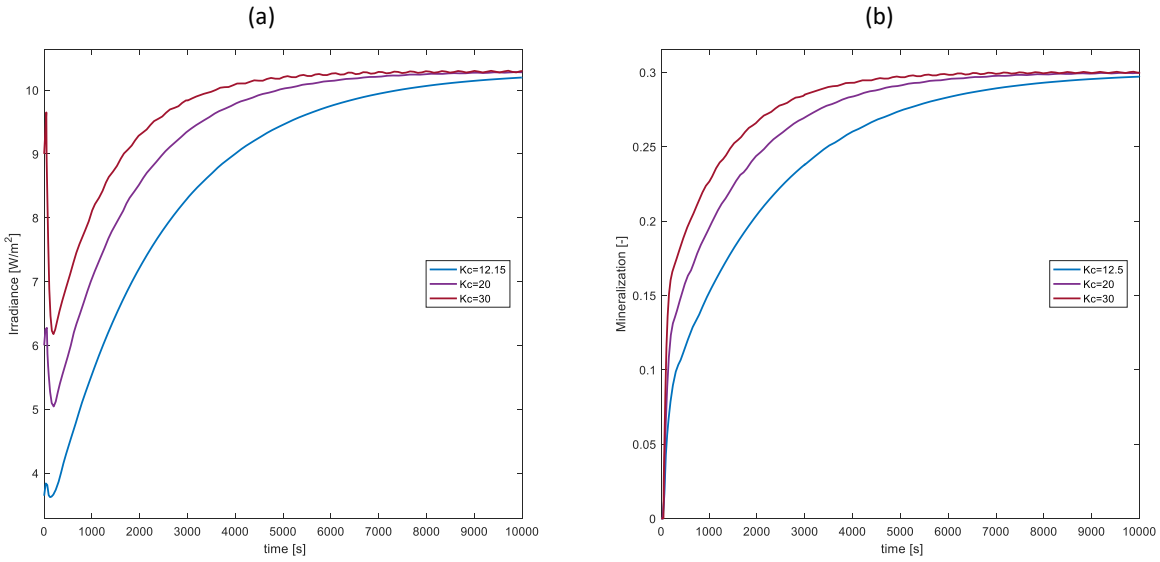

Figure E.2: System response to different values of the controller gain: (a) Irradiance; (b) Toluene mineralization